

Palladium Mediated Activation of Molecular Oxygen

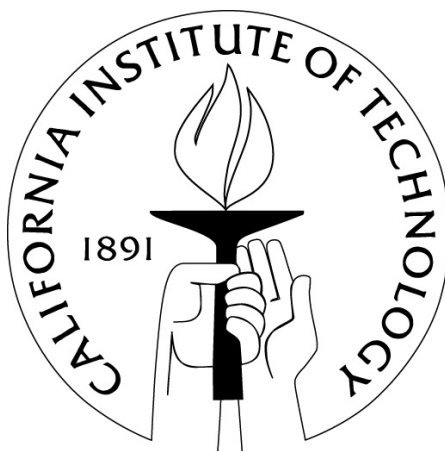
Thesis by

Jason M. Keith

In Partial Fulfillment of the Requirements for the

degree of

Doctor of Philosophy



California Institute of Technology

Pasadena, California

2008

(Defended May 27, 2008)

© 2008

Jason M. Keith

All Rights Reserved

In memoriam—Angel Luis “Louie” Castillo, 1978-2004

Acknowledgements

The person most responsible for my development as a scientist and to the completion of this body of work is my advisor, William A. Goddard, III. Bill has endowed me with the invaluable tools to accomplish my professional goals through my experiences as researcher, student, and teacher, and I hope one day to have the opportunity to mean as much to a young aspiring scientist.

I thank my collaborators and mentors Robert “Smith” Nielsen and Jonas Oxgaard for their patience and continued support from my first days learning Unix® to my final days working on this manuscript. I could not have accomplished what I have without you.

I would also like to thank the numerous members of the Goddard group during my tenure here with special mention to all the members of the catalysis subgroup. Exposure to new ideas and opinions occurred almost on a daily basis.

As an eager source of information for all things experimental, I would like to thank Chris Thomas for all her helpful discussions and friendship.

Outside of the realm of science several people played an important role in my life while in graduate school by providing friendship and support at times when it was most needed. Alex “Foos” Papandrew, Nathan Lundblad, Chris Harris, Matt Lucas, Patrick Dondl and Luke Wilson all did this in their own unique way and I am deeply indebted to them for their friendship. I would also like to thanks all the past and present members of the Caltech Rugby Football Club and the Caltech Spirits Club for providing a much needed distraction and social outlet.

Finally I would like to thank my parents, Chip and Karen, my brother Kris and his wife Amy, and my grandparents Wayland, Evelyn, and Rose for their love and support. My strong family bonds are something that I regularly rely on in my daily life. I would also like to give a posthumous thank you to my grandfather Ken for teaching me at a young age to be a resourceful problem solver and to always question why, traits that contributed directly to my affinity for science.

I have graciously been supported through an nsf fellowship and by grants from the National Science Foundation and Chevron-Texaco Energy Research and Technology Company. The computational facilities at the Materials and Process Simulation Center were funded by grants from ARO-DURIP, ONR-DURIP, IBM-SUR, and the Beckman Institute.

Abstract

In developing environmentally benign chemistries, it is most important to use dioxygen directly in lieu of toxic and/or corrosive stoichiometric oxidants. Unfortunately, for many processes such as direct oxidations this has not yet become practical. To help develop such processes, we elucidate here the mechanism for the reaction of molecular oxygen with palladium-hydride complexes in nonpolar solvent using quantum mechanics (B3LYP/LACVP** with the PBF polarizable continuum solvent model) for several Pd^{II} complexes, specifically focusing on the pathways proceeding through Pd⁰ and on the direct insertion of oxygen into the Pd-H bond. All the chapters presented herein constitute independent publications focusing on different aspects of the total problem as follows:

Chapter 1: Activation of Molecular Oxygen by ((-)-Sparteine)PdHCl: Direct Insertion presents the first proposal of a hydrogen atom abstraction from a palladium-hydride complex by triplet oxygen along with calculated potential energy surfaces and structures that demonstrate the feasibility of this mechanism. Aspects of the spin conversion and importance of adjacent hydrogen bond acceptors are also examined in detail.

Chapter 2: Activation of Molecular Oxygen by [1,3-(CH₂P^tBu₂)₂-C₆H₃]PdH presents calculated potential energy surfaces, structures and calculated kinetic isotope effects for an experimentally isolated palladium-hydride complex from which formation of Pd⁰ has been deemed unlikely. The calculated direct insertion mechanism coincides with the experimental results and the calculated KIE has fair agreement with experimental numbers, thus proving the previously predicted mechanism to be active in a known system.

Chapter 3: Activation of Molecular Oxygen by ((-)-Sparteine)PdHCl: Pd⁰ presents a thorough investigation of possible base-assisted reductive elimination pathways that can lead to the formation of Pd⁰ in the ((-)-Sparteine)PdHCl system initially investigated in Chapter 1. Calculated potential energy surfaces and structures are presented and, when compared to the previously reported direct insertion mechanism, demonstrate that the direct insertion mechanism is in fact the process involved in this system ($\Delta\Delta H^\ddagger = 6.2$ kcal/mol, $\Delta\Delta G^\ddagger = 7.5$ kcal/mol). At the time this work was completed it, along with Chapter 1, was among the earliest examinations of these two mechanisms for one system (and the first for a bidentate ligand system) and the first that definitively stated a preference for the direct insertion pathway when both pathways were accessible.

Chapter 4: Activation of Molecular Oxygen by ((-)-Sparteine)Pd(OAc)H: Pd⁰ vs. Direct Insertion presents calculated potential energy surfaces and structures of the ((-)-Sparteine)PdH substituting OAc ion for Cl. The acetate ligand's ability to act as a base while chelating the Pd deems the external base unnecessary and significantly lowers the energy involved in the Pd⁰ pathway, switching the calculated preference to the Pd⁰ pathway ($\Delta\Delta H^\ddagger = -1.0$ kcal/mol, $\Delta\Delta G^\ddagger = 7.7$ kcal/mol).

Chapter 5: Activation of Molecular Oxygen by (Pyridine)₂Pd(OAc)H: Pd⁰ vs. Direct Insertion presents calculated potential energy surfaces and structures for the reaction of (Pyridine)₂Pd(OAc)H with O₂. The ability for the two pyridine ligands to obtain both a *cis* and *trans* configuration is examined, and the direct insertion and Pd⁰ mechanisms are examined for both starting structures and with the assistance of an additional HOAc molecule. This work represents the first examination of these two mechanisms for both the *cis* and *trans* isomers of a system employing two monodentate ligands and the first case of acid-assisted reductive elimination from a square planar Pd-H. The calculated mechanisms present feasible *cis/trans* isomerisation and demonstrate that the Pd⁰ pathway is the favored pathway for both the *cis* ($\Delta\Delta H^\ddagger = 2.2$ kcal/mol,

$\Delta\Delta G^\ddagger = 9.3$ kcal/mol) and the *trans* (HOAc-assisted; $\Delta\Delta H^\ddagger = -2.6$ kcal/mol, $\Delta\Delta G^\ddagger = 5.8$ kcal/mol) cases.

Appendix I: Enantioselective Oxidations of Secondary Alcohols by (–)-Sparteine-Pd^{II} Complexes is a report on previous results that examine the mechanism of specific Pd oxidation catalysis focusing on alcohol binding, deprotonation to form the corresponding alkoxide and the subsequent β -hydride elimination to form the ketone product. Calculated potential energy surfaces and structures are presented for the reaction of ((–)-Sparteine)PdX₂ + PhCH₂OH \rightarrow ((–)-Sparteine)PdHX + HX + PhC(H)=O (X = Cl, OAc) focusing on the deprotonation and β -hydride elimination transition states and paying special attention to variations due to X-group, solvent, substrate, and exogenous base. The calculated mechanisms are used to compare experimental enantioselectivities with excellent correlation ($s_{\text{calc}}/s_{\text{exp}}$ values of 17.7/20.0, 7.4/8.8 and 1.5/NA X = Cl, OAc, none).

Contents

Acknowledgements	iv
Abstract	vi
List of Figures	xiv
List of Tables	xvii
Chapter 1: Activation of Molecular Oxygen by (Spar)PdHCl:	
Direct Insertion	1
1.1 Introduction	1
1.2 Computational Methodology	2
1.3 Results and Discussion	4
1.3.1 (Spar)Pd Mechanism	4
1.3.1.1 Triplet H Abstraction-Dioxygen Rotation Mechanism for Dioxygen Insertion	4
1.3.1.2 Alternative Mechanisms	8
1.3.1.3 The 3A Intermediate	8
1.3.1.4 Transition from Triplet to Singlet (3A to 4)	9
1.3.1.5 Completion of the Catalytic Cycle	10
1.3.2 (Bipy)Pd Mechanism	10

1.3.3 Spin Transition	11
1.3.4 Role of Hydrogen Bonding.....	13
1.3.5 Comparison of Computational Methodologies	18
1.4 Conclusions	19
Chapter 2 Activation of Molecular Oxygen by (PCP)PdH	20
2.1 Introduction	20
2.2 Computational Methodology	21
2.3 Results and Discussion.....	21
2.3.1 Pd-H Insertion	21
2.3.1.1 Mechanistic Pathway	22
2.3.1.2 Spin Conversion.....	24
2.3.1.3 Radical Initiation.....	24
2.3.2 Pd ⁰ Pathways	24
2.3.3 Comparison to Previous Results with (Spar)PdHCl	25
2.3.4 Kinetic Isotope Effect	26
2.4 Conclusions	27
Chapter 3 Activation of Molecular Oxygen by (Spar)PdHCl: Pd⁰	28
3.1 Introduction	28
3.2 Computational Methodology	32
3.3 Results and Discussion.....	35
3.3.1 Base-Assisted Formation of Pd ⁰	35
3.3.1.1 Primary Pathway.....	35

3.3.1.2 Alternate Pathway Starting at 6_{sing}	42
3.3.1.3 Alternate Pathway Starting at 4_{trip}	42
3.3.2 Unassisted Formation of Pd^0	44
3.3.2.1 “Naked” Pd^0	44
3.3.2.2 Pd^0 with O_2	46
3.3.2.3 Pd^0 with Ketone	46
3.4 Conclusions	50
Chapter 4 Activation of Molecular Oxygen by (Spar)PdHOAc:	
Pd^0 vs. Direct Insertion	52
4.1 Introduction	52
4.2 Computational Methodology	55
4.3 Results and Discussion	57
4.3.1 Direct Insertion Pathway	57
4.3.2 Pd^0 Pathway: Unassisted Reductive Elimination of HOAc	60
4.4 Conclusions	64
Chapter 5 Activation of Molecular Oxygen by (Pyr)$_2\text{PdHOAc}$:	
Pd^0 vs. Direct Insertion	66
5.1 Introduction	66
5.2 Computational Methodology	71
5.3 Results and Discussion	73
5.3.1 <i>Cis/Trans</i> Isomerisation	73
5.3.2 Pd^0 Direct Insertion Pathway	74

5.3.2.1 <i>Trans</i> Pathway	75
5.3.2.2 <i>Cis</i> Pathway	77
5.3.3 Pd ⁰ Pathway: Unassisted Reductive Elimination of HOAc.....	79
5.3.3.1 <i>Cis</i> Pathway	79
5.3.3.2 <i>Trans</i> Pathway	82
5.3.4 Pd ⁰ Pathway: HOAc-Assisted Reductive Elimination of HOAc.....	85
5.4 Conclusions	87
Appendix Enantioselective Oxidations of Secondary Alcohols	
by (Spar)Pd^{II} Complexes	91
A.1 Introduction.....	91
A.2 Computational Methodology	93
A.3 Mechanism.....	94
A.3.1 General	94
A.3.2 Chloride vs. Acetate	99
A.4 Selectivity	101
A.4.1 General	101
A.4.2 Solvent Effects	105
A.4.3 Substrate and Ions	107
A.4.4 Thermodynamics.....	108
A.5 Discussion.....	109
A.6 Conclusions	110

Bibliography	112
---------------------------	------------

List of Figures

<i>Number</i>	<i>Page</i>
1.1 (Spar)PdHCl•O ₂ Insertion Potential Energy Surface	5
1.2 (Spar)PdHCl•O ₂ Insertion Detailed Structural View	6
1.3 (Spar)PdHCl•O ₂ Insertion Orbitals and Spin Density	7
1.4 (Bipy)PdHCl•O ₂ Insertion Potential Energy Surface	10
1.5 Pd(OOH)Cl Triplet-Singlet Crossing.....	12
1.6 Pd(OOH)Cl Triplet-Singlet Crossing Point Structure	13
1.7 PdCl•OOH Relaxation Path	15
1.8 (Bipy)PdHCH ₃ Direct Insertion Potential Energy Surface	16
2.1 (PCP)PdH•O ₂ Insertion Potential Energy Surface.....	21
2.2 (PCP)PdH•O ₂ Insertion Detailed Structural View.....	22
2.3 (PCP)PdH Pd ⁰ Structures	25
3.1 Direct Insertion vs. Pd ⁰ : Catalytic Cycles	29
3.2 Direct Insertion vs. Pd ⁰ : Recently Studied Systems	30
3.3 (Spar)PdHCl Pd ⁰ Potential Energy Surface	36
3.4 (Spar)PdHCl Pd ⁰ Detailed Structural View	37

3.5 Pd(η^2 OOH)•Cl Substitution Detailed Structural View.....	41
3.6 “Naked” (Spar)Pd Pd ⁰ Potential Energy Surface.....	45
3.7 Pd(η^2 O=R)•O ₂ Substitution Detailed Structural View	47
3.8 Pd(η^2 O ₂)•O=R Substitution Detailed Structural View	48
3.9 (Spar)PdHCl Direct Insertion vs. Pd ⁰ : Energetics Comparison	50
4.1 Pd ⁰ and Direct Insertion Pathways for Pd-H + O ₂	53
4.2 (Spar)PdHCl Direct Insertion vs. Pd ⁰ : Energetics Comparison	54
4.3 (Spar)PdHOAc•O ₂ Insertion Potential Energy Surface.....	57
4.4 (Spar)PdHOAc•O ₂ Insertion Detailed Structural View.....	58
4.5 (Spar)PdHOAc Pd ⁰ Potential Energy Surface	61
4.6 (Spar)PdHOAc Pd ⁰ Detailed Structural View	63
4.7 (Spar)PdHOAc Direct Insertion vs. Pd ⁰ : Energetics Comparison	65
5.1 Pd ⁰ and Direct Insertion Pathways for Pd-H + O ₂	68
5.2 Transition State Structures for (IMes) ₂ PdHOAc + O ₂	69
5.3 (Pyr) ₂ PdHOAc <i>Cis/Trans</i> Isomerisation Potential Energy Surface	73
5.4 (Pyr) ₂ PdHOAc•O ₂ Insertion Potential Energy Surface	74
5.5 (Pyr) ₂ PdHOAc•O ₂ Insertion Detailed Structural View	76
5.6 <i>Cis</i> -(Pyr) ₂ PdHOAc Pd ⁰ Potential Energy Surface.....	79
5.7 (Pyr) ₂ PdHOAc Pd ⁰ Detailed Structural View.....	80
5.8 <i>Trans</i> -(Pyr) ₂ PdHOAc Pd ⁰ Potential Energy Surface.....	82
5.9 <i>Trans</i> -(Pyr) ₂ PdHOAc Pd ⁰ Potential Energy Surface Continued.....	84
5.10 HOAc assisted <i>Trans</i> -(Pyr) ₂ PdHOAc Pd ⁰ Potential Energy Surface	85

5.11 HOAc assisted <i>Trans</i> -(Pyr) ₂ PdHOAc Pd ⁰ Detailed Structural View	86
5.12 (Pyr) ₂ PdHOAc Direct Insertion vs. Pd ⁰ : Energetics Comparison.....	88
A.1 (Spar)PdCl ₂ Ground State and Improbable Intermediates.....	94
A.2 (Spar)PdCl ₂ βHE Potential Energy Surface.....	95
A.3 (Spar)PdCl ₂ βHE Detailed Structural View.....	96
A.4 (Spar)PdOAc ₂ βHE Potential Energy Surface.....	97
A.5 (Spar)PdX ₂ βHE Halide Effects.....	99
A.6 Enantioselectivities: Calculated vs. Experimental.....	104

List of Tables

<i>Number</i>	<i>Page</i>
1.1 Halide Effects in (Spar)Pd(H)Cl•O ₂ Insertion.....	17
1.2 Basis Set and Functional Comparison	18
A.1 Halide, Solvent, and Substrate Effects in (Spar)PdCl ₂ βHE	103

Chapter 1

Activation of Molecular Oxygen by ((-)-Sparteine)PdHCl: Direct Insertion

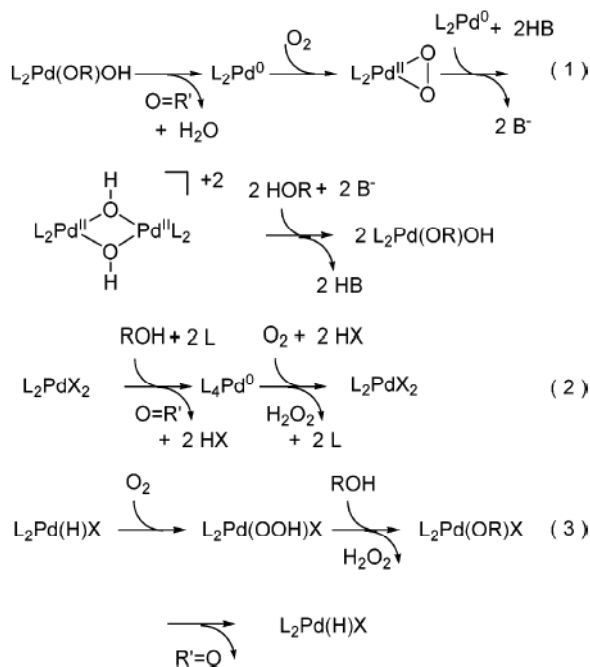
1.1 Introduction

¹Homogeneous catalytic systems involving Pd^{II} complexes have been used as efficient oxidization catalysts with the use of molecular oxygen as a terminal oxidant [1–4]. Molecular oxygen is an ideal oxidant due to its availability, its solubility in common solvents, and its production of environmentally safe byproducts such as water and hydrogen peroxide, itself a commercially important chemical. Despite its importance, the mechanistic details of the involvement of O₂ in these processes are largely unknown.

There are currently three major mechanistic proposals to explain the role of dioxygen in these processes. The first two mechanisms, as proposed by Sheldon [2] (eq. 1) and Bianchi [3] (eq. 2), proceed via a Pd⁰ intermediate, which subsequently reacts with the dioxygen. The third mechanism, as proposed by Hosokawa and Murahashi (eq. 3), postulates the direct insertion of O₂ in a Pd-H bond, thus avoiding Pd⁰ altogether [4]. Later experimental

¹ Reproduced with permission from *J. Am. Chem. Soc.* **2005**, *127*, 13172. Copyright 2005 American Chemical Society.

work by Stahl suggested a variant of eq. 1 where the L_2PdO_2 species is protonated directly, thus avoiding dimerisation [5].



As part of our work on Pd-catalyzed oxidation of alcohols in nonpolar media², we investigated the interaction of O_2 with Pd^{II} hydride in a direct insertion mechanism. While alternative Pd^0 mechanisms are currently under investigation, we have found that the direct insertion is indeed plausible, but only for a select subset of Pd complexes. In this report we will demonstrate a detailed mechanistic picture and discuss the structural requirements of this process, as well as introduce some new aspects of the triplet-singlet crossover involved.

1.2 Computational Methodology

All calculations were performed using the hybrid DFT functional B3LYP as implemented by the Jaguar 5.5 program package [6]. This DFT functional utilizes the Becke three-

² See Appendix.

parameter functional (B3) [7] combined with the correlation functional of Lee, Yang, and Parr (LYP) [8], and is known to produce good descriptions of reaction profiles for transition-metal-containing compounds [9,10]. Pd was described with the LACVP** effective core potential and basis set (18 explicit electrons) [11]. All other elements were described including the core electrons, using the Pople 6-31G** basis set [12], but with 3s combination of the six d-like functions reduced to five. Diffuse functions were also added to Cl. The resulting basis set is denoted LACVP**^(a).

All geometries were optimized and evaluated for the correct number of imaginary frequencies through vibrational frequency calculations using the analytic Hessian. Zero imaginary frequencies correspond to a local minimum, while one imaginary frequency corresponds to a transition structure.

Implicit solvent effects were calculated with the Poisson-Boltzmann (PBF) continuum approximation [13], using the parameters $\epsilon = 2.379$ and solvent radius = 2.762 Å. Here we use the solvent-accessible surface of the molecular complex built using standard van der Waals radii. The solvation effects were calculated at geometries optimized for the gas phase.

Using the analytic Hessian, we calculated the zero-point energy corrections at 0 K and added this to the solvation correction and the QM energy [$\Delta(E)$] to obtain the enthalpy at 0 K [$\Delta H(0\text{ K})$]. Similarly, the vibrational frequencies were used to calculate the entropy and enthalpy corrections to 298.15 K, to obtain $(\Delta H - T\Delta S) = \Delta G(298.15\text{ K})$.

On the basis of previous results, we expect that relative energies on the $\Delta H(0\text{ K})$ surface are accurate to ~ 3 kcal/mol for stable intermediates, and to ~ 5 kcal/mol for transition structures. Probably the relative energies on the $\Delta G(298\text{ K})$ surface are less accurate, due to the use of the PBF model [14].

DFT is formulated in terms of Slater determinants built from Kohn-Sham orbitals that are calculated self-consistently. This process is consistent for states that are well described with closed-shell orbitals (up and down spins in the same orbitals), the normal situation for most DFT applications. However, in the studies reported here it was necessary to consider triplet states. With DFT this is done by having two more spin orbitals with up spin than down spin (unrestricted DFT or UDFT). We refer to this as the triplet state, but it need not be an eigenstate of the spin operator, S^2 . Rather it is an eigenfunction of S_z , leading to $M_S = 1$. The problem with this formulation occurs when it is necessary to consider transitions between triplet and singlet states, the topic of this paper. Thus, starting with the true triplet orbitals of O_2 and calculating the energy of the singlet state should lead to a component of $^1\Delta_g$, with an excitation energy of 22.5 kcal/mol. In fact, UDFT gives an excitation energy of 10.5 kcal/mol. The reason is that the $M_S = 0$ wave function we consider to describe the singlet state also has a component of triplet character. This can be treated by applying the spin projection operator, which leads to true singlet excited state and singlet-triplet splitting of 20.5 kcal/mol [15a], nearly twice the value from UDFT [15b]. In this paper all results are UDFT, and hence for triplet ground states the excitation energies to the excited singlet states are expected to be about half the rigorous value [15b].

1.3 Results and Discussion

1.3.1 Pd(sparteine) Mechanism

1.3.1.1 Triplet H Abstraction-Dioxygen Rotation Mechanism for Dioxygen Insertion

As the starting point for this study we chose (–)-sparteine- $Pd^{II}(H)(Cl)$ (**1**, Figure 1.1). Introducing (triplet) molecular oxygen to **1** leads immediately to the formation of a weakly bound van der Waals complex $[(spar)Pd^{II}(H)(Cl)]\cdot O_2$ (**2**), with $\Delta H = -0.8$ kcal/mol. There is negligible electron transfer between the O_2 and the Pd complex (the Mulliken charges on the two oxygens change from 0 and 0 to 0.06 and -0.02 electron, with the positively charged oxygen closest to the hydride, while the Pd gains 0.04

electron). Spin analysis shows that all unpaired spins in **2** are on the O₂ fragment (one π^* orbital in the plane, hereafter the σ electron, and the other π^* orbital perpendicular to the plane, hereafter the π electron).

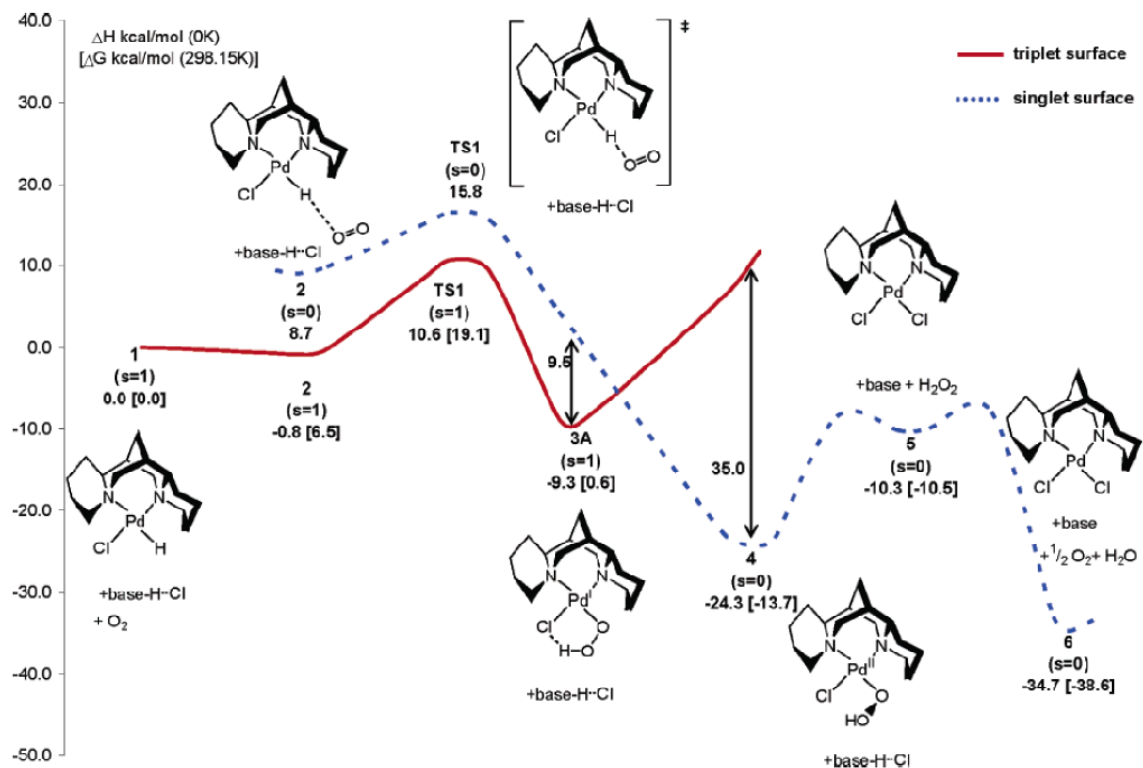


Figure 1.1. Calculated mechanism for O₂ insertion in (spar)Pd(H)(Cl) in toluene (base = spar). Here the triplet surface is shown by the solid (red) line while the singlet surface is shown with the dotted (blue) line. The triplet-singlet crossing between **3A** and **4** is discussed in Section 3.3 and shown in Figure 2.5.

The corresponding fully optimized singlet species is significantly higher in energy ($\Delta H = 9.5$ kcal/mol), indicating that the spin transition cannot occur at this stage in the reaction mechanism. Similar to O₂, discussed above in section 2, the UDFT calculation for the $M_S = 0$ or “singlet” state of **2** is contaminated with a significant amount of triplet character, leading to an energy that is far too low³.

³ Similar to O₂, the unrestricted singlet species of **2** and **TS1** have S^2 values of 1.004 and 1.017, demonstrating significant spin contamination, and therefore the energy gaps of 9.5 and 5.2 kcal/mol are underestimated by ~ 10 and ~ 5 kcal/mol, respectively,

From **2** we find an unexpected mechanism for O₂ insertion. Here the transition state, **TS1** (Figure 1.2a), has the triplet O₂ positioned to abstract the H from the Pd with $\Delta H^\ddagger = 10.6$ kcal/mol. Thus from **1** to **TS1** the Pd-H bond length stretches from 1.52 to 1.68 Å, indicating a decrease in bond order from 1 to ~ 0.7 . At the same time the O-O bond distance increases from 1.21 to 1.26 Å, indicating a decrease in bond order of ~ 0.2 . On the other hand, the O-H distance of 1.33 Å (compared to 0.96 Å in HO₂) indicates the O-H bond has not yet formed. At this point the π unpaired spin (perpendicular to the O₂-H-Pd plane) remains on the O₂, while the σ unpaired spin (in the plane) has partly delocalized onto the Pd d_{x²-y²} orbital (where Pd-H is the x direction and the plane is the xy plane; this orbital is shown in Figure 1.3). Spin population (shown in Figure 1.3) for the O₂ moiety is 1.53 (equally distributed across both O's), and that for Pd is 0.38.

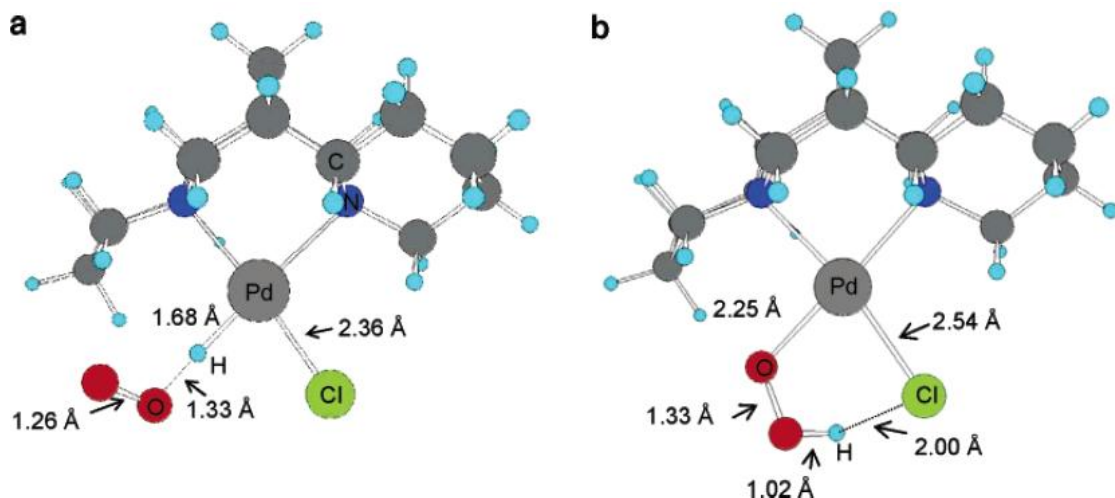


Figure 1.2. (a) Transition-state structure (**TS1**) for hydrogen abstraction/O₂ insertion mechanism. (b) Triplet species **3A**

From **TS1** the energy falls monotonically by 19.1 kcal/mol while the HO₂ rotates in the plane to form **3A** (further discussed in Section 1.3.1.3), in which the H is now bonded to the inner O (H-O = 1.02 Å) while the outer O is now bonded to the Pd (Pd-O = 2.25

although spin projections were not performed. In the singlet hydroperoxo species, **4**, spin contamination is not present ($S^2 = 0.000$). For further discussion on spin projections of singlet dioxygen, see ref [15].

Å). Here the two unpaired spin orbitals are similar to species **TS1**, in which the π unpaired spin remains on the O_2 , while the σ unpaired spin (in the plane) has further delocalized onto the Pd $d_{x^2-y^2}$ orbital.

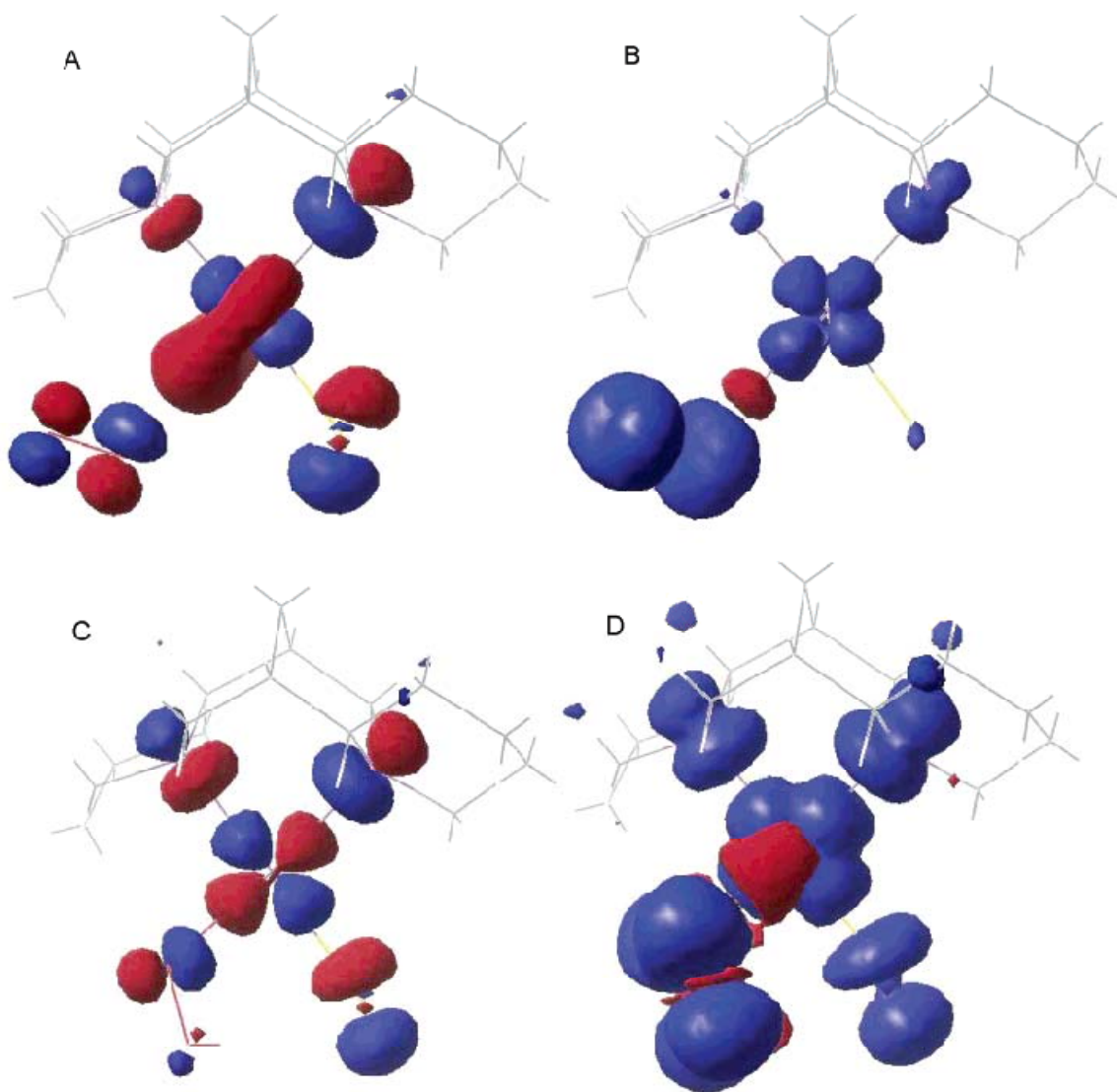


Figure 1.3. Highest SOMO orbital and spin densities for **TS1** and **3A**, illustrating the contribution from the Pd $d_{x^2-y^2}$. (A) Highest SOMO for **TS1**. (B) Spin distribution of **TS1**. (C) Highest SOMO of **3A**. (D) Spin distribution of **3A**

In this **TS1** structure the corresponding UDFT singlet state is higher than the triplet state by 5.2 kcal/mol ($\Delta H = 15.8$ kcal/mol). This species is contaminated with a

significant amount of triplet character, leading to an energy that is far too low³, demonstrating that a spin transition need not occur in the O₂ insertion step.

1.3.1.2 Alternative Mechanisms

Initially we assumed that the mechanism might proceed through a “2 + 2”-like transition state in which the Pd-O and O-H bonds are formed simultaneously with the Pd-H bond being broken. After initial failures to find such a transition state, we carried out geometry searches in which we constrained the Pd-O distance at successively shorter bond lengths from 5.0 to 2.0 Å. However, we found that the energy increased as the distance decreased until the ΔH was above 18.9 kcal/mol by the point at which Pd-O = 2.0 Å. As an alternative we constrained the Pd-O and Pd-H distances simultaneously (Pd-O from 2.0 to 5.0 Å and Pd-H from 1.5 to 3.5 Å), with similarly negative results.

We also examined the stepwise process in which a five-coordinate Pd species is first formed, followed by an insertion. However all attempts to find a stable five-coordinate intermediate were unsuccessful, with the geometries collapsing to Pd-(H)(Cl) + O₂. These attempts included cases in which the H, Cl, and O₂ in turn were each placed in the axial position in a square pyramidal geometry, as well as several trigonal bipyramidal geometries.

Only by allowing the O₂ to move away from the metal center and varying the O-H distance with no other constraints were we able to find the mechanism described in Section 1.3.1.1.

1.3.1.3 The 3A Intermediate

The mechanism through **TS1** leads to the planar Pd-OOH species **3A** (Figure 1.2b), with a ΔH of -9.3 kcal/mol with respect to **1**. The triplet state in **3A** is best described as a square planar Pd^I radical (unpaired spin in the Pd d_{x²-y²} orbital; this orbital shown in Figure 1.3) complexed with the HO₂• peroxy radical (π orbital perpendicular to the plane) acting as a donor ligand. The spin density (shown in Figure 1.3) for the O₂ moiety

is 0.98 (0.66 of which resides on the O nearest Pd), and that for Pd is 0.77. Since the unpaired orbitals are orthogonal by symmetry and localized on different centers, they have little interaction and **3A** is a biradical. Indeed, the Pd-O bond distance of 2.25 Å indicates a weak donor-acceptor bond, compared to the significantly shorter value of 2.09 Å expected for a Pd^{II}-O single bond [16]. The O-O bond distance of 1.33 Å is typical of a peroxy radical species (O-O = 1.33 Å in free HO₂), halfway between common single and double bond distances of 1.48 and 1.21 Å. The O-H bond distance of 1.02 Å is similar to that of free HO₂• (1.00 Å). Finally, the Pd-Cl bond distance of 2.54 Å and the Pd-N distances of 2.30 (*trans* to Cl) and 2.35 Å (*cis* to Cl) are elongated by 0.25, 0.19, and 0.24 Å compared to the bond lengths in other Pd^{II} complexes [17], as expected for a Pd^I center. An interesting feature of **3A** is the H-Cl distance of 2.00 Å between the Cl and the H of the peroxy radical, which indicates some internal hydrogen bonding. We find that this contributes to the exothermicity of this part of the reaction by significantly stabilizing this intermediate.

In the optimum geometry for the triplet state, the singlet state for **3A** is 9.5 kcal/mol higher in energy (spin contamination is negligible at this point, with $S^2 = 0.020$).

1.3.1.4 Transition from Triplet to Singlet (**3A** to **4**)

Given the O₂ π and Pd $d_{x^2-y^2}$ unpaired orbitals of triplet **3A**, we expect the transition to the singlet to occur by merely rotating the HO₂ about the O-O axis, where it can overlap the Pd $d_{x^2-y^2}$ unpaired orbital and start bonding to form the final Pd-O bond. This leads to **4**, with $\Delta H = -24.3$ kcal/mol. **4** is clearly a Pd^{II}OOH complex: the Pd-O bond distance of 1.97 Å is consistent with the covalent Pd-O bond in similar species [16], while the O-O bond distance of 1.43 Å is slightly shorter than a normal single bond distance of 1.48 Å. The O-H bond distance of 0.98 Å is consistent with an O-H bond distance in H₂O₂. The Pd-Cl bond distance of 2.42 Å and the Pd-N distances of 2.19 (*trans* to Cl) and 2.24 Å (*cis* to Cl) are as expected for Pd^{II}.

1.3.1.5 Completion of the Catalytic Cycle

The catalytic cycle is completed with protonation of **4** by an external acid (in this case protonated sparteine, spar-H), which yields **5**, PdCl₂, and H₂O₂. This process is energetically uphill by 14.0 kcal/mol. Even though this step is endothermic, the strongly exothermic disproportionation of H₂O₂ to water and O₂ is believed to be sufficient to drive the reaction forward. The mechanism for the conversion of **4** to **5** is well documented and not presented here [18].

1.3.2 Pd(bipyridine) Mechanism

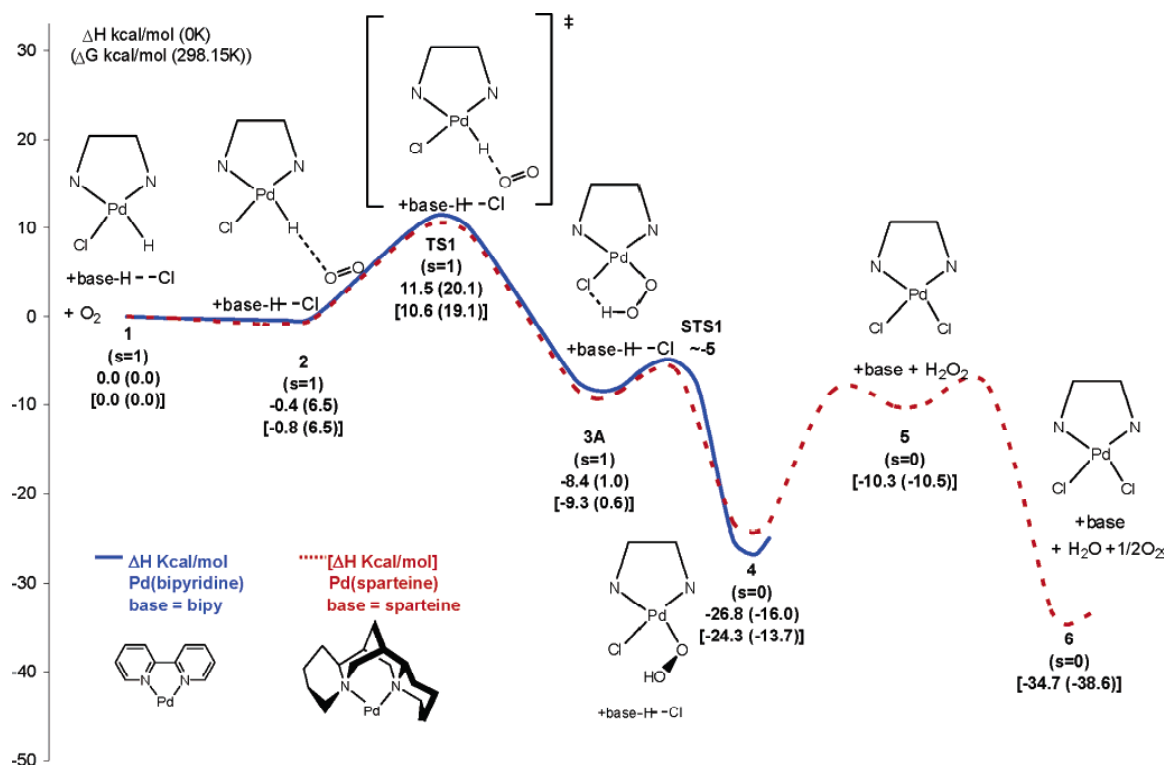


Figure 1.4. Calculated mechanism for O₂ insertion in (L)Pd(H)(Cl) in toluene (L = bipy, [spar]). The upper numbers refer to the solid (blue) energies using bipy as the base, while the lower numbers in brackets and the dotted (red) line use sparteine as the base. The first numbers are ΔH, while the numbers in parentheses are ΔG.

Further studies were conducted to confirm our expectation that **3A** can easily undergo a spin transition and to explore the rearrangement that connects **TS1** with **3A**. However, to reduce the costs of such calculations, we replaced the sparteine ligand in Pd(sparteine)(Cl)₂ with a significantly smaller analogue, (bipyridine)Pd(Cl)₂ [19]. Bipyridine (bipy) was chosen as a simple *cis*-restricted bidentate diamine ligand partly to maintain some of the structural restrictions of (–)sparteine, and partly to provide a more general model applicable to a broad range of systems. While (bipy)Pd(Cl)₂ has been shown experimentally to not be a competent catalyst for the aerobic oxidation of alcohols [4c], our previous computational results indicate that this is due to difficulties in the deprotonation of the alcohol and does thus not imply an inability for (bipy)Pd(Cl)(H) to react with O₂. Furthermore, as illustrated in Figure 1.4 (solid line), the energetic profiles of the bipy and sparteine systems are very similar. We thus believe bipy to be a good ligand substitute for the larger sparteine.

1.3.3 Spin Transition

As mentioned above, a key concern of the insertion mechanism is whether a spin transition between structures **3A** and **4** is feasible. Such “spin-forbidden” processes are fastest when the minimum of the initial state is crossed nearby by the other spin state, to allow metal-mediated spin-orbit coupling. Crossings of different spin-state surfaces are difficult to predict because of spin dependence of correlation energies and DFT functionals. However, the barrier can be estimated by finding the minimum energy crossing point (MECP) between the surfaces, a methodology which Harvey and co-workers showed to adequately model spin crossings in organometallic systems [20, 21].

We implemented a methodology similar to that used by Harvey to obtain an approximate crossing point. Singlet calculations established that the singlet surface is not accessible prior to **3A**. However, optimization of the singlet starting from the **3A_{bipy}** triplet geometry led to structure **4_{bipy}**, a significantly more stable structure, with the resulting triplet/singlet gap of –18.4 kcal/mol, implying spin crossover between **3A_{bipy}**

and **4_{bipy}**. The vertical singlet/triplet gap⁴ for **3A_{bipy}** was calculated to be 9.5 kcal/mol. While too high for a facile crossover, this indicates that **3A_{bipy}** and **4_{bipy}** must have significantly different geometries since relaxation yields 27.9 kcal/mol. Inspection of the triplet **3A_{bipy}** and the singlet **4_{bipy}** suggested that the major geometric difference between the two is the torsion angle Cl-Pd-O-O, which goes from 0° in **3A_{bipy}** to 74.9° in **4_{bipy}**.

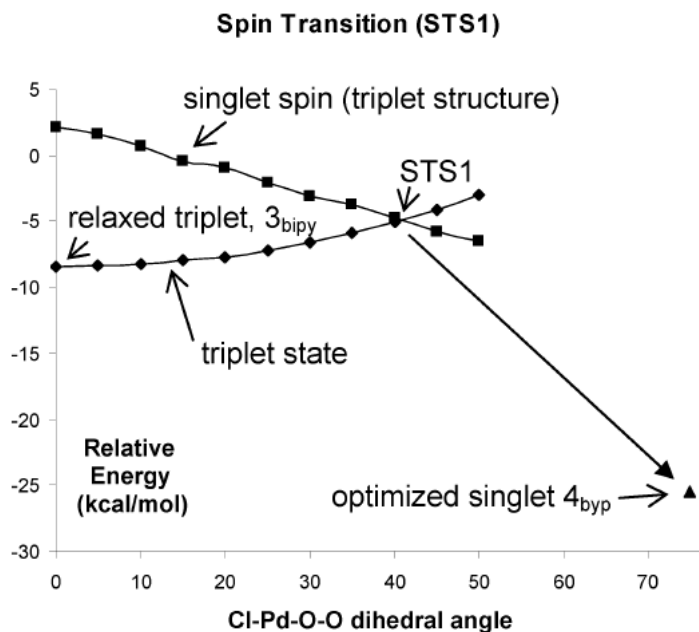


Figure 1.5. Triplet-singlet spin transition, approximated by varying the Cl-Pd-O-O torsion angle, θ , starting with the stable triplet species **3**, $\theta = 0^\circ$, until a structure was found in which the singlet and triplet spins had the same gas-phase energy, **STS1**, $\theta = \sim 41^\circ$. Singlet **STS1** was then allowed to relax to product and proceeded directly to species **4**, $\theta = 74.9^\circ$.

Consequently, a search for the MECP was undertaken by optimizing triplet structures of **3A_{bipy}**, where the Cl-Pd-O-O torsion angle was constrained at values ranging from the equilibrium position of 0° to larger values within the range of vibrational motion of the molecule (in this case up to 55°), while allowing the rest of the structure to relax. Starting with the $M_S = 1$ unrestricted triplet-state optimum geometries, we carried out single-point calculations for $M_S = 0$ by flipping the spin of one orbital and calculating self-

⁴ Vertical singlet-triplet gap: the difference in energy between the singlet and triplet wave functions with the same geometry.

consistently. This led to S^2 ranging from 0.000 to 0.020, demonstrating that spin contamination is quite small. We consider these states to accurately describe points on the singlet potential energy surface (Figure 1.5).

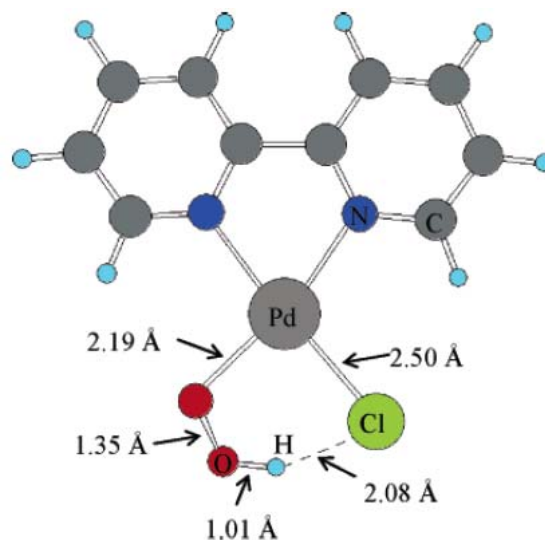


Figure 1.6. Spin transition-state structure (STS1) for spin conversion from triplet to singlet. Here the Cl-Pd-O-O torsion angle is $\sim 41^\circ$.

Through this process an intersection was found (Figure 1.6) with Cl-Pd-O-O torsional angle of $\sim 41^\circ$ and an energy 3.6 kcal/mol higher than that of the stable triplet species in the gas phase. In this crossing point the Pd-O bond length of 2.19 Å, the O-O bond distance of 1.35 Å, the H-Cl hydrogen-bonding distance of 2.08 Å, and the O-H bond distance of 1.01 Å are all very similar to those of **3A_{bipy}**. The only considerable structural differences between this structure and **3A_{bipy}** are the Cl-Pd-O-O and Pd-O-O-H torsional angles, and the spin transition point is thus accessible through the vibrational motion of **3A_{bipy}**.

1.3.4 Role of Hydrogen Bonding

One remaining concern was the possibility that **TS1** did not connect complex **2** with triplet species **3A**. It is not obvious how breaking of the Pd-H bond by O₂ results in the formation of the Pd-O-O-H system, and visual inspection of the imaginary frequency

showed only a motion of the hydride along the Pd-H-O axis. Intrinsic reaction coordinate calculations from TS1 were unsuccessful, due to the flatness of the hypersurface. Instead we elected to follow the relaxation of the geometry shortly after the transition state. **TS1_{bipy}** was moved slightly along the reaction pathway toward product (the Pd-H bond distance was stretched 0.07 Å from **TS1_{bipy}**) and then allowed to fully relax. Figure 2.7 shows the progression of the relaxation from the nudged transition state **A** to product **E**, which corresponds exactly with species **3A_{bipy}**. Structure **A** is identical to **TS1_{bipy}** except for the elongated Pd-H bond; structure **B** exhibits further elongation of the Pd-H distance resulting in the formation of two distinct species, HO₂• and a Pd^I T-complex; structure **C** shows the HO₂• moving toward the Cl ligand and forming an H-bond; structure **D** shows the HO₂• rotating in order to bring the Pd and O closer together while maintaining the H-bond; finally, structure **E** shows the formation of the Pd-O bond and the formation of the triplet product. This progression demonstrates that the hydrogen bonding which is important for stabilization of **3A** is also important for the formation of **3A** from **TS1**.

Since relaxation from the transition state is not conclusive proof of an uninterrupted pathway, we also elected to investigate the mechanism of a non-hydrogen-bonding analogue, (bipy)Pd(CH₃)(H) (see Figure 1.8). When the transition state in this case is nudged toward products and relaxed, as discussed above, the -CH₃ species does not proceed to the expected product **3A_{bipy}-CH₃**, but instead forms complex **3B_{bipy}-CH₃**, at 12.8 kcal/mol. **3B_{bipy}-CH₃** can be described as a Pd^I T-complex with unpaired spin in the orbital formerly covalently bonded to the hydride, while the hydrogen in the HO₂• radical is coordinating to the same orbital in an agostic fashion. Control calculations of a (bipy)Pd(Cl)(OOH) triplet complex with the starting coordinates of the Pd^I-HOO• moiety taken from **3B_{bipy}-CH₃** again optimized to **3A_{bipy}-Cl**, reinforcing our belief that an intermediate **3B_{bipy}-Cl** is not part of the mechanistic pathway.

Having concluded that eliminating the possibility of internal hydrogen bonding changes the mechanism for hydrogen abstraction, we also elected to determine what effect this has for the overall mechanism. A transition state for the conversion of

$3\mathbf{B}_{\text{bipy}}\text{-CH}_3$ to $3\mathbf{A}_{\text{bipy}}\text{-CH}_3$ was not located, but an upper bound for this process is the infinite dissociation of the Pd^{I} and $\bullet\text{OOH}$ radicals, calculated to be 19.0 kcal/mol, from $1_{\text{bipy}}\text{-CH}_3$.

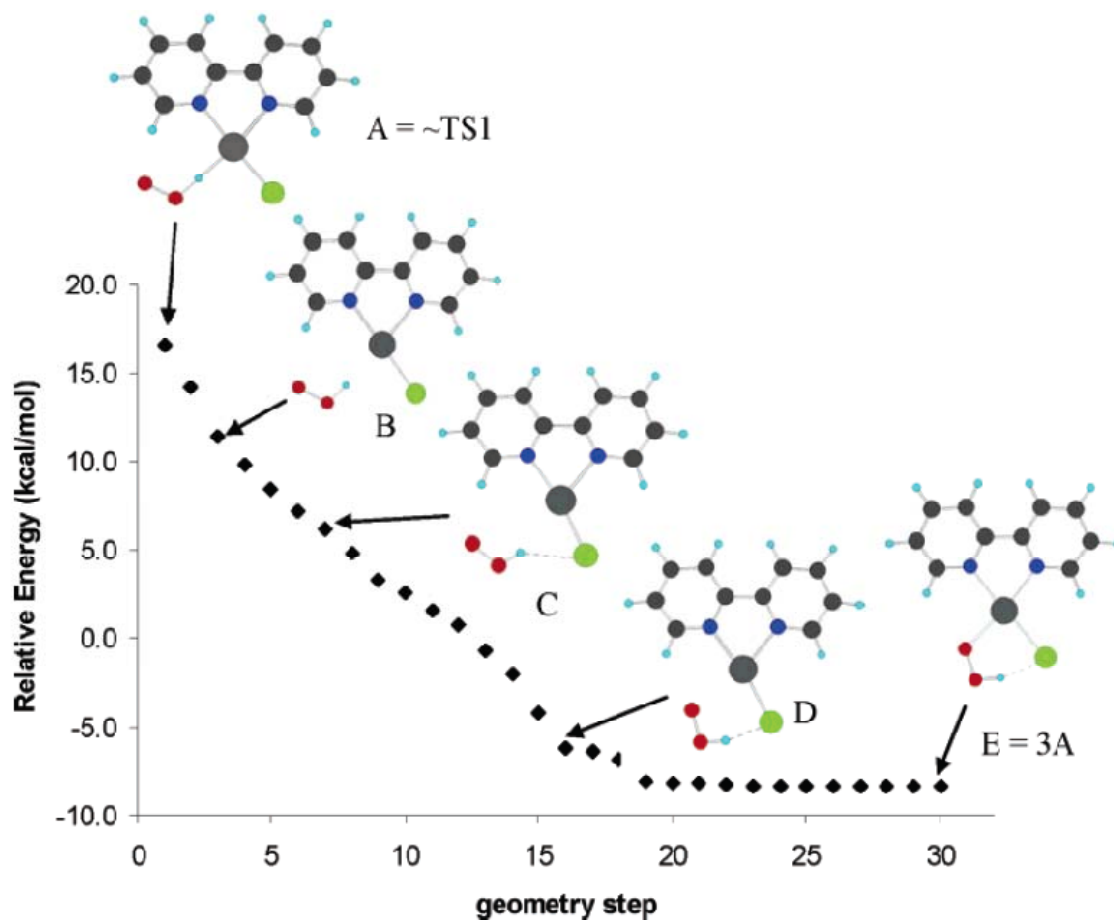


Figure 1.7. Energetics of the transition-state relaxation reaction pathway from the transition state $\text{TS}1_{\text{bipy}}$ ($\sim \mathbf{A}$) to the stable triplet $3\mathbf{A}_{\text{bipy}}$ (\mathbf{E}).

However, whether $3\mathbf{B}_{\text{bipy}}\text{-CH}_3$ can convert to $3\mathbf{A}_{\text{bipy}}\text{-CH}_3$ appears to be a moot point. $3\mathbf{A}_{\text{bipy}}\text{-CH}_3$ is surprisingly high in energy, 12.0 kcal/mol higher than $1_{\text{bipy}}\text{-CH}_3$. This is in contrast to $3\mathbf{A}_{\text{bipy}}\text{-Cl}$, which is 8.4 kcal/mol lower in energy than $1_{\text{bipy}}\text{-Cl}$. The difference of ~ 20 kcal/mol is too large to be solely attributed to the lack of hydrogen bonding,

estimated at 8–10 kcal/mol. The remaining energy change is most likely caused by the increased σ -donor ability of the $-\text{CH}_3$ substituent, which destabilizes the relatively electron-rich Pd^{I} complex. Moreover, the increased energy of the $3\text{A}_{\text{bipy}}\text{-CH}_3$ triplet pushes it above the $3\text{A}_{\text{bipy}}\text{-CH}_3$ singlet, thus causing the spin transition to be inaccessible at this point. Furthermore, since the singlet becomes significantly more stable than the triplet as the mechanism progresses, it is our belief that for this case to proceed through an O_2 insertion, the spin transition must occur earlier in the mechanism.

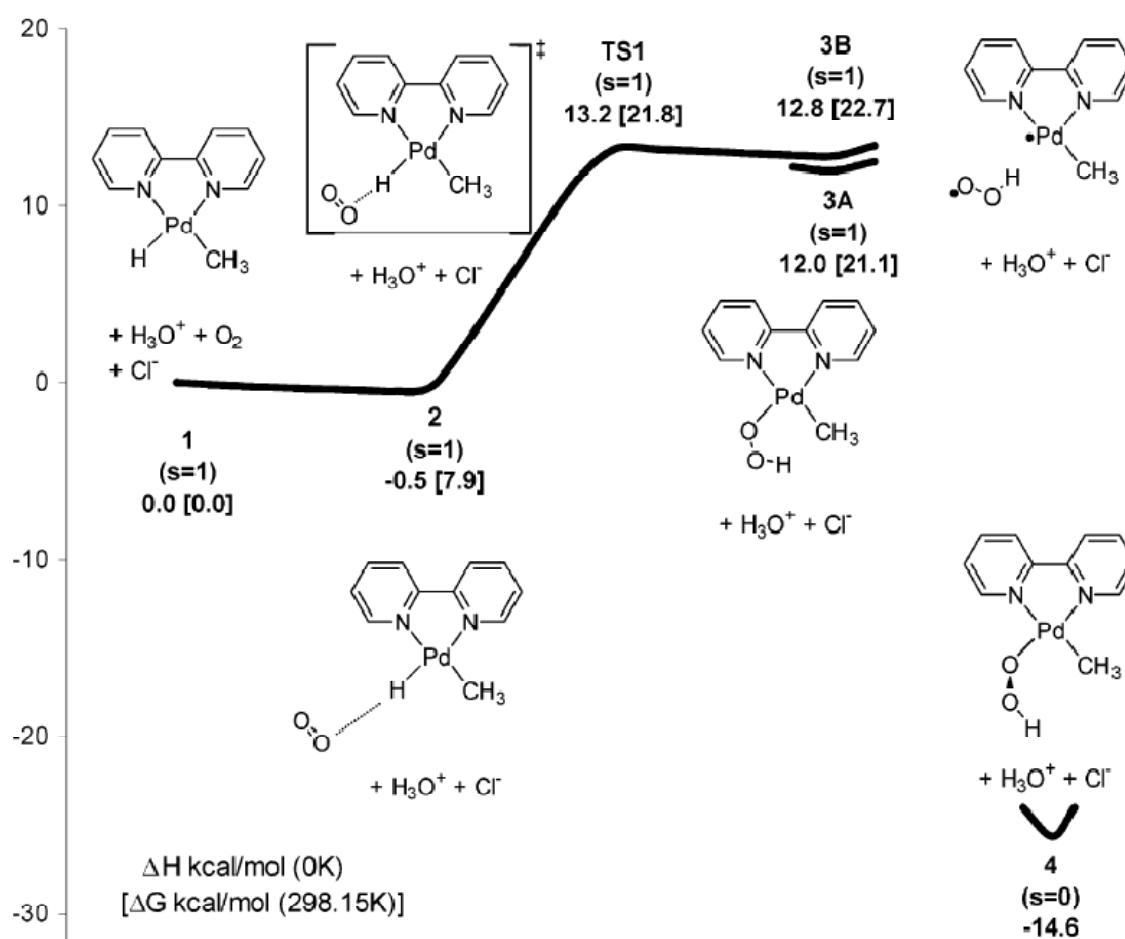


Figure 1.8. Calculated mechanism for O_2 insertion in $\text{Pd}(\text{bipy})(\text{H})(\text{CH}_3)$ in toluene

Indeed, calculations show that the relative energy of the $3\text{B}_{\text{bipy}}\text{-CH}_3$ singlet is 13.2 kcal/mol, i.e., within the margin of error identical to the $3\text{B}_{\text{bipy}}\text{-CH}_3$ triplet. This is not

unexpected, since the two unpaired spins in **3B_{bipy}-CH₃** are essentially disconnected. Even so, the strong spin-orbit coupling of the Pd atom should facilitate the spin crossing, and we do not expect the barrier to be prohibitively high. Conversion of the **3B_{bipy}-CH₃** singlet to **4_{bipy}-CH₃** should occur via a mechanism similar to the conversion of triplet **3B** → **3A**, and thus has an upper bound barrier of 19.0 kcal/mol. With a barrier to activation between 13.2 and 19.0 kcal/mol, the reaction is expected to be feasible, but significantly slower than the analogous reaction with the -Cl species.

Further insight into the H-bonding effects is obtained by comparison of structures **1**, **2**, **TS1**, **3**, and **4** with a variety of ligands of varying electronic properties (Table 1.1). It can easily be seen that as the X-ligand's ability to accept a hydrogen bond is reduced and then completely eliminated through the substitution from ligands such as OAc, Cl, and I to ligands like CN, CF₃, and finally CH₃; the energy of **3A** is increased with respect to all the other species.

ligand	X-group	1	2	TS1	3A	3B	4
spar	Cl	0	-0.8	10.6	-9.3	N/A ^a	-24.3
		[0.0]	[6.5]	[19.1]	[0.6]		[-13.7]
bipy	OAc	0	-0.6	10.4	-14.0	N/A ^a	-30.0
		[0.0]	[6.1]	[19.0]	[5.3]		[-18.7]
bipy	Cl	0	-0.4	11.5	-8.4	N/A ^a	-26.8
		[0.0]	[6.5]	[20.1]	[1.0]		[-22.7]
bipy	I	0	-0.7	12.3	-4.6	N/A ^a	-24.6
		[0.0]	[6.5]	[20.5]	[4.9]		[-13.7]
bipy	CN	0	-0.6	13.5	3.0	N/A ^a	-23.4
		[0.0]	[6.5]	[22.3]	[12.1]		[-12.8]
bipy	CF ₃	0	-0.5	13.5	7.0	N/A ^a	-26.0
		[0.0]	[5.5]	[21.0]	[14.5]		[-14.7]
bipy	CH ₃	0	-0.5	13.2	12.0	12.8	-25.6
		[0.0]	[7.9]	[21.8]	[21.1]	[22.7]	[-14.6]

Table 1.1. ΔH [ΔG] (kcal/mol) values for intermediates and transition states of the various systems studied. ^a Unstable with respect to **3A**

1.3.5 Comparison of Computational Methodologies

To ensure that the results described here are not artifacts caused by the particular methodology employed, we optimized the geometries of **1**, **2**, **TS1**, **3**, and **4** using B3LYP with a triple- ζ basis set (LACV3P**++) as well as two other density functionals (BLYP and BP86). The results are summarized in Table 1.2, where it can be seen that the use of the larger basis set changes the energies very little. The largest change on the ΔH surface is for **1** \rightarrow **4**, which is exothermic by -26.8 kcal/mol using LACVP** and -24.5 kcal/mol using LACV3P**++. The changes on the ΔG surface mimic the changes on the ΔH surface and do not warrant further comment. The BLYP and BP86 surfaces correspond very closely to the B3LYP surface, with the exception of the transition state **TS1**. The calculated BLYP ΔH^\ddagger is 5.7 kcal/mol with respect to **1** and 7.6 kcal/mol with respect to **2**, while the BP86 ΔH^\ddagger is 4.6 and 5.0 kcal/mol, respectively. This is compared to the B3LYP ΔH^\ddagger , which is calculated to be 11.5 and 11.9 kcal/mol, respectively. The B3LYP barrier is roughly twice as high as the BLYP and BP86 barriers. However, it should be noted that BP86 is known to yield lower barriers than B3LYP, and there is some indication that the B3LYP barrier corresponds better to experimental values [22].

functional	basis set	1	2	TS1	3A	4
B3LYP	LACVP** ^a	0	-0.4	11.5	-8.4	-26.8
		[0.0]	[6.5]	[20.1]	[1.0]	[-16.0]
B3LYP	LACV3P**++	0	-0.1	11.9	-7.3	-24.5
		[0.0]	[4.5]	[20.5]	[0.4]	[-14.1]
BLYP	LACVP** ^a	0	-1.9	5.7	-9.3	-27.6
		[0.0]	[5.9]	[13.8]	[1.4]	[-17.1]
BP86	LACVP** ^a	0	-0.4	4.6	-9.5	-28.8
		[0.0]	[7.1]	[14.4]	[0.6]	[-18.3]

Table 1.2. Optimized ΔH [ΔG] (kcal/mol) values for intermediates and transition states of the various systems studied. ^a Diffuse functions added to chloride

1.4 Conclusions

A direct insertion of triplet O_2 into Pd^{II} hydride to form a final singlet state is accessible with certain limitations. The reaction proceeds through abstracting the hydrogen from palladium by O_2 , which in our case immediately forms a hydrogen bond with the neighboring X-type ligand. The H-bonded complex relaxes to a triplet Pd^I -OOH species, which subsequently undergoes a spin transition to the corresponding singlet Pd^{II} -OOH. This singlet species is then protonated, and hydrogen peroxide is replaced by another X-type ligand to complete the catalytic cycle. The limitations involved in the spin transition, the formation of the triplet Pd^I -OOH species, and the stability of that triplet species are all dependent on the presence of an H-bond acceptor *cis* to the hydride and the electronic characteristics of the other ligands which may or may not stabilize the Pd^I species. Without this *cis* H-bond acceptor and/or electron-withdrawing ligands that can stabilize Pd^I , the reaction will not proceed via the palladium hydride insertion mechanism. We are now building on these results to focus on evaluating the Pd^0 mechanisms (eqs. 1 and 2) using known catalysts in order to compare relative barriers in systems where the direct insertion mechanism is feasible.

Chapter 2

Activation of Molecular Oxygen by $[1,3-(\text{CH}_2\text{P}^t\text{Bu}_2)_2\text{-C}_6\text{H}_3]\text{PdH}$

2.1 Introduction

⁵The activation of molecular oxygen by transition metals, especially palladium, has been widely discussed in recent years. However, there are still numerous questions regarding the mechanism or mechanisms at play. The two current schools of thought focus on either a direct insertion of oxygen into a palladium-hydride bond or the interaction of oxygen with a palladium(0) complex. There is some indication that both mechanisms are feasible under varying conditions [5b–c, 23, 24], although support for the former mechanism was previously found only in our theoretical work⁶.

Recently, however, Goldberg and co-workers experimentally isolated a palladium-hydride species, $[1,3-(\text{CH}_2\text{P}^t\text{Bu}_2)_2\text{-C}_6\text{H}_3]\text{PdH}$, and tracked the progress of a reaction between this species and oxygen [24]. The results suggested that the reaction proceeds by the aforementioned palladium-hydride insertion mechanism and should thus be a direct counterpart to our earlier theoretical work⁶. Consequently, we performed a detailed

⁵ Reproduced with permission from *Inorg. Chem.* **2006**, *45*, 9631. Copyright 2006 American Chemical Society.

⁶ See Chapter 1.

theoretical examination of the mechanism involved. We demonstrate that an insertion mechanism not only is possible but also is the only plausible solution. We discuss differences and similarities between this system and our previously studied (sparteine)Pd(Cl)(H) system⁶.

2.2 Computational Methodology

All calculations were performed using B3LYP/LACVP** as implemented by the Jaguar 6.5 program package [25]. Implicit solvent effects for benzene were calculated with the Poisson-Boltzmann (PBF) continuum approximation [13], using the parameter $\epsilon = 2.284$ and solvent radius = 2.60 Å. 1,3-(CH₂PH₂)₂C₆H₃ (PCP) was also substituted for the 1,3-(CH₂P^tBu)₂C₆H₃ ligand. This methodology was found to be an adequate level of theory in our previous, more exhaustive, study of (sparteine)Pd(Cl)(H)⁶.

2.3 Results and Discussion

2.3.1 Pd-H Insertion

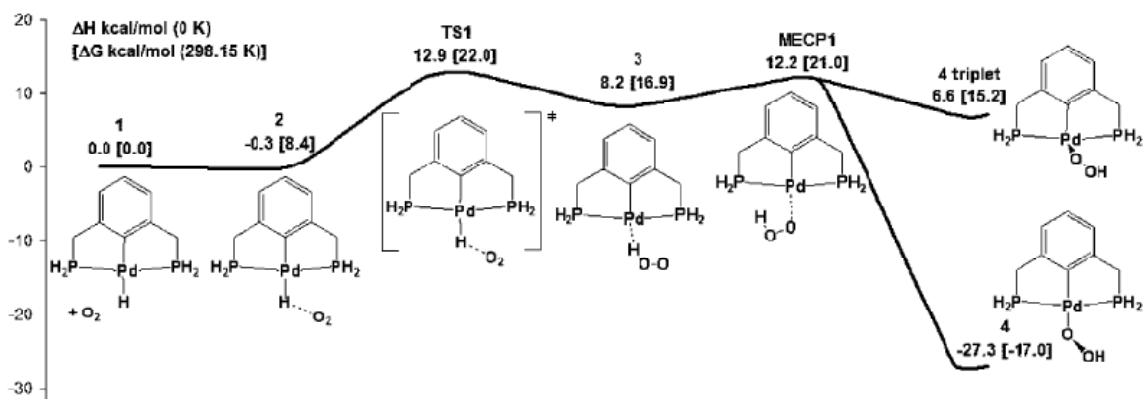


Figure 2.1. Calculated mechanism for oxygen insertion in (PCP)PdH in benzene. Energies are in kilocalories per mole (ΔH [ΔG]).

2.3.1.1 Mechanistic Pathway

As the starting point for the study, we chose [1,3-(CH₂-PH₂)₂C₆H₃]PdH (**1**; Figure 2.1), also abbreviated (PCP)PdH. Introduction of (triplet) molecular oxygen leads immediately to the formation of a weakly bound van der Waals complex [(PCP)PdH]•O₂ (**2**), with $\Delta H = -0.3$ kcal/mol, where the O₂ is coordinating to the hydride in the plane (forming pseudo-*C_s* symmetry) and not to the metal. All attempts at finding a starting point where the O₂ coordinates directly to the metal failed, instead collapsing to **1** and free O₂ or to complex **2**. This is similar to our findings for (sparteine)Pd(Cl)(H)⁶ and is most likely due to repulsion between the electron-rich oxygens and the filled d orbitals on the metal.

Electron transfer in **2** is negligible between the oxygen and the palladium complex (Mulliken charges on the two oxygens change from 0 and 0 to 0.02 and 0.01 electrons, while the palladium gains 0.03 electrons). Spin analysis demonstrates that all unpaired spins reside on the oxygen (one π orbital parallel to the plane and one π orbital perpendicular to the plane).

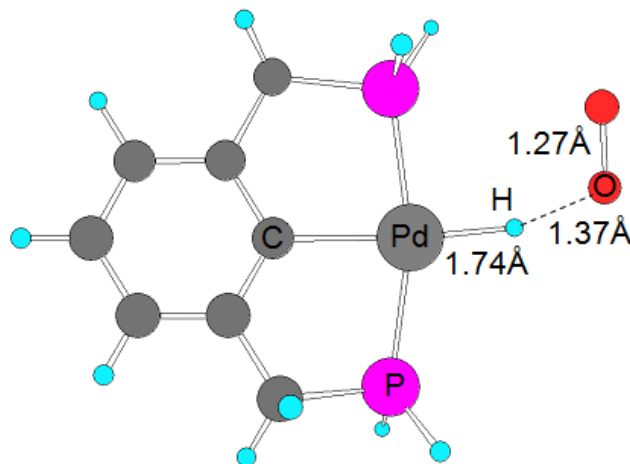


Figure 2.2. Transition-state structure for the hydrogen abstraction/oxygen insertion mechanism

From **2**, we explored the transition state for the oxygen insertion mechanism. The transition state, **TS1** (Figure 2.2), has triplet oxygen positioned to abstract the hydrogen from the palladium center with ΔH^\ddagger 12.9 kcal/mol. This results in a stretching of the Pd-H bond distance from 1.62 to 1.74 Å, while the O-O bond distance increases from 1.21 to 1.27 Å. The O-H distance of 1.37 Å (compared to 0.96 Å in HO₂) indicates that the O-H bond has not yet formed. The spin population for the oxygen moiety is ~ 0.75 electrons on each oxygen atom, while that for palladium and the adjacent carbon are 0.19 and 0.26 electrons, respectively.

The reaction proceeds from the transition state to form the triplet species **3**, which can be best described as a Pd^I T-complex with a closely associated HO₂ radical, with an overall $\Delta H = 8.2$ kcal/mol. The O-H bond length of 1.01 Å is similar to that of free HO₂, and the elongated Pd-H bond distance of 2.36 Å demonstrates the complete breaking of the Pd-H bond. Further analysis shows that one of the unpaired spins resides on the palladium in the orbital formerly bonded to hydrogen while the HO₂ fragment coordinates to the same orbital in an agostic fashion. **TS1** and **3** are almost planar; in both cases, the O-O moiety angles out of the (PCP)Pd plane by $\sim 5^\circ$. Calculations using bulkier substituents on the phosphorus ligand show more deviation from planarity, but we do not expect this to significantly alter the overall mechanism.

From species **3**, the reaction proceeds to the singlet (η^1 -hydroperoxo)palladium(II) product [**4**; (PCP)Pd-OOH] by rotation of the HO₂ fragment. ΔH for the formation of product) -27.3 kcal/mol. A triplet version of **4** is also possible, although higher in energy, and is thus expected to be short-lived. **4** is clearly a Pd^{II}OOH complex: the Pd-O bond distance of 2.04 Å is consistent with those of similar species⁶, while the O-O bond distance of 1.47 Å is what would be expected for a normal O-O single bond. The O-H bond distance of 0.97 Å is comparable to that in H₂O₂. It should also be noted that the calculated bond lengths are in close agreement with the bond lengths in the crystal structure from ref [24a] [Pd-O = 2.074(3) Å and O-O = 1.470(4) Å].

2.3.1.2 Spin Conversion

We used the method of Harvey and co-workers [20, 26] to compute the minimum energy crossing point structure (**MECP1**) between the singlet and triplet potential energy surfaces close to structure **3**. This structure has an energy $\Delta H = 12.2$ kcal/mol, and its structure is quite similar to that of triplet **4**, although with a slight rotation out of the plane around the Pd-O axis. The fact that the energy of **MECP1** is only marginally higher than the energy of **3** suggests that **3** will repeatedly explore the parts of the potential energy surface that contain the MECP and make a spin-forbidden transition possible.

2.3.1.3 Radical Initiation

We also considered a dissociative process, where the (PCP)Pd and OOH moieties separate in the solution to isolated radical species. Reassociation with a radical of the appropriate spin could then generate the singlet **4** without a formally forbidden spin crossing. Our calculations show that this dissociative process is less favorable than the concerted process on the ΔH surface, with a calculated ΔH of 13.1 kcal/mol, but more favorable on the ΔG surface, with a calculated ΔG of 11.1 kcal/mol. However, the accuracy of these solution-phase ΔG calculations is uncertain, and we thus cannot for sure state which mechanism is preferred.

2.3.2 Pd⁰ Pathways

While the above results show the viability of the direct insertion, various possible palladium(0) pathways should also be excluded. The tridentate ligand employed in this process excludes the commonly proposed square-planar η^2 -O₂ complex without manipulation of the PCP backbone. However, two viable candidates were considered, assuming various possible ligand deformations (**5** and **6**; Figure 3.3). **5** is simply the product of an intramolecular reductive elimination of the hydride with the adjacent phosphorus moiety. This species was not found despite numerous attempts, all of which

instead collapsed to either species **1**, **7**, or **8**. No mechanisms through **7** and **8** were pursued because both are too high in energy (19.6 and 17.5 kcal/mol greater than **1**).

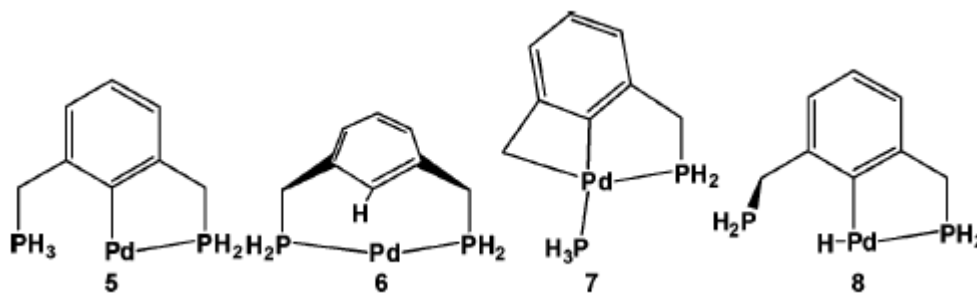


Figure 2.3. Possible candidates examined along the hypothetical palladium-(0) pathway

6, on the other hand, is a stable linear palladium(0) species with $\Delta H = -14.7$ kcal/mol. Despite the favorable energetics, **6** has two main problems: (1) The linear nature of the bonding does not allow for bonding of O_2 in an η^2 fashion. (2) Examination of the surrounding surface did not demonstrate a feasible barrier from **1** to **6**. Furthermore, because **6** is so much lower in energy than **1**, this should be the resting state of the catalyst if a low-energy mechanism for interconversion exists. Because the resting state of this (PCP)-PdH complex is experimentally known to be species **1**, this indicates that no such mechanism exists, and **6** is thus not considered to be a viable intermediate.

2.3.3 Comparison to Previous Results with (Spar)PdHCl

These results are in contrast to our previous study of (sparteine)Pd(Cl)(H), where the possibility of palladium(0) pathways are not yet excluded. Indeed, preliminary studies suggest that palladium(0) pathways are competitive for the same system in coordinating solvents. Nevertheless, these palladium(0) pathways are not viable for the current system because the PCP ligand seemingly prevents the formation of palladium(0).

The current direct insertion mechanism is, however, in the initial aspects similar to the insertion mechanism we previously described for an analogue Pd(sparteine) system without

a hydrogen-bonding X-type ligand⁶. Indeed, **TS1** is almost identical with the corresponding transition state in the (sparteine)PdHCH₃ system, both energetically (12.9 and 13.2 kcal/mol, respectively) and geometrically (Pd-H 1.74 and 1.72 Å, O-H 1.37 and 1.27 Å, and O-O 1.27 and 1.28 Å, respectively). Conversely, while the hydrogen-abstraction transition states are similar, the resulting intermediate in the present case is lower with $\Delta H = 8.2$ kcal/mol, compared to 12.5 kcal/mol for the previous case. Similarly, the dissociation energy of the HO₂ radical (which we believed to be energetically prohibitive to the process in the previous study) is lowered from 19.0 to 13.0 kcal/mol, allowing the reaction to proceed without excessive barriers.

2.3.4 Kinetic Isotope Effect

In addition to the correlation between the Pd(sparteine) and the Goldberg system, we also examined the kinetic isotope effect (KIE) present when the hydrogen atom attached to palladium is switched to a deuterium atom. For **TS1**, we calculate a classical KIE value of 2.49. To correct for tunneling, this should be multiplied by an additional transmission coefficient, which we estimate as 5.2, based on a one-dimensional parabolic approximation of the potential barrier outlined by Skodje and Truhlar [27]. The total KIE (12.9), while off by a factor of 2 if we assume our classical KIE is correct, is still in fair agreement with Goldberg's reported KIE of 5.8. Indeed, our results thus validate the suggestion by Goldberg and co-workers that tunneling makes an important contribution to the total KIE (they postulate that the classical part of the measured KIE should be < 3.3) [24a].

We also explored the possibility of **MECP1** being the rate determining step. The corresponding KIE should be [28]

$$\kappa = \frac{\kappa(\mathbf{TS1}) \kappa(\mathbf{MECP})}{\kappa(-\mathbf{TS1})}$$

While we cannot at this point calculate the tunneling contribution from **MECP1**, the calculated classical KIE values are $\kappa(\mathbf{TS1}) = 2.49$, $\kappa(\mathbf{MECP1}) = 0.75$ (as both singlet and

triplet), and $\kappa(-\text{TS1}) = 7.46$. The calculated κ for this case is 0.25, i.e., an inverse effect. While it is technically possible that the tunneling contribution could alter this value to the observed KIE of 5.8, it would require a tunneling coefficient for the MEC1 of 23.2, which is unrealistic. Also, calculations of the equilibrium isotope effect of the isolated radicals described above show a similar ratio (0.38). Consequently, we believe the possibility of the spin crossing being the rate-determining step can be ruled out.

2.4 Conclusions

In conclusion, a direct insertion of triplet O_2 into a specific Pd-H bond to form a (η^1 -hydroperoxo)palladium(II) species has been established. The mechanism starts with abstraction of a hydrogen atom by molecular oxygen, which then forms a $\text{Pd}^{\text{I}}/\text{HO}_2$ radical pair. The HO_2 moiety rotates and flips the spins, resulting in the product hydroperoxo species. It is not clear whether this occurs through a concerted or dissociative mechanism. The calculated mechanism presented here agrees with the experimental evidence put forward by Goldberg and co-workers and supports our previous hypothesis that this type of insertion mechanism is both possible and in some cases the only viable process.

Chapter 3

Activation of Molecular Oxygen by ((-)-Sparteine)PdHCl: Pd⁰

3.1 Introduction

⁷Palladium catalysis enables a broad spectrum of selective oxidation reactions of organic substrates, frequently employing molecular oxygen as the stoichiometric oxidant [4a, 23, 30]. Oxygen is the ideal oxidant for green chemistry, as it is inexpensive, abundant, noncorrosive, and environmentally benign. Thus, enabling the use of molecular oxygen is highly desirable. Indeed, significant effort has been devoted to this goal, and Pd/O₂ systems have been developed for selective oxidation of alcohols [1b, 1e, 31], intermolecular oxidative amination of alkenes [32], oxidative C-C bond cleavage in tertiary alcohols [33], intermolecular heterocyclization of alkenes [34], and the synthesis of hydrogen peroxide [35]. Nevertheless, the subset of oxygen-utilizing Pd systems constitute only a fraction of the important reactions involving Pd systems, leaving a vast pool of potential reactions where use of oxygen as the oxidant would be most valuable [4a, 23, 30].

The palladium-catalyzed oxidations mentioned above are believed to proceed through an “oxidase” pathway, in which oxidation of the substrate by the palladium species occurs

⁷ Reproduced with permission from *J. Am. Chem. Soc.* **2007**, *129*, 10361. Copyright 2007 American Chemical Society.

first, followed by reoxidation of palladium by O_2 [23, 30a]. However, the details of this reoxidation are not clear, which significantly hampers the rational design of further uses. Consequently, much work has been performed in an effort to ascertain the mechanism or mechanisms involved, including the necessary spin conversion from triplet to singlet [4a, 5b–c, 23, 24, 30, 36–38]^{8,9}.

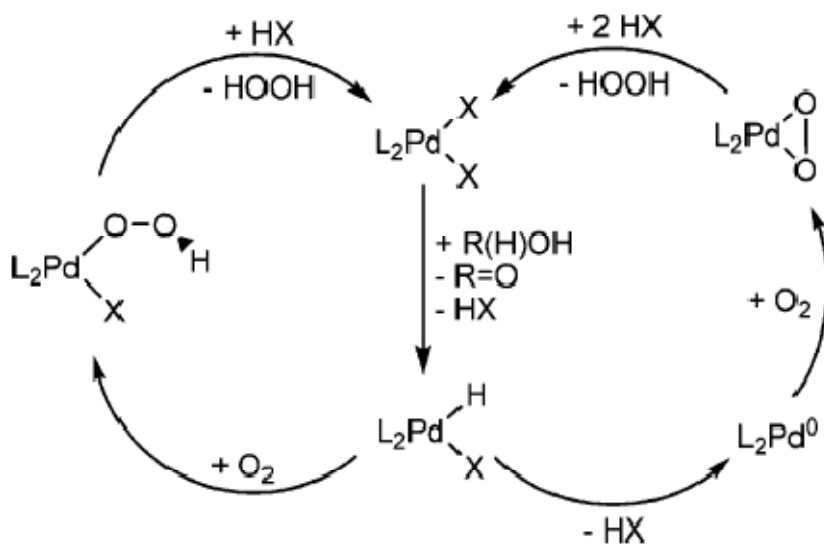


Figure 3.1. Competing Pathways for the Catalytic Cycle of Palladium-Catalyzed Oxidation of Alcohols

Two competing pathways for the reoxidation step are currently receiving considerable attention in the literature (Figure 3.1) [4a, 5b–c, 23, 24, 30, 36–38]^{8,9}. The first involves the formation of Pd^0 through the reductive elimination of HX followed by reaction with O_2 to form an η^2 -peroxo species (Figure 3.1, right side), whereas the other involves the direct insertion of O_2 into a Pd^{II} hydride (Figure 3.1, left side). In particular, several experimental studies on the direct reaction of Pd^0 with O_2 have been reported, demonstrating both the formation of a stable η^2 -peroxo Pd^{II} complex (see Figure 3.1, right) and the eventual products hydrogen peroxide and $Pd^{II}X_2$, after treatment with HX [5b–c, 36–37]. Although

⁸ See Chapter 1.

⁹ See Chapter 2.

this is not conclusive proof, it demonstrates the feasibility of the Pd^0 pathway under select conditions. In addition to the experimental work, Landis and co-workers used density functional theory (DFT) to examine the feasibility of a spin crossover for several Pd^0 systems and showed that after the triplet Pd^{I} -superoxide complex is formed, the pathway to the singlet Pd^{II} -peroxo complex is significantly downhill, making the barrier for the spin-crossing practically negligible [37].

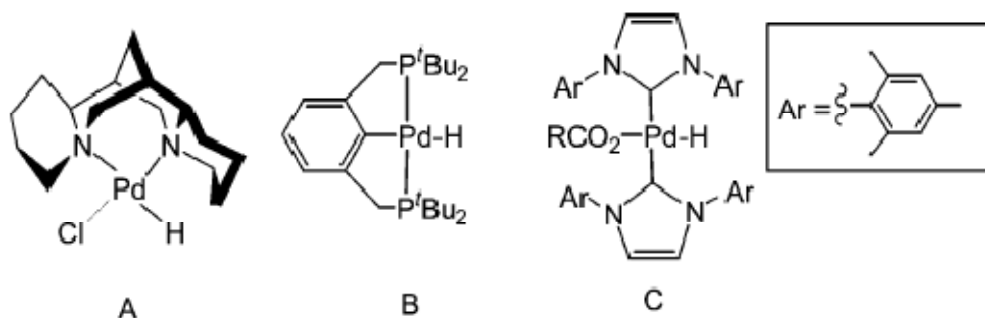


Figure 3.2. Pd species recently examined in the $\text{Pd}^0/\text{Pd-H}$ insertion debate

Studies on the direct insertion have been less common. Our group reported DFT studies on a $\text{Pd}(\text{sparteine})$ system used in enantioselective oxidation of alcohols, where the direct insertion is calculated to be feasible (Figure 3.2, species **A**)⁸. The insertion mechanism reported therein proceeds through the abstraction of a hydrogen atom by oxygen to form a Pd^{I} radical T-complex and $\text{HOO}\cdot$ which subsequently leads to the formation of triplet palladium hydroperoxo species. After undergoing a spin-flip to form the singlet hydroperoxo species the reaction proceeds through the addition of a proton to form H_2O_2 and the corresponding PdCl_2 . We concluded that the re-formation of the two radical species and the existence of the *cis* hydrogen bond acceptor were intimately correlated and removal of the *cis* hydrogen bond acceptor substantially increased the reaction barrier as the radical pair must first undergo a spin conversion before directly forming the singlet hydroperoxo species en route to completing the catalytic cycle. In addition, Privalov et al. conducted investigations on a chelating $\text{Pd}(\text{phenyl-pyridine})\text{-(H)(pyridine)}$ complex and concluded

that direct insertion after O₂ complexation to Pd^{II} was a feasible mechanism for this system [38].

One of the problems associated with experimental explorations of the direct insertion mechanism is the possibility that a stable palladium hydride could reductively eliminate under reaction conditions, preventing the evaluation of the direct insertion method. However, Denney et al. studied a Pd-H complex specifically designed not to allow reductive elimination (Figure 3.2, species **B**) [24a]. Upon treatment with O₂, **B** is converted into the corresponding Pd-OOH species and thus experimentally verifies a direct insertion. Subsequently, a report by Konnick et al. appeared where O₂ reacts with the Pd-H complex **C**, forming the corresponding Pd-OOH species. The data presented suggests a reversible reductive elimination pathway, but Konnick et al. could not entirely rule out the possibility of a direct insertion mechanism [24b].

The mechanism of Denney et al.'s (PCP)Pd(H) + O₂ → (PCP)Pd(OOH) reaction was computationally explored by us and was found to react through a mechanism very similar to our previously studied Pd(sparteine) system⁹. However, our results also confirmed that the Pd⁰ mechanism is indeed not viable for this system, therefore shedding little light on the competition between the two pathways. Consequently, a study on a system where both pathways are potentially viable would be tremendously useful in understanding what factors enable these mechanisms. Thus, we are now complementing our previous work on the direct insertion with a study of the Pd⁰ pathways for Pd(sparteine). In particular, we are focusing on the formation of Pd⁰, the subsequent formation of η²-peroxo Pd^{II}, the spin-crossing from triplet to singlet, and the eventual formation of the corresponding Pd^{II}X₂ and H₂O₂ complexes. Herein we will present a detailed mechanistic view of this reaction mechanism. These new results, coupled with our previous work on the direct O₂ insertion mechanism on the identical system, provide a complete picture of both possible pathways and define the preferred path both for our system and those closely related.

3.2 Computational Methodology

All calculations were performed using the hybrid DFT functional B3LYP, as implemented by the Jaguar 6.5 program package [25]. This DFT functional utilizes the Becke three-parameter functional (B3) [7] combined with the correlation functional of Lee, Yang, and Parr (LYP) [8] and is known to produce good descriptions of reaction profiles for transition-metal-containing compounds [9, 10]. Pd was described with the LACVP** effective core potential and basis set (18 explicit electrons) [11]. All other elements were described including the core electrons, using the Pople 6-31G** basis set [12], but with 3s combination of the six d-like functions reduced to five.

All geometries were optimized and evaluated for the correct number of imaginary frequencies through vibrational frequency calculations using the analytic Hessian. Zero imaginary frequencies correspond to a local minimum, whereas one imaginary frequency corresponds to a transition structure.

Implicit solvent effects were calculated with the Poisson-Boltzmann (PBF) continuum approximation [13], using the parameters $\epsilon = 2.38$ and solvent radius = 2.76 Å. Here we use the solvent accessible surface of the molecular complex built using standard vdW radii. The solvation effects were calculated at geometries optimized for the gas phase.

Using the analytic Hessian we calculated the zero-point energy corrections at 0 K and added this to the solvation correction and the QM energy ($\Delta[E]$) to obtain the enthalpy at 0 K, $\Delta H[0 \text{ K}]$. Similarly, the vibrational frequencies were used to calculate the entropy and enthalpy corrections to 298.15 K, to obtain $(\Delta H - T\Delta S) = \Delta G[298.15 \text{ K}]$.

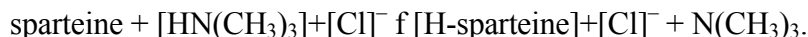
On the basis of previous results we expect that relative energies on the $\Delta H[0 \text{ K}]$ surface are accurate to ~ 3 kcal/mol for stable intermediates and to ~ 5 kcal/mol for transition structures. Probably the relative energies on the $\Delta G[298 \text{ K}]$ surface are less accurate, due to the use of the PBF model [14]. This methodology was found to be at an adequate level of

theory in our previous study of Pd(sparteine)(Cl)(H) when compared to various other functionals and basis sets⁸.

DFT is formulated in terms of Slater determinants built from Kohn-Sham orbitals that are calculated self-consistently. This process is consistent for states that are well described with closed-shell orbitals (up and down spins in the same orbitals), the normal situation for most DFT applications. However, in the studies carried out here it was necessary to start with a triplet state. With DFT this is done by having two more spin orbitals with up spin than down spin (unrestricted DFT or UDFT). We refer to this as the triplet state, but it need not be an eigenstate of the spin operator, S^2 . Rather, it is an eigenfunction of S_z , leading to $M_s = 1$. The problem with this formulation occurs when considering a transition between triplet and singlet states, a topic of this paper. Thus, starting with the true triplet orbitals of O_2 and calculating the energy of the singlet state should lead to a component of $^1\Delta_g$ with an excitation energy of 22.5 kcal/mol. In fact, UDFT gives an excitation energy of 10.5 kcal/mol. The reason is that the $M_s = 0$ wavefunction we consider to describe the singlet state also has a mixture of triplet character. This can be treated by applying the spin projection operator, which will lead to a rigorous energy for the singlet-triplet splitting (20.5 kcal/mol) [15a] but neither the orbitals nor the geometry are optimum after spin projection. Bally and Borden has suggested simply doubling the calculated energy gap in order to approximate the true gap, which in this case yields an energy gap of 21.0 kcal/mol for O_2 [15b]. Thus, in the case of O_2 both methods produce similar results. All results reported here are UDFT.

In addition, we used the method of Harvey and co-workers [20, 26] to compute the minimum energy crossing point structure (MECP) between the singlet and triplet potential energy surfaces close to various structures in this study. This technique combines the energies and gradients of the singlet and triplet surfaces into effective gradients that can be followed to locate the position of the MECP structure.

Trimethylamine $[\text{N}(\text{CH}_3)_3]$ was used as a model base in place of an additional sparteine molecule, as this considerably cuts down on the computational cost of the calculations. To illustrate the result of this substitution we calculate a ΔH of -0.9 kcal/mol for the reaction



As a result, we expect our use of trimethylamine to impart an artificial increase in barrier heights for the base-assisted reactions, although only at a magnitude of ~ 1 kcal/mol. Sparteine could potentially present significant steric hindrance to the structures which could increase the energy in those cases. However, several species were examined to a limited extent with a full sparteine base, and we could find no case where the bulk of sparteine seriously impacted any of the pathways presented herein.

It should also be noted that the ligand employed in this study, (–)-sparteine, is one stereocenter removed from C_2 symmetry, and although enantiomerically pure it still presents the dilemma of doubling the number of isomers for most of the steps involved. We found the differences in energy and geometry to be negligible and chose to present only the pathway starting at the (–)-sparteine- $\text{Pd}^{\text{II}}(\text{H})(\text{Cl})$ species that corresponds with the favorable alcohol oxidation transition state from our previous study on the use of this catalyst in the selective oxidation of alcohols¹⁰.

In addition, it is relevant to explain that direct formation of Pd^0 during the alcohol oxidation is not feasible in this system. Although one might expect that the (spar)- $\text{Pd}(\text{Cl})(\text{OC}(\text{H})(\text{R})\text{R}')$ (alkoxide species) could undergo deprotonation by an exogenous base [leading to either $[(\text{spar})-\text{Pd}^0(\text{Cl})(\text{O}=\text{C}(\text{R})\text{R}')]^-$ or directly to $(\text{spar})-\text{Pd}^0(\eta^2-\text{O}=\text{C}(\text{R})\text{R}')$] as a corollary to the reactivity of a related N-heterocyclic carbene $\text{Pd}^{\text{II}}(\text{OAc})_2(\text{OH}_2)$ complex studied by Nielsen and Goddard [39] but that is not the case here. First, the Pd-H is significantly destabilized in the carbene system as compared to the sparteine system^{8,10} and the related pyridine system [39]. Second, formation of HCl or even

¹⁰ See Appendix.

$[\text{base-H}]^+[\text{Cl}]^-$ in the sparteine system is significantly less favorable than the formation of HOAc in the carbene system. Third, removal of the second proton/H atom from the bound alkoxide (either through deprotonation or β -hydride elimination) is known to be the enantioselective step, and in the case of the possible deprotonation, the activity in the transition state is too far away from the chiral portion of the catalysts to provide the enantioselectivity observed.

3.3 Results and Discussion

3.3.1 Base-Assisted Formation of Pd^0

3.3.1.1 Primary Pathway

Similar to our previous studies on this system, we chose κ^2 -(-)-sparteine- $\text{Pd}^{\text{II}}(\text{H})(\text{Cl})$ (**1**, Figure 3.3) as the starting point. Initially an attempt was made to examine the H-Cl reductive elimination pathway leading to a “naked” (-)-sparteine- Pd^0 and HCl, but this was determined to be energetically prohibitive¹¹. Instead, we elected to focus on a base-assisted deprotonation pathway. Under experimental condition an excess amount of sparteine is present and should, thus, be our first choice of an external base. However, sparteine is also quite large, and to reduce computational time, we elected to model sparteine with the significantly smaller trimethylamine $[\text{N}(\text{CH}_3)_3]$. Introduction of our model base to **1** resulted in the formation of a weakly bound van der Waals complex $[\kappa^2\text{-(spar)}\text{Pd}^{\text{II}}(\text{H})(\text{Cl})] \cdots \text{N}(\text{CH}_3)_3$ (**2**), with $\Delta H^\circ = -0.5$ kcal/mol. The trimethylamine remains significantly removed from the Pd species and does not appear to have any significant interaction (N-H distance is > 8.0 Å). There is negligible electron transfer between the base and the Pd complex (the Mulliken charges on the trimethylamine and the Pd and adjacent H do not change).

¹¹ See Section 4.3.2 for further discussion on this topic.

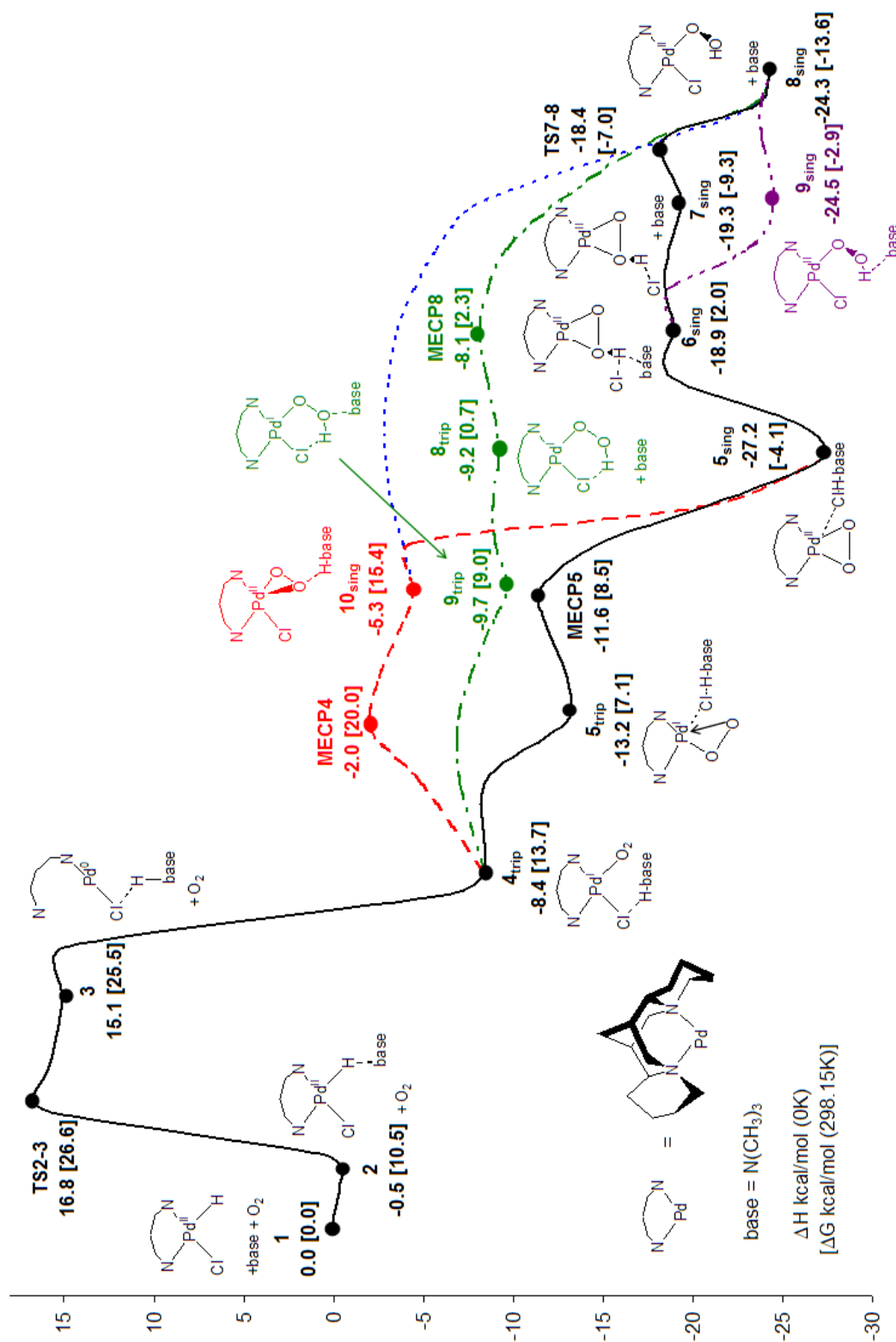


Figure 3.3. Calculated mechanism for the Pd^0 pathway for $\text{Pd}(\text{spar})(\text{H})(\text{Cl}) + \text{O}_2$ in toluene (base = trimethylamine). Intermediates are shown, while transition states (TSX-Y) are shown separately.

From **2** we found a deprotonation transition state, **TS2-3** (Figure 3.4), in which the base deprotonates the κ^2 -(spar)Pd^{II} complex resulting in the formation of a linear $[\kappa^1$ -(spar)Pd⁰-(Cl)]⁻[HN(CH₃)₃]⁺ ion pair, **3**. The ΔH^\ddagger for **TS2-3** is 16.8 kcal/mol. **TS2-3** is a fairly late transition state. The Pd-H distance has stretched from 1.52 to 2.40 Å, indicating that the Pd-H bond is completely broken, while the N-H distance has decreased from 8.29 to 1.08 Å, indicating that the N-H bond is fully formed. The imaginary frequency corresponds to a mode in which the proton transfers from the Pd to Cl while keeping the N-H bond intact, indicating the formation of a [(spar)Pd-Cl]⁻[HN(CH₃)₃]⁺ ion pair. Also of note is that the Pd-N (*cis* to Cl) distance has increased from 2.34 to 2.80 Å, indicating a loss of bonding, consistent with the hybridization of the available orbitals on a d¹⁰ Pd⁰ species. As a result of the change in formal oxidation state of the Pd, the Pd-N (*trans* to Cl) and Pd-Cl distances have both increased from 2.18 and 2.35 Å to 2.31 and 2.43 Å, respectively. Finally, the resulting Cl-H distance of 2.10 Å is consistent with that of a hydrogen bond.

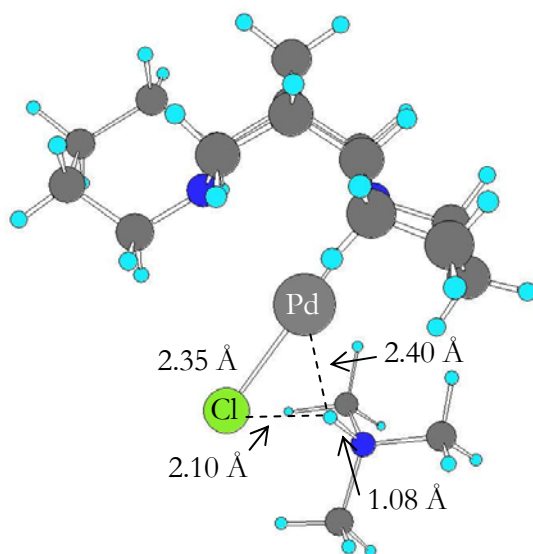


Figure 3.4. Detail view of **TS2-3**

From **TS2-3** the energy falls 1.7 kcal/mol when forming species **3**, a linear Pd⁰ complex very similar to the preceding transition state. Indeed, the only significant changes are the further stretching of the Pd-H distance (to 2.96 Å), the reduction of the Cl-H distance (to

1.84 Å), and movement of the $\text{HN}(\text{CH}_3)_3$ moiety out of the plane of the molecule spanned by the Pd, the Cl, and both N_{sparS} . Breaking the Pd-Cl bond followed by complete removal of the $\text{Cl}^-[\text{HN}(\text{CH}_3)_3]^+$ ion pair is energetically prohibitive (uphill 13.5 kcal/mol). It could, however, be accessible in related systems and will thus be discussed in detail in Section 3.2.

Instead of removing $\text{Cl}^-[\text{HN}(\text{CH}_3)_3]^+$, triplet oxygen was added to **3**. We could not isolate any unbound $\text{Pd}^0\text{-O}_2$ species, as all attempts immediately optimized to a four-coordinate triplet $[\kappa^2\text{-(spar)Pd}^{\text{I}}(\text{Cl})(\text{O}_2)]^+[\text{HN}(\text{CH}_3)_3]^+$ ion pair, **4_{trip}**, with a ΔH of -8.4 kcal/mol. The new Pd-O bond and the electron transfer to form Pd^{I} are the main factors governing the exothermicity of this step. In this species the two N_{sparS} , the Cl, and the bonding O of the end-on O_2 moiety all reside in a square plane. Spin analysis of complex **4_{trip}** shows a spin density of 1.16 electrons on the two oxygens (0.62 on the O α to Pd and 0.54 on the O β to Pd), a spin density of 0.67 electrons on the Pd atom, and the remaining spin density (0.17 electrons) distributed over the sparteine and $\text{Cl}^-[\text{HN}(\text{CH}_3)_3]^+$ ion pair, indicating that this complex should be considered a Pd^{I} species. The O-O bond of 1.32 Å is typical for a peroxy radical species (1.33 Å in free HO_2), halfway between common single- and double-bond distances of 1.48 and 1.21 Å, respectively. The Pd-N distances of 2.39 Å (*trans* to Cl) and 2.42 Å (*cis* to Cl) and the Pd-Cl distance of 2.69 Å are elongated compared to those of other Pd^{II} complexes, as expected for a Pd^{I} center. The new Pd-O and Cl-H bond lengths are 2.17 and 1.93 Å. The energy to break the ion pair at this point is 38.8 kcal/mol on the ΔH surface, and the protonated base will therefore remain associated with the complex until the Pd-Cl bond has been broken.

Species **4_{trip}** reacts further through an internal substitution step, in which a Pd-O-O three-membered ring is formed and the Pd-Cl bond is broken. This transition can be described as an intermolecular substitution that involves the simultaneous lengthening of the Pd-Cl bond and the shrinking of the P-O-O bond angle. The energy surface around species **4_{trip}** is quite flat, as made apparent by a scan of the Pd-Cl distance. The energy remains almost constant until the Pd-Cl bond is stretched to 3.8 Å ($\Delta\text{E} = -10.4$ kcal/mol), at

which point the structure relaxes to species **5_{trip}**. Several transition state calculations were attempted in this area with various starting conditions and geometries, all of which continually tested the surrounding area, maintained sufficiently small gradients, and showed virtually no energy fluctuation, yet all failed to converge to a stationary point. This is most likely a function of the flatness of the surface. Thus, as a result of this exhaustive search and the low energy of the apparent transition point we conclude that there is virtually no barrier for this process.

The new species, **5_{trip}**, has Pd-O distances of 2.10 and 2.47 Å and an O-O distance of 1.32 Å, forming an unsymmetrical three-membered ring. The Pd- distances are now 2.38 Å (*cis* to the Pd-O bond) and 2.25 Å (*trans* to Pd-O bond). The new Pd-Cl distance of 4.30 Å demonstrates that this bond has been completely broken. $[\text{Cl}]^-[\text{HN}(\text{CH}_3)_3]^+$ is, as expected, a bound ion pair (Cl-H distance of 1.84 Å), forming a van der Waals complex with the Pd(O₂) species. The spin densities have changed little from **4_{trip}** (0.62 electrons for Pd, 0.60 electrons for O closest to Pd, and 0.66 electrons for O furthest from Pd), implying that this is still a Pd^I species. The calculated ΔH for this complex is -13.2 kcal/mol. The complexation energy of the $[\text{Cl}]^-[\text{HN}(\text{CH}_3)_3]^+$ ion pair is calculated to be 4.4 kcal/mol (see species **12_{trip}** in Section 3.3.2.2), thus suggesting that while the ion pair could stay complexed throughout the mechanism, it is not particularly strongly bound. The effect of removing the ion pair is explored in Section 3.3.2.2.

Continuing along the preferred pathway, **5_{trip}** now relaxes to **5_{sing}** with a ΔH of -27.2 kcal/mol. The MECP for these two surfaces was first explored without the $[\text{Cl}]^-[\text{HN}(\text{CH}_3)_3]^+$ ion pair for computational expedience. (In addition to increasing the computational cost of the optimization, the complexed ion pair also introduces several small oscillating rotational modes that complicate the procedure.) Thus, the corresponding MECP sans ion pair (**MECP12** in Section 3.3.2) was first identified using the methodology by Harvey and co-workers outlined above and has a $\Delta H = -7.9$ kcal/mol. The geometry of the MECP was then frozen and the ion pair reintroduced, followed by an optimization of the ion pair next to the frozen MECP. This approximate MECP was found to have a ΔH of

–11.6 kcal/mol. The geometry of the crossing point is unsymmetrical with respect to the Pd-O-O ring structure, with Pd-O distances of 2.12 and 2.21 Å, the latter being halfway between that of **5_{sing}** (2.01 Å) and **5_{trip}** (2.47 Å), while the former has remained virtually unchanged from the triplet. Thus, the main nucleic motion associated with the state-crossing is the creation of a Pd-O single bond from the two previously unpaired electrons. Indeed, neither the O-O distance of 1.33 Å nor the Pd-N distances of 2.35 (*cis* to the close O) and 2.29 Å (*trans* to the close O) have changed noticeably from **5_{trip}**, which also demonstrates the close proximity of the MECF to the higher energy spin state. This low-energy crossing combined with significant spin-orbit coupling from Pd suggests that the barrier for this formally forbidden spin-flip should be small.

The MECF connects to the stable singlet Pd^{II} species **5_{sing}**. This complex is structurally similar to **5_{trip}**, although the Pd-O distances are now almost equivalent (2.01 and 2.02 Å) while the O-O distance is slightly elongated (1.39 Å). The Pd- distances have both decreased to 2.20 Å, consistent with the formation of a Pd^{II} species. Indeed, the calculated spin densities (employing an unrestricted wavefunction) on Pd and both O's are now all 0.0, as would be expected from closed-shell Pd^{II} species. The [Cl][–][HN(CH₃)₃]⁺ ion pair is still forming a van der Waals complex with the Pd species, with a complexation energy of 8.4 kcal/mol (see species **12_{sing}** in Section 3.3.2.2).

Next, the acidic proton from HN(CH₃)₃⁺ is passed to one of the two O's, forming species **6_{sing}** with a ΔH of –18.9 kcal/mol. Species **6_{sing}** can best be described as a palladium hydroperoxo species with the β-O also acting as a donor ligand, forming an unsymmetrical three-membered ring and with the hydrogen forming a hydrogen bond to the chloride ion. The O-H bond is orthogonal to the square plane, and the O-HCl bond angle is 158°. The Pd-O bond distances are 1.98 and 2.17 Å, consistent with one Pd-O covalent bond and one donor-acceptor bond similar to the short bond in species **5_{trip}**. The O-O bond distance of 1.41 Å is consistent with an O-O single bond. The O-H bond length of 1.04 Å is consistent with a single bond, and the H-Cl distance of 1.90 Å is consistent with a hydrogen bond. The Pd-N distances of 2.14 and 2.15 Å are still indicative of Pd^{II} complex. The base is still

in the calculation but is merely forming a van der Waals complex with the Pd species. Removal of the base results in species **7_{sing}**, which is structurally identical to **6_{sing}** except for the absence of the base. The complexation energy of the base is very low (0.4 kcal/mol), resulting in a ΔH of -19.3 kcal/mol for **7_{sing}**.

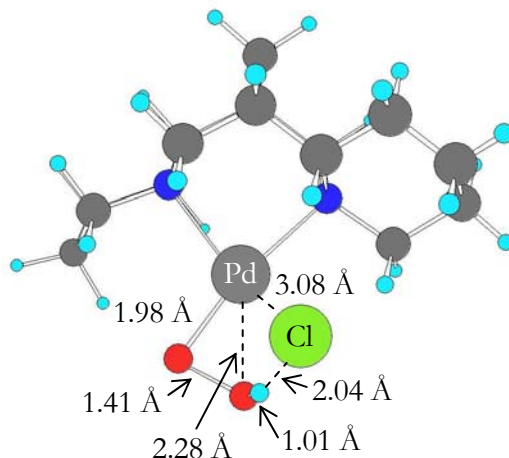


Figure 3.5. Detail view of **TS7-8**

From **7_{sing}**, the mechanism proceeds through a substitution where the Cl displaces the weakly bound O (referred to as the β -O above) forming a Pd(OOH)(Cl) species, **8_{sing}**, through transition state **TS7-8** (Figure 3.5). The ΔH^\ddagger for **TS7-8** is -18.4 kcal/mol, and it can be described as an associative substitution process in which the Cl approaches from out of the square plane ($\sim 45^\circ$) while the Pd-O(β) is dissociating. The Pd-O(β) distance has stretched from 2.17 to 2.28 Å, demonstrating that the Pd-O(β) coordination has not yet completely disappeared, while the Pd-O(α) and O-O distances are unchanged. The Pd-Cl distance has reduced from 3.37 to 3.08 Å but is still significantly longer than the Pd-Cl distance of 2.42 Å in **8_{sing}**, and the Cl still resides out of the plane. The O-H distance has decreased from 1.04 to 1.01 Å, while the H-Cl distance has increased from 1.89 to 2.04 Å, both consistent with the weakening of the H-bond. The Pd-N distances have remained at ~ 2.15 Å.

8_{sing} is a stable Pd^{II} hydroperoxo species with a ΔH of -24.3 kcal/mol. The Pd-O distance of 1.98 Å is consistent with a single bond. The O-O bond distance of 1.43 Å is slightly shorter than the corresponding distance of 1.48 Å in HOOH, while the O-H bond distance of 0.98 Å is almost identical. The Pd-N distances of 2.20 (*trans* to Cl) and 2.24 Å (*cis* to Cl) and Pd-Cl distance of 2.42 Å are also consistent with Pd^{II} complex. At this point we have merged with the pathway in our previous work on the direct O₂ insertion into a Pd-H bond⁸. The remaining steps to form (spar)PdCl₂ are described in detail in this previous report and will not be repeated here.

It should also be mentioned that Stahl et al. demonstrated that when HOAc or H₂SO₄ is added to a bathocuproine-Pd^{II}- η^2 -peroxo species it immediately reacts to form H₂O₂ and the corresponding PdX₂ [X₂ = (OAc)₂, SO₄] complex [7a]. This corresponds quite well with our calculated mechanism from **5_{sing}** to product.

3.3.1.2 Alternate Pathway Starting at **6_{sing}**

We also examined the effect of leaving the base complexed to species **6_{sing}** on the further mechanism. The dissociative substitution of the Cl to **6_{sing}** results in complex **9_{sing}** (structurally identical to **8_{sing}**, except for the van der Waals complexed base). ΔH for **9_{sing}** is -24.5 kcal/mol, and the complexation energy of the base is thus only 0.2 kcal/mol. Thus, it can be stated that the process from **6_{sing}** to **8_{sing}** can proceed first by the loss of complexed base followed by substitution of the chloride or vice versa with no relevant energy barriers.

3.3.1.3 Alternate Pathway Starting at **4_{trip}**

Although all feasible Pd⁰ pathways we found proceed through **TS2-3**, several competitive pathways exist between species **4_{sing}** and **8_{sing}** (Figure 3.3, dotted lines). The first obvious choice is to carry out the proton-transfer step immediately. The resulting species, **9_{trip}**, is significantly higher in energy than any of the other pathways discussed, although energetically similar to **4_{trip}** with ΔH of -9.7 kcal/mol. Upon removal of the base from the system ΔH changes only slightly to -9.2 kcal/mol, and the Pd structure, **8_{trip}**, remains the

same. At this point we have merged with the direct insertion pathway in our previous paper⁸, and we will not repeat the remaining steps to form (spar)PdCl₂ aside from an improved approximation of the barrier for spin crossover **MECP8**, ΔH) -8.1 kcal/mol, as a result of our improved methods concerning MECPs, as discussed in Section 3.2. Although this pathway ($4 \rightarrow 9$) does not seem to have prohibitively high barriers and is competitive with the previous pathway ($4 \rightarrow 5$), we believe it is less favorable due to the virtual lack of a barrier from **4_{trip}** to **5_{trip}** and the observation that the previous pathway remains lower in energy throughout the entirety of the mechanism.

Another alternate direction from species **4_{trip}** could be to reverse the ordering of the spin conversion and the intramolecular substitution. It should also be noted that before species **4_{trip}** the singlet-triplet splitting is too large to even consider the spin-flip (corresponding to the singlet-triplet separation for free O₂, as discussed in our preceding paper)⁸. The MECP of these two surfaces (designated **MECP4**) has a ΔH of -2.0 kcal/ mol. **MECP4** looks very similar to **4_{trip}**, and the only notable geometrical changes include a shortening of the Pd-O distance from 2.17 to 2.01 Å, a lengthening of the Pd-Cl distance from 2.60 to 2.69 Å, and a decrease in the Pd-O-O bond angle from 120.3° to 111.5°.

The hypothetical resulting species **4_{sing}** is not stable and immediately relaxes to form species **10_{sing}** with a ΔH of -5.3 kcal/mol. **10_{sing}** is similar to **4_{trip}** except that the O₂ species has now formed an unsymmetrical three-membered ring with the Pd perpendicular to the original square plane. The new Pd-O distances are 1.94 and 2.51 Å, while the Pd-Cl distance is 2.61 Å.

From species **10_{sing}** there are two pathways resulting in either **5_{sing}** or **8_{sing}**. In the former, the mechanism would proceed by breaking the Pd-Cl bond followed by relaxation of the Pd-O-O heterocycle. The latter would require the transfer of the proton from the base to one of the two O's, followed by relaxation of the hydroperoxo moiety. However, neither of the two transition states responsible for these mechanisms were explored, as they both occur after **MECP4** which is too high in energy to compete with the pathways which

proceed from **4_{trip}** to species **5_{trip}** and **9_{trip}**. That being said, we do expect both transition states to be energetically accessible based on their similarities to the transition between **4_{trip}** and **5_{trip}** and the transition from **5_{sing}** to **6_{sing}**, and it is thus not inconceivable that they could be favored in other catalytic systems.

3.3.2 Unassisted Formation of Pd⁰

3.3.2.1 “Naked” Pd⁰

In the literature, a Pd⁰ species that retains the bonding of the two donor ligands (in our case, the κ^2 -(–)-sparteine ligand) without any other inner-sphere interactions, or simply “naked”, is commonly invoked [5b–c, 23, 24b, 30a]. The proposals for this type of mechanism include reductive elimination transition states (which would coincide with the elimination of H-Cl in our system), while some studies have simply examined this type of Pd⁰ species as a possible intermediate along the catalytic pathway without concern for its origin [5b–c]. For instance, Stahl and coworkers synthesized a bathocuproine-Pd⁰ species as well as the corresponding bathocuproine-Pd^{II}-peroxo complex [5c]. Although this bathocuproine system has been shown to be a competent catalyst for the formation of H₂O₂ [35] there is no evidence that the catalytic cycle actually involves this Pd⁰ species. Showing that the Pd⁰ complex can access the catalytic cycle does not prove that Pd⁰ is accessed during the catalytic cycle, as it is possible that the synthesized Pd⁰ complex converts to the active catalyst prior to reaction, instead of the other way around. Consequently, in order to ascertain whether the Pd⁰ or the direct insertion pathway is more favorable, an analysis of the entire catalytic cycle must be made.

We find that, for systems with nitrogen ligands where the putative Pd⁰ species is prevented from attaining a geometry with the two donor nitrogens at 180° from each other, the energy of the Pd⁰ intermediate is prohibitively high. (In contrast, for systems such as (pyridine)₂Pd(H)(Cl) the energy of the Pd⁰ intermediate is quite accessible, as it is for

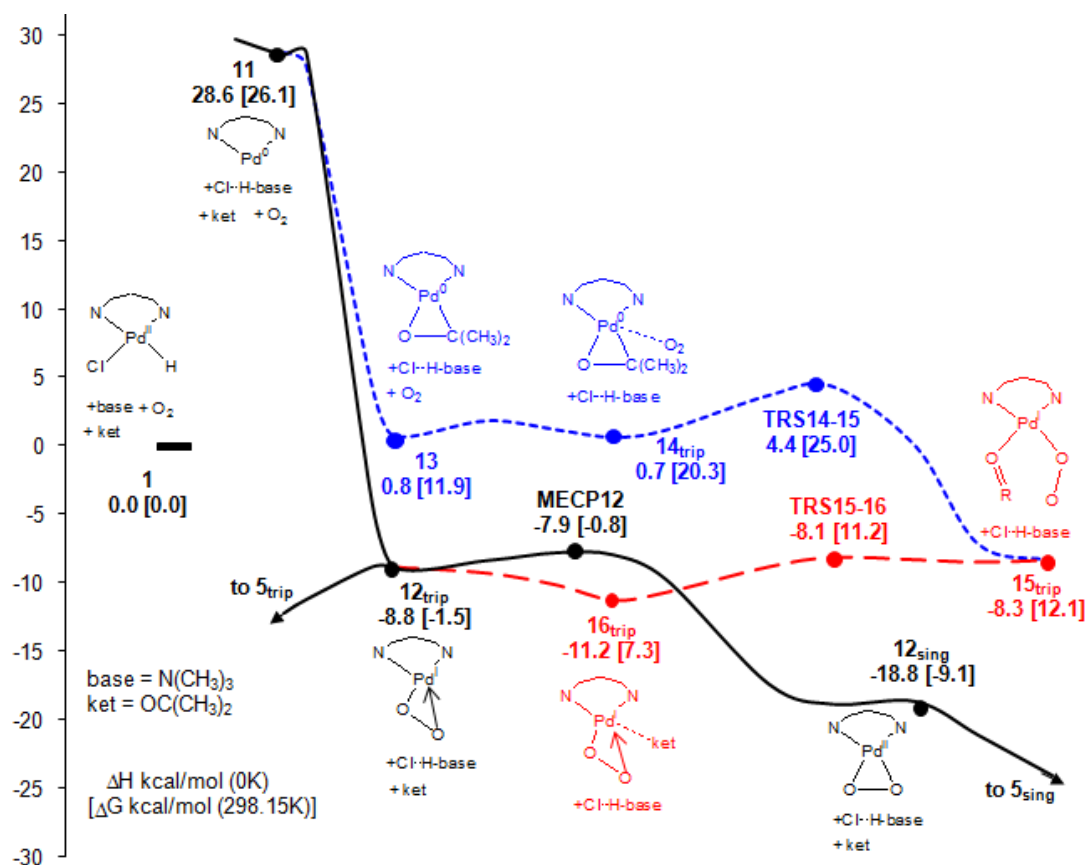


Figure 3.6. Calculated mechanism for naked $\text{Pd}^0(\text{spar})$. Intermediates are shown, while transition states (TSX-Y) are shown separately.

systems with, for example, a chelating diphosphine ligand.) In our current case, the formation of the naked sparteine- Pd^0 even with the formation of $[\text{Cl}]^-[\text{HN}(\text{CH}_3)_3]^+$ ion pair to help in stabilization is still 28.6 kcal/mol uphill in energy (Figure 3.6, species **11**), and without the aid of the base it is 51.1 kcal/mol uphill (not shown). Thus, the energy of the intermediate alone is too high to be accessible from species **1**, without considering the energy of the transition states leading to and from **11**. However, although not accessible in this catalytic process, intermediates similar to **11** could very well be accessed in reaction profiles of analogue systems. Moreover, the addition of solvent molecules, molecular oxygen, or other interacting species could realistically lower the energy and play an important role in this and other processes. Indeed, we find that addition of O_2 or of a simple model ketone such as acetone can provide a great deal of stabilization to the Pd^0 species,

although none of the species we investigated could stabilize **11** enough to make it energetically competitive with the direct insertion pathway. Nevertheless, the results will be discussed in detail and do appear to shed some light on related processes.

3.3.2.2 Pd⁰ with O₂

Addition of triplet oxygen to **11** generates **12_{trip}**, with an overall $\Delta H = -8.8$ kcal/mol. We could not find a transition state for this process, as **12_{trip}** is formed immediately when triplet O₂ is introduced to **11**. Indeed, attempts at scanning the energy as a function of Pd-O distance showed a monotonic energy increase with increasing distance, until a plateau was reached. **12_{trip}** is an η^2 -O₂ complex with Pd, which could be characterized as **5_{trip}** with the [Cl]⁻[HN(CH₃)₃]⁺ ion pair removed from the system. By adding the [Cl]⁻[HN(CH₃)₃]⁺ ion pair back, this pathway can easily merge to the primary pathway at species **5_{trip}** and proceed to products. Alternatively, **12_{trip}** could immediately undergo a spin-flip. The MECF for this process, **MECF12**, has an energy of -7.9 kcal/mol and was previously described in detail in Section 3.3.1.1.

The resulting species, **12_{sing}**, is identical to **5_{sing}** with the [Cl]⁻[HN(CH₃)₃]⁺ ion pair removed from the system, and again this pathway could merge with the primary pathway with the simple addition of the [Cl]⁻[HN(CH₃)₃]⁺ ion pair. The relative ΔH for **12_{sing}** is -18.8 kcal/mol.

3.3.2.3 Pd⁰ with Ketone

In addition to adding O₂ to **11**, we also considered the possibility that other donating ligands could stabilize the Pd⁰ species. As mentioned above, our original focus for the investigation involved the oxidation of alcohols to ketones using a (s^{par})Pd(Cl)₂ catalyst, and as a result there is an abundance of ketone in the reaction mixture. Consequently, we decided to use the ketone acetone as a model donating ligand, designated ket in Figure 3.6. Addition of acetone to **11** forms the complex **13**, with a $\Delta H = 0.8$ kcal/mol. No transition state was sought for this process as the addition of acetone to species **11** converges

monotonically to **13**, much like what was observed for O₂. **13** is an η^2 -acetone complex with Pd, with a Pd-O distance of 2.07 Å and a Pd-C distance of 2.14 Å. In addition, the C-O distance of 1.30 Å is increased from the free ketone C-O distance of 1.22 Å, while the Pd-C-C bond angles have distorted to 113° and 155°. The Pd- distances of 2.30 (*trans* to O) and 2.43 Å (*cis* to O) are both consistent with Pd⁰ and similar to what we saw in **5**_{trip}. Although acetone did act to stabilize the Pd⁰ species, it does not participate in the remainder of the reaction and will need to be displaced. Despite the fact that this is not the most favorable pathway to proceed from **11** and does not seem to contribute any new information for our specific sparteine system, **13** is similar to known complexes that are known to react to form H₂O₂ and are therefore relevant to the discussion. Of particular note here is the comparison between **13** and the toluene analogue in which toluene is bound to the Pd in an η^2 fashion to the aromatic carbons α and β to the methyl (not shown), $\Delta H = 7.1$ kcal/mol. Since there is no energetic advantage in complexing toluene compared to acetone, and both pathways would need to proceed in parallel directions, the toluene-assisted pathway is considered redundant and will not be presented here.

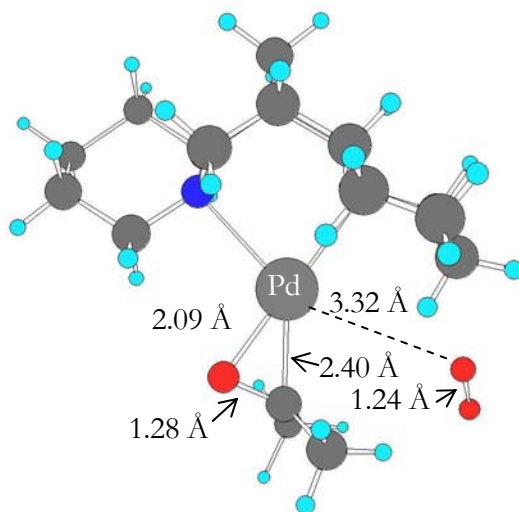


Figure 3.7. Detail view of TS14-15

To proceed from **13**, addition of oxygen is required. A weakly bound van der Waals complex, **14_{trip}**, is formed when O₂ is added, with a $\Delta H = 0.7$ kcal/mol. The geometry of **14_{trip}** has not changed noticeably from **13** despite the addition of O₂, which lies behind the acetone methyls near the Pd square plane. The distances from the Pd to both O's are 5 Å or greater and are indicative of no bonding. Mulliken populations demonstrate that no charge has been transferred between the O₂ and the Pd species, while spin analysis confirms that both unpaired spins still reside on the oxygen.

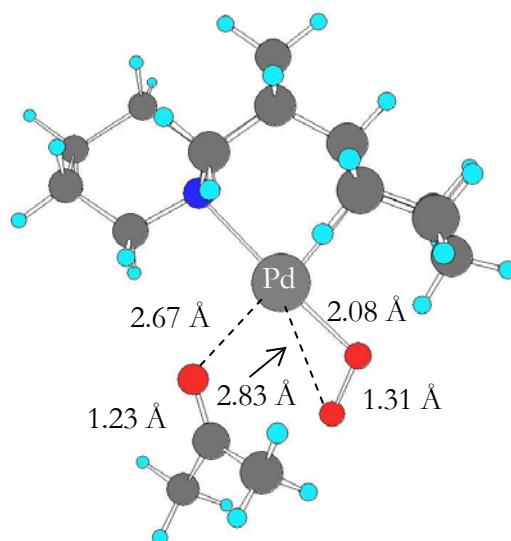


Figure 3.8. Detail view of TS15-16

14_{trip} proceeds through an intermolecular substitution reaction in which the O₂ bonds end on to the Pd, and the Pd-C interaction is broken. The resulting Pd^I species, **15_{trip}**, is a square planar Pd complex with both O₂ and acetone bonding with the Pd in an η^1 fashion. The transition state, **TS14-15** (Figure 3.7), maintains close interaction between the Pd and the O of the acetone while the Pd-C distance has increased resulting in distances of 2.09 and 2.40 Å, respectively. The O₂ is now significantly closer but still unbound with a Pd-O distance of 3.32 Å and an O-O distance of 1.24 Å. The Pd- distances of 2.30 (*trans* to ket) and 2.49 Å (*cis* to ket) have not changed significantly from **14_{trip}**. ΔH^\ddagger for this step is 4.4 kcal/mol.

The resulting species, **15_{trip}**, is significantly more stable, $\Delta H = -8.3$ kcal/mol. The new Pd-O distances are 2.21 (O₂) and 2.23 Å (ket) similar to those seen in previous Pd^I species. The new O-O distance of 1.31 Å is consistent with a peroxy radical species and further suggests Pd^I species. Indeed, spin analysis shows 0.72 electrons of unpaired spin on the Pd and 1.06 electrons combined on both O's. Of further interest is the C-O distance of 1.26 Å, halfway between that of **14_{trip}** and of free acetone, and that the two methyls are still distorted out of plane. The Pd- distances are now 2.32 (*trans* to ket) and 2.34 Å (*cis* to ket).

15_{trip} can easily undergo an intramolecular substitution, losing the ketone and forming an η^2 -O₂-Pd complex, **16_{trip}**, with a $\Delta H = -11.2$ kcal/mol. **16_{trip}** can be described as a weakly bound van der Waals complex and is structurally identical to both **5_{trip}** and **12_{trip}** except for the nonbonded species involved. **TRS15-16** (Figure 3.8) has Pd-O distances of 2.67 (ket), 2.08 (α-O of O₂), and 2.83 Å (β-O of O₂) demonstrating that the ketone is already unbound, even though the second O has not yet coordinated to the Pd. The O-O distance of 1.31 Å has not changed, but the C-O distance has decreased to 1.23 Å, and the ketone is now planar, just as in free acetone. The Pd-N distances are 2.32 Å (formerly *cis* to ket) and 2.41 Å (formerly *trans* to ket). Spin analysis show that Pd still has 0.65 electrons of unpaired spin and oxygen has a combined 1.21 electrons of unpaired spin, suggesting that the transition state is still a Pd^I species, whereas **16_{trip}** should be considered a Pd⁰ species. ΔH^\ddagger for this transition state is -8.1 kcal/mol. At this point **16_{trip}** can lose the complexed ketone, resulting in the formation of **12_{trip}**, thus merging with the previous pathway and completing the cycle.

3.4 Conclusion

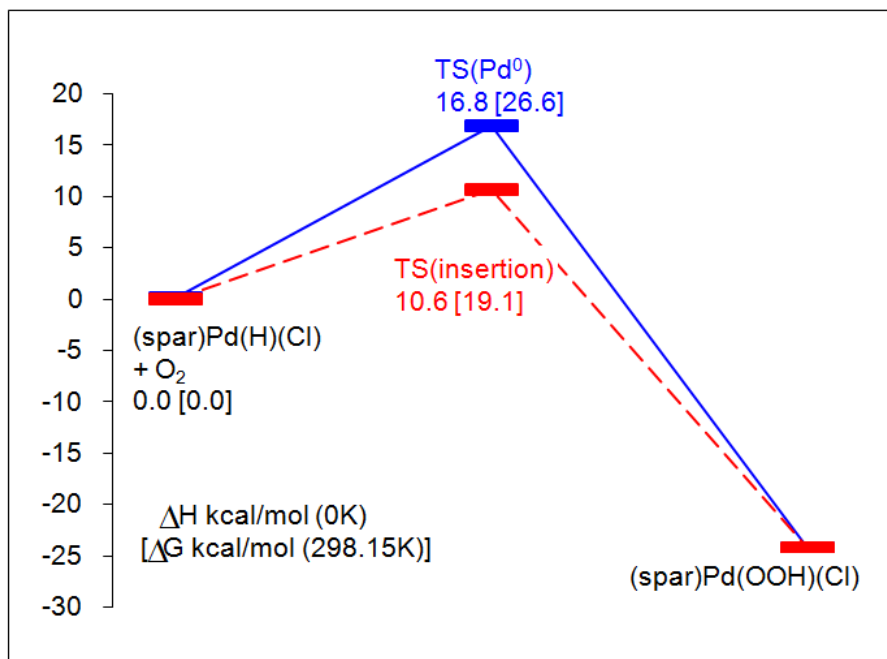


Figure 3.9. Comparison of Pd⁰ (solid blue line) and insertion (dotted red line) energetics for (sparateine)Pd(H)(Cl) + O₂

We conclude that a base-assisted pathway for the formation of Pd⁰ from Pd^{II} hydride with the subsequent formation of an η^2 -peroxo Pd⁰ is energetically accessible for bidentate nitrogen ligand systems such as sparteine. The reaction must proceed as follows:

- (1) first through the deprotonation of the hydride to form a linear (κ^1 -sparteine)Pd⁰-Cl anion (in which one of the two chelating nitrogens has dissociated),
- (2) followed by incorporation of molecular oxygen (O₂[‡]).

The result is (κ^2 -sparteine)Pd^I(Cl)(η^1 -O₂), which has one unpaired spin on the Pd and one delocalized over the two oxygens. This rearranges through loss of Cl⁻ and the associated protonated base coupled with a spin-crossing to the singlet surface. The result is a (κ^2 -sparteine)Pd⁰(η^2 -O₂) singlet. Protonation of this species leads to the formation of a

Pd^{II} hydroperoxo complex, and reaction with a second equivalent of HX completes the catalytic cycle by producing $\text{Pd}^{\text{II}}\text{X}_2$ and H_2O_2 .

The barrier for the Pd^0 pathway ($\Delta H^\ddagger = 16.8$ kcal/mol, $\Delta G^\ddagger = 26.6$ kcal/mol, Figure 3.9) is considerably higher than that of the direct oxygen insertion mechanism previously described for the same system ($\Delta\Delta H^\ddagger = 6.2$ kcal/mol, $\Delta\Delta G^\ddagger = 7.5$ kcal/mol)⁸. We believe these results should apply to all Pd systems which employ bidentate N,N ligands. Indeed, based on these results, we postulate that the bidentate character of the ligand significantly disfavors the palladium(0) pathway, as the resulting d^{10} complex can only be stabilized by one of the two donor atoms. However, this could be alleviated through the use of other donor atoms that are strongly π -accepting, such as P. In addition, disconnecting the tether and allowing the two donor ligands to obtain a *trans* configuration should also favor the palladium(0) pathway. Finally we speculate that both the insertion and palladium(0) pathways would be stabilized through the employment of more σ -withdrawing ligands, although further testing is required.

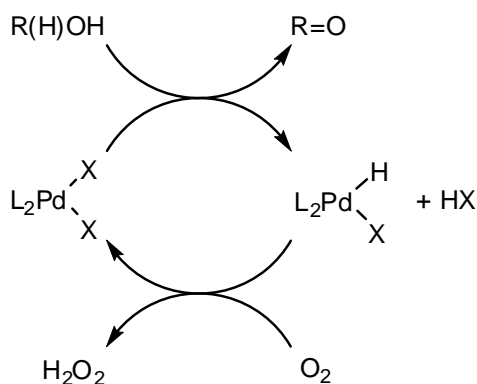
Together with our previous report, we now have a complete picture of the two competing pathways at work in a specific palladium oxidase system. We expect this to provide a framework for further studies in this area, and in order to provide further understanding of palladium oxidase chemistry, we are now expanding these studies to such other ligand systems as bipyridine ligands, phosphorus-containing ligands, and tridentate (pincer-type) ligands.

Chapter 4

Activation of Molecular Oxygen by ((-)-Sparteine)Pd(OAc)H: Pd⁰ vs. Direct Insertion

4.1 Introduction

Scheme 4.1



Enabling the use of molecular oxygen is highly desirable as the stoichiometric oxidant in inorganic catalysis due to its low cost, abundance, and its conversion to environmentally benign byproducts such as H_2O_2 . Indeed, studies on Pd/O_2 systems have become ubiquitous in recent years [4, 23, 30, 31, 40–41]. These palladium-catalyzed oxidations are believed to

proceed through an “oxidase” pathway, in which oxidation of the substrate by the palladium species occurs first, followed by reoxidation of palladium by O₂ (Scheme 4.1) [23, 30a]. Despite this knowledge of the mechanism the specific details of this reoxidation are actively debated, which significantly hinders the rational design of new catalysts. Consequently, much work has been performed in an effort to ascertain the mechanism or mechanisms involved and has narrowed the discussion down to two main pathways for the majority the systems involved [4a, 5b–c, 23, 24, 30, 36–38, 40–41]^{12,13,14}. The first of these two pathways involves the direct insertion of O₂ into a Pd^{II}-hydride brought about by the abstraction of the hydrogen atom by O₂ followed by rearrangement of the HOO• fragment and spin conversion (Figure 4.1, “Direct Insertion”), whereas the other involves the formation of Pd⁰ through the reductive elimination of HX followed by reaction with O₂ (Figure 4.1, “Pd⁰”).

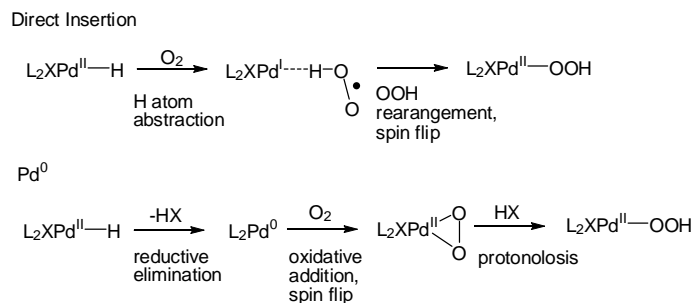


Figure 4.1. The two feasible mechanisms previously shown to be at work for the aerobic oxidation of L₂PdHX

Our group first demonstrated the feasibility of the direct insertion pathway through DFT studies on a (spar)PdHCl system used in enantioselective oxidation of alcohols and later demonstrated a preference for this mechanism in the same system ($\Delta\Delta\text{H}^\ddagger = 6.2$ kcal/mol, $\Delta\Delta\text{G}^\ddagger = 7.5$ kcal/mol). The insertion mechanism reported therein proceeds through the

¹² Two additional pathways proposed for this process are: 1) The oxidative addition of O₂ to form an octahedral Pd^{IV} complex; 2) The substitution of O₂ for the X-ligand forming a cationic LPd^{III}H-superoxide. In our efforts and those of others these pathways have been eliminated due to unreasonably high energy intermediates and will not be examined here. For more information including a computational examination of these pathways see Popp and Stahl [41].

¹³ See Chapters 1 and 3.

¹⁴ See Chapter 2.

abstraction of a hydrogen atom by oxygen to form a Pd^{I} radical T-complex and $\text{HOO}\bullet$ which subsequently leads to the formation of triplet palladium hydroperoxo species. After undergoing a spin-flip to form the singlet hydroperoxo species the reaction proceeds through the addition of a proton to form H_2O_2 and the corresponding PdCl_2 . We concluded that the re-formation of the two radical species and the existence of the *cis* hydrogen bond acceptor were intimately correlated. The observed preference is most likely due to the bidentate character of the ligand which prevents the formation of a linear Pd^0 species and the need for an exogenous base. The substitution of OAc for Cl in this study allows a direct comparison to the previous results and allows us to see the results of a X-ligand with the ability to chelate to the metal after the reductive elimination and the basicity to avoid the need for the exogenous base.

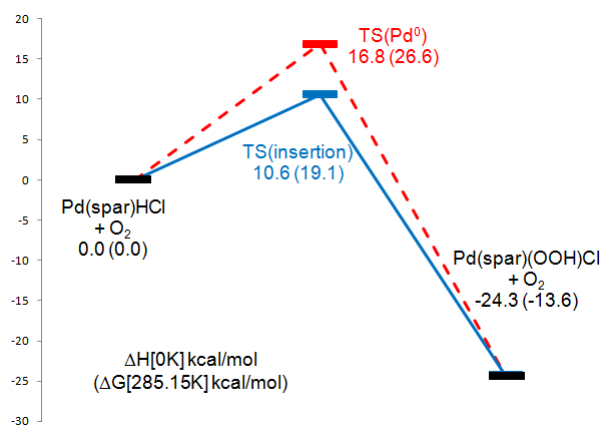


Figure 4.2. Comparison of Pd^0 (dotted red line) and insertion (solid blue line) energetics for $(\text{spar})\text{PdHCl} + \text{O}_2 \rightarrow (\text{spar})\text{Pd}(\text{OOH})\text{Cl}$ in toluene

Submitted shortly before our results completing the $(\text{spar})\text{PdClH}$ study, Popp and Stahl published a thorough examination of $(\text{IMes})_2\text{PdHOAc} + \text{O}_2$ [41]. Based on their calculations and their “tentative” results for the addition of exogenous carboxylic acid they conclude that “the HX reductive elimination pathway is the most likely mechanism for catalyst oxidation under typical reaction conditions”.

Herein we will present a detailed mechanistic view of the reaction of O_2 with $(\text{spar})\text{PdHOAc}$ focusing on direct insertion and Pd^0 mechanisms. These new results present

substantial changes in the mechanistic pathway through the inclusion of a chelating base as the X-ligand and provide a tool for developing new catalytic systems with the ability to steer toward or away from a specific reoxidation pathway.

4.2 Computational Methodology

All calculations were performed using the hybrid DFT functional B3LYP, as implemented by the Jaguar 7.0 program package [44]. This DFT functional utilizes the Becke three-parameter functional (B3) [7] combined with the correlation functional of Lee, Yang, and Parr (LYP) [8] and is known to produce good descriptions of reaction profiles for transition-metal-containing compounds [9,10]. Pd was described with the LACVP** effective core potential and basis set (18 explicit electrons) [11]. All other elements were described including the core electrons, using the Pople 6-31G** basis set [12], but with 3s combination of the six d-like functions reduced to five.

All geometries were optimized and evaluated for the correct number of imaginary frequencies through vibrational frequency calculations using the analytic Hessian. Zero imaginary frequencies correspond to a local minimum, whereas one imaginary frequency corresponds to a transition structure.

Implicit solvent effects for toluene were calculated with the Poisson-Boltzmann (PBF) continuum approximation [13], using the parameters $\epsilon = 2.38$ and solvent radius = 2.76 Å. Here we use the solvent accessible surface of the molecular complex built using standard vdW radii. The solvation effects were calculated at geometries optimized for the gas phase.

Using the analytic Hessian we calculated the zero-point energy corrections at 0 K and added this to the solvation correction and the QM energy ($\Delta[E]$) to obtain the enthalpy at 0 K, $\Delta H[0\text{ K}]$. Similarly, the vibrational frequencies were used to calculate the entropy and enthalpy corrections to 298.15 K, to obtain $(\Delta H - T\Delta S) = \Delta G[298.15\text{ K}]$.

On the basis of previous results we expect that relative energies on the $\Delta H[0\text{ K}]$ surface are accurate to ~ 3 kcal/mol for stable intermediates and to ~ 5 kcal/mol for transition structures. Probably the relative energies on the $\Delta G[298\text{ K}]$ surface are less accurate, due to the use of the PBF model [14]. This methodology was found to be an adequate level of theory in our previous study of (sparteine)Pd(Cl)(H) when compared to various other functionals and basis sets¹³.

DFT is formulated in terms of Slater determinants built from Kohn-Sham orbitals that are calculated self-consistently. This process is consistent for states that are well described with closed-shell orbitals (up and down spins in the same orbitals), the normal situation for most DFT applications. However, in the studies carried out here it was necessary to also include some triplet states. With DFT this is done by having two more spin orbitals with up spin than down spin (unrestricted DFT or UDFT). We refer to this as the triplet state, but it need not be an eigenstate of the spin operator, S^2 . Rather, it is an eigenfunction of S_z , leading to $M_S = 1$. The problem with this formulation occurs when considering a transition between triplet and singlet states, a topic of this paper. Thus, starting with the true triplet orbitals of O_2 and calculating the energy of the singlet state should lead to a component of $^1\Delta_g$ with an excitation energy of 22.5 kcal/mol. In fact, UDFT gives an excitation energy of 10.5 kcal/mol. The reason is that the $M_S = 0$ wavefunction we consider to describe the singlet state also has a mixture of triplet character. This can be treated by applying the spin projection operator, which will lead to a rigorous energy for the singlet-triplet splitting (20.5 kcal/mol) [15a] but neither the orbitals nor the geometry are optimum after spin projection. Bally and Borden has suggested simply doubling the calculated energy gap in order to approximate the true gap, which in this case yields an energy gap of 21.0 kcal/mol for O_2 [15b]. Thus, in the case of O_2 both methods produce similar results. All results reported here are UDFT.

It should also be noted that the ligand employed in this study, (–)-sparteine, is one stereocenter removed from C_2 symmetry, and although enantiomerically pure it still presents the dilemma of doubling the number of isomers for most of the steps involved. We

found the differences in energy and geometry to be negligible and chose to present only the pathway starting at the (–)-sparteine-Pd^{II}(H)(Cl) species that corresponds with the favorable alcohol oxidation transition state from our previous study on the use of this catalyst in the selective oxidation of alcohols¹⁵.

4.3 Results and Discussion

4.3.1 Direct Insertion Pathway

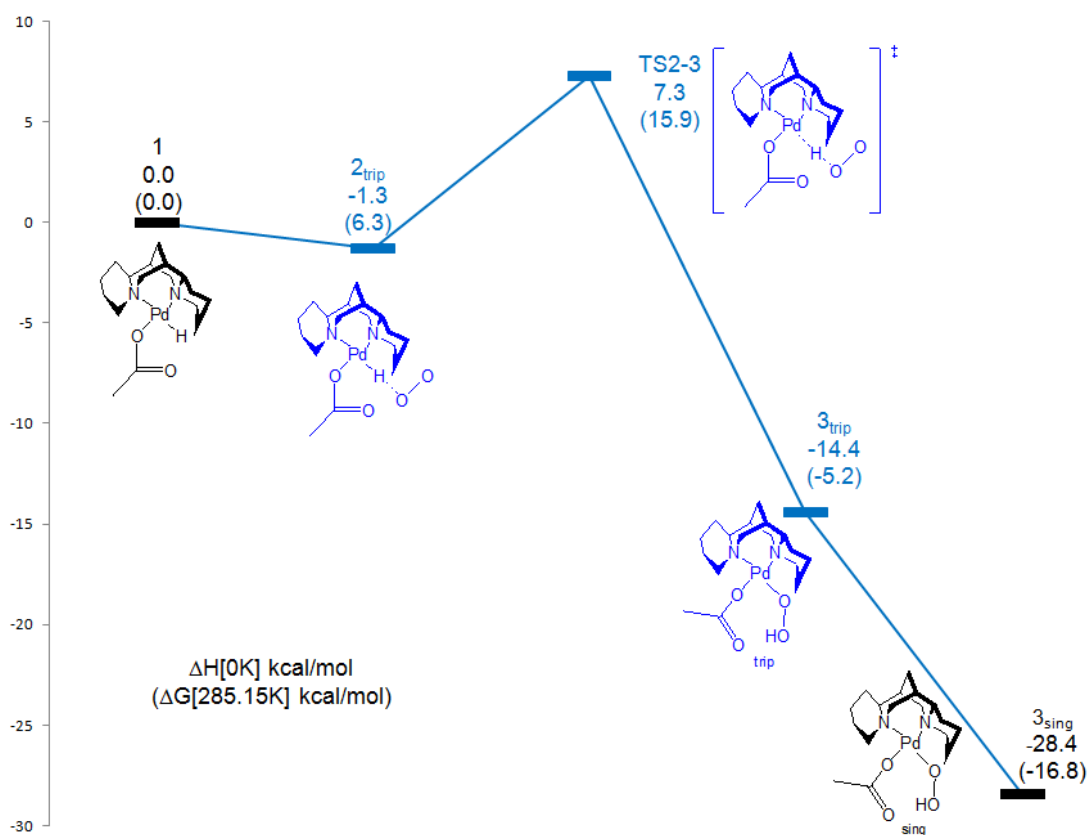


Figure 4.3. Calculated mechanism for the direct O₂ insertion pathway for (spar)PdHOAc + O₂ → (spar)Pd(OOH)OAc in toluene

¹⁵ See Appendix.

As the starting point for this study we chose κ^2 -(-)-sparteine-Pd^{II}HOAc (**1**, Figure 4.3). Introducing (triplet) molecular oxygen to **1** leads immediately to the formation of a weakly bound van der Waals complex [(spar)Pd^{II}HCl]•O₂ (**2**, Figure 4.4 upper left), with $\Delta H = -1.3$ kcal/mol. There is negligible electron transfer between the O₂ and the Pd complex. Spin analysis shows that all unpaired spins in **2** are on the O₂ fragment (one π^* orbital in the plane, hereafter the σ electron, and the other π^* orbital perpendicular to the plane, hereafter the π electron).

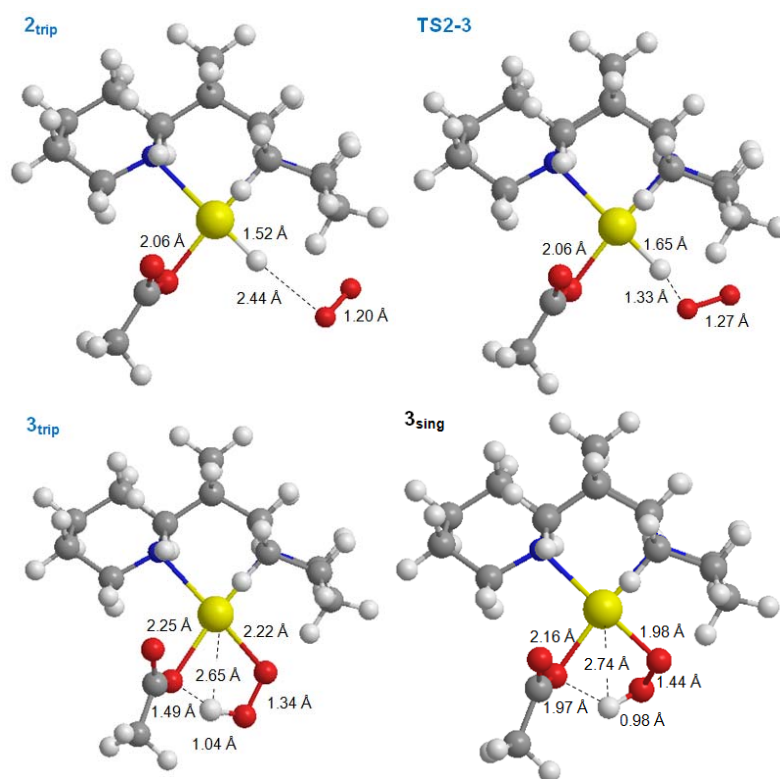


Figure 4.4. Detailed structures along direct O₂ insertion pathway

From **2** we find the transition state for direct O₂ insertion. Here the transition state, **TS2-3** (Figure 4.4 upper right), has the triplet O₂ positioned to abstract the H from the Pd with $\Delta H^\ddagger = 7.3$ kcal/mol. Thus from **1** to **TS2-3** the Pd-H bond length stretches from 1.52 to 1.65 Å, indicating a decrease in bond order from 1 to ~ 0.7 . At the same time the O-O bond distance increases from 1.20 to 1.27 Å, indicating a decrease in bond order of ~ 0.2 .

On the other hand, the O-H distance of 1.33 Å (compared to 0.96 Å in HO₂) indicates the O-H bond has not yet formed. At this point the π unpaired spin (perpendicular to the O₂-H-Pd plane) remains on the O₂, while the σ unpaired spin (in the plane) has partly delocalized onto the Pd $d_{x^2-y^2}$ orbital (where Pd-H is the x direction and the plane is the xy plane). Spin population for the O₂ moiety is 1.50 (with 0.71 on the O nearest to Pd), and that for Pd is 0.39.

From **TS2-3** the energy falls monotonically by 19.1 kcal/mol while the HO₂ rotates in the plane to form **3_{trip}** in which the H is now bonded to the inner O (H-O = 1.04 Å) while the outer O is now bonded to the Pd (Pd-O = 2.22 Å). Here the two unpaired spin orbitals are similar to species **TS2-3**, in which the π unpaired spin remains on the O₂, while the σ unpaired spin (in the plane) has further delocalized onto the Pd $d_{x^2-y^2}$ orbital.

The mechanism through **TS2-3** leads to the Pd-OOH species **3_{trip}** (Figure 4.4 lower left), with a ΔH of -14.4 kcal/mol with respect to **1**. **3_{trip}** is best described as a square planar Pd^I radical (unpaired spin in the Pd $d_{x^2-y^2}$ orbital) complexed with the HO₂• peroxy radical (π orbital perpendicular to the plane) acting as a donor ligand. The spin density for the O₂ moiety is 0.97 (0.65 of which resides on the O nearest Pd), and that for Pd is 0.81. Since the unpaired orbitals are orthogonal by symmetry and localized on different centers, they have little interaction and **3_{trip}** is a biradical. Indeed, the Pd-O bond distance of 2.22 Å indicates a weak donor-acceptor bond, compared to the significantly shorter value of 2.00 Å expected for a Pd^{II}-O single bond. The O-O bond distance of 1.34 Å is typical of a peroxy radical species (O-O = 1.33 Å in free HO₂), halfway between common single and double bond distances of 1.48 and 1.21 Å. The O-H bond distance of 1.04 Å is close to that of free HO₂• (1.00 Å). Finally, the Pd-O _{α} OAc bond distance of 2.25 Å and the Pd-N distances of 2.29 (*trans* to OAc) and 2.34 Å (*cis* to OAc) are elongated by 0.09, 0.13, and 0.14 Å compared to the bond lengths in the corresponding Pd^{II} complex, as expected for a Pd^I center. An interesting feature of **3_{trip}** is the H-O _{α} OAc distance of 1.49 Å, which indicates some internal hydrogen bonding. We find that this

contributes to the exothermicity of this part of the reaction by significantly stabilizing this intermediate.

Conversion to the singlet state leads to $\mathbf{3}_{\text{sing}}$ (Figure 4.4 lower right), with $\Delta H = -28.4$ kcal/mol. $\mathbf{3}_{\text{sing}}$ is clearly a $\text{Pd}^{\text{II}}\text{OOH}$ complex: the Pd-O bond distance of 1.98 Å is consistent with the covalent Pd-O bond in similar species [16], while the O-O bond distance of 1.44 Å is slightly shorter than a normal single bond distance of 1.48 Å. The O-H bond distance of 0.98 Å is consistent with an O-H bond distance in H_2O_2 . The Pd- O_{OAc} bond distance of 2.16 Å and the Pd-N distances of 2.16 (*trans* to Cl) and 2.20 Å (*cis* to Cl) are as expected for Pd^{II} .

As discussed in Section 4.1 spin conversions in related complexes have been thoroughly examined and we feel it is unnecessary to calculate a MECP for the conversion of $\mathbf{3}_{\text{trip}}$ to $\mathbf{3}_{\text{sing}}$. From here reaction with a second equivalent of HOAc completes the catalytic cycle by producing $\text{Pd}^{\text{II}}\text{OAc}_2$ and H_2O_2 .

4.3.2 Pd^0 Pathway: Unassisted Reductive Elimination of HOAc

Similar to Section 4.3.1, we chose $\kappa^2(-)\text{-sparteine-Pd}^{\text{II}}\text{HOAc}$ (**1**, Figure 4.5, Figure 4.6 upper left) as the starting point. From **1** we found a reductive elimination transition state, **TS1-4** (Figure 4.6 upper right), in which the Pd complex goes through an intermolecular proton transfer from the Pd to the OAc resulting in the formation of a linear $\kappa^1\text{-}(\text{spar})\text{Pd}^0\text{-acetic acid}$ complex, **4**. The ΔH^\ddagger for **TS1-4** is 8.3 kcal/mol. The Pd-H distance has stretched from 1.52 to 1.69 Å, indicating that the Pd-H bond has not completely broken, while the $\text{O}_{\gamma\text{OAc}}\text{-H}$ distance has decreased from 2.35 to 1.30 Å, indicating that the $\text{O}_{\gamma\text{OAc}}\text{-H}$ bond is not fully formed. The imaginary frequency corresponds to a mode in which the proton transfers from the Pd to $\text{O}_{\gamma\text{OAc}}$ with little other molecular motion except for slight stretching of the Pd-N (*cis* to OAc) distance. Also of note is that the Pd-N (*cis* to OAc) distance has increased from 2.34 to 2.54 Å, indicating a loss of bonding, consistent with the hybridization of the available orbitals on a $\text{d}^{10} \text{Pd}^0$ species. As a result of the change in

formal oxidation state of the Pd, the Pd-N (*trans* to OAc) and Pd-O _{α} OAc distances have both increased from 2.18 and 2.03 Å to 2.23 and 2.16 Å, respectively.

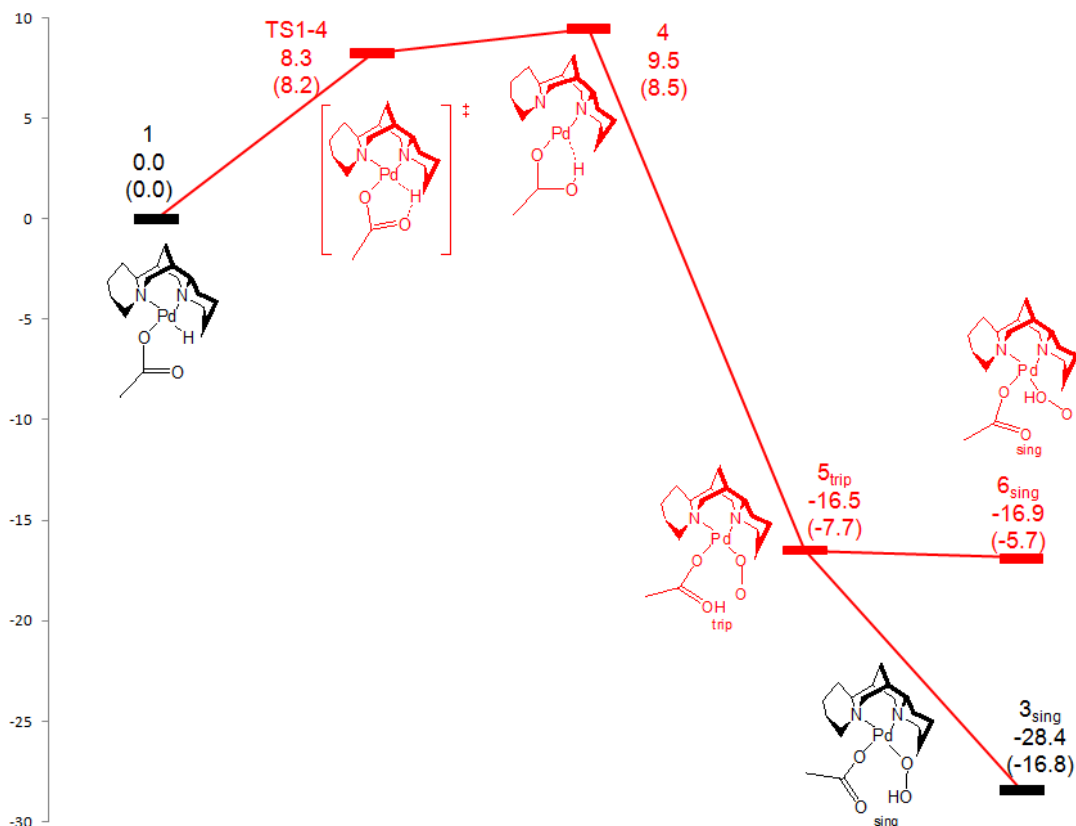


Figure 4.5. Calculated mechanism for the Pd⁰ pathway for (spar)PdHOAc + O₂ → (spar)Pd(OOH)OAc in toluene. Intermediates are shown, while transition states (TSX-Y) are shown separately.

From **TS1-4** the reaction proceeds to species **4**, a linear Pd⁰ complex very similar to the preceding transition state (Figure 4.6 middle left). Indeed, the only significant changes are the further stretching of the Pd-H distance (to 2.06 Å), the reduction of the O _{γ} OAc-H distance (to 1.04 Å), and further stretching of Pd-N (*cis* to OAc) distance (to 2.66 Å). Species **4** is downhill 2.6 kcal/mol on the ΔE_{gas} surface and is indeed the product formed through this transition state. When solvation corrections and ZPE corrections are added to

these species the result is that intermediate **4** is *uphill*¹⁶ from the previous transition state with $\Delta H = 9.5$ kcal/mol. Breaking the Pd- O _{α OAc} bond followed by complete removal of the HOAc is energetically prohibitive (uphill 22.1 kcal/mol).

Instead of removing HOAc, triplet oxygen was added to **4**. We could not isolate any unbound Pd⁰-O₂ species, as all attempts immediately optimized to a four-coordinate triplet κ^2 -(spar)Pd^I(η^1 -O₂)-acetic acid complex, **5_{trip}**, with a ΔH of -16.5 kcal/mol (Figure 4.6 middle right). The new Pd-O₂ bond and the electron transfer to form Pd^I are the main factors governing the exothermicity of this step. In this species the two N_{sparS}, the O _{α OAc}, and the bonding O of the end-on O₂ moiety all reside in a square plane. Spin analysis of complex **5_{trip}** shows a spin density of 1.11 on the two oxygens (0.66 on the O α to Pd and 0.45 on the O β to Pd), a spin density of 0.71 on the Pd atom, and the remaining spin density (0.18) distributed over the sparteine and HOAc, indicating that this complex should be considered a Pd^I species. The O-O bond of 1.33 Å is typical for a superoxide species (1.33 Å in free O₂⁻), halfway between common single- and double-bond distances of 1.48 and 1.21 Å, respectively. The Pd-N distances of 2.33 Å (*trans* to OAc) and 2.34 Å (*cis* to OAc) and the Pd-O _{α OAc} distance of 2.41 Å are elongated compared to those of corresponding Pd^{II} complexes, as expected for a Pd^I center. The new Pd-O, O-H and O _{γ OAc}-H bond lengths are 2.17, 1.47, and 1.04 Å. The energy to remove the HOAc moiety is uphill 10.8 kcal/mol and would only require the reintroduction at a latter point so it will not be discussed further.

Attempts to locate the corresponding species **5_{sing}** are not successful with the resulting structures relaxing to either **3_{sing}** or **6_{sing}**, both the results of a proton transfer from O _{γ OAc} to the α or β O of the O₂ moiety. Species **6_{sing}** (Figure 4.6 bottom) corresponds to the proton transfer to the α O of the O₂¹⁷. The O-O bond of 1.42 Å is similar to that of a single-bond distances of 1.48. The Pd-N distances of 2.22 Å for both N's and the Pd-O _{α OAc} distance of

¹⁶ This result is most likely due to the uncertainties involved in ZPE. For a similar example see the process from 18 \rightarrow TS9 \rightarrow 19 in ref [42].

¹⁷ Our previous examinations did not consider species such as **6_{sing}** until they were previously reported in ref [43].

2.12 Å are consistent with Pd^{II} . The new Pd-O, O-H, and $\text{O}_{\gamma\text{OAc}}\text{-H}$ bond lengths are 2.03, 1.04, and 1.47 Å.

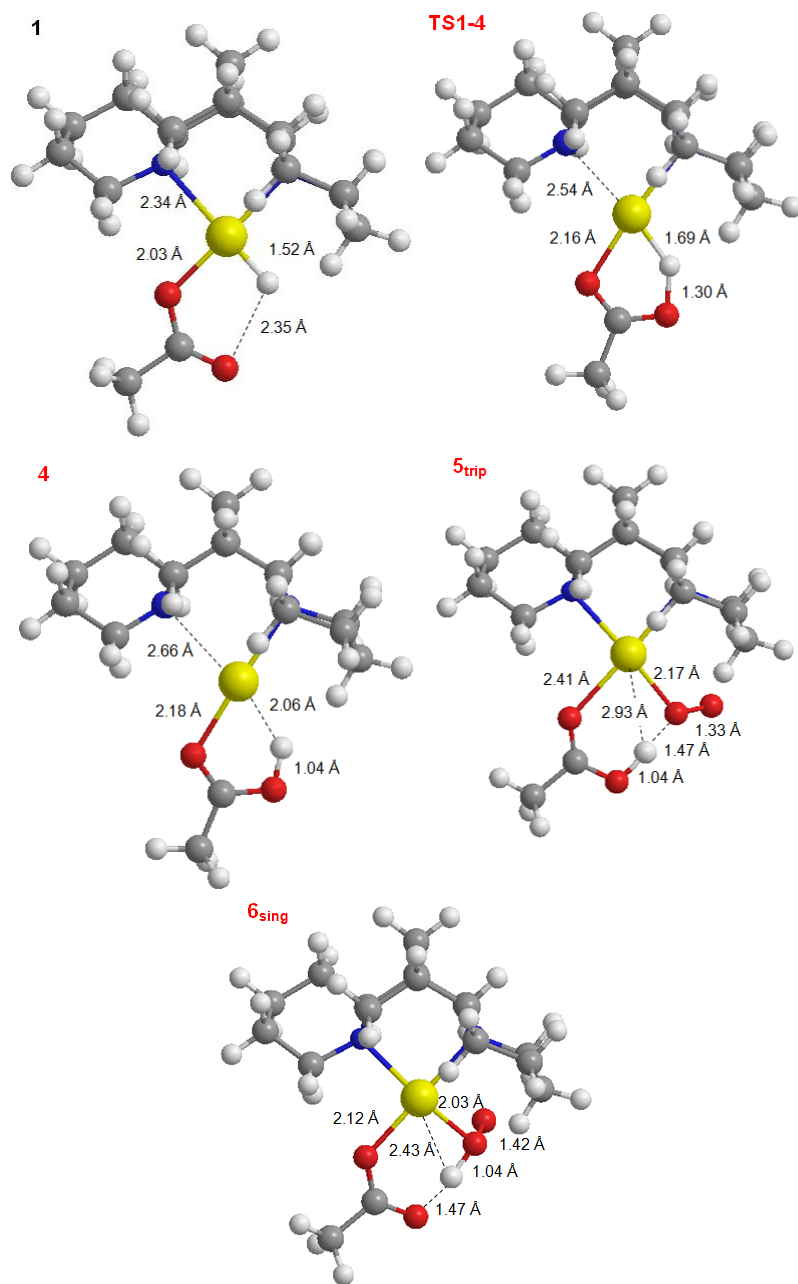


Figure 4.6. Detailed structures along direct O_2 insertion pathway

As discussed in Section 4.1 spin conversions in related complexes have been thoroughly examined and we feel it is unnecessary to calculate a MECP for the conversion of **5**_{trip} to **5**_{sing}. From here reaction of either **3**_{sing} or **6**_{sing} with a second equivalent of HOAc completes the catalytic cycle by producing Pd^{II}OAc₂ and H₂O₂ (alternatively **6**_{sing} can proceed first to **3**_{sing}) and will not be discussed further.

4.4 Conclusions

We conclude that the formation of Pd⁰ from Pd^{II}-hydride with the subsequent reaction with triplet oxygen is energetically accessible for bidentate nitrogen ligand systems such as sparteine and the inclusion of a basic chelating X-ligand such as OAc lowers the reaction barrier for the Pd⁰ pathway to the point that it is favored over the direct insertion. The reaction must proceed as follows:

(1) first through the intramolecular deprotonation of the hydride from the *cis* OAc ligand resulting in the formation of a linear (κ^1 -sparteine)Pd⁰-acetic acid complex (in which the chelating nitrogen originally *trans* to the hydride has dissociated),

(2) followed by incorporation of molecular oxygen (O₂[‡]).

The result is (κ^2 -sparteine)Pd^I(HOAC)(η^1 -O₂), which has one unpaired spin on the Pd and one delocalized over the two oxygens. Upon spin conversion the resulting complex proceeds monotonically downhill through a proton transfer to the adjacent O₂ moiety forming a Pd^{II}-hydroperoxo complex. Reaction with a second equivalent of HOAc completes the catalytic cycle by producing Pd^{II}OAc₂ and H₂O₂.

The barrier for the Pd⁰ pathway ($\Delta H^\ddagger = 8.3$ kcal/mol, $\Delta G^\ddagger = 8.2$ kcal/mol, Figure 4.7, **dotted line**) is competitive with that of the direct oxygen insertion mechanism (**TS2-3** Figure 4.7, **solid line**) on the ΔH surface and considerably more favorable on the ΔG surface ($\Delta\Delta H^\ddagger = -1.0$ kcal/mol, $\Delta\Delta G^\ddagger = 7.7$ kcal/mol). We believe these results should apply to all Pd systems which employ bidentate N,N-ligands and a basic chelating X-

ligand. Based on these results, we demonstrate that despite the fact that the bidentate character of the ligand significantly disfavors the Pd^0 pathway, the chelating HOAc moiety can alleviate the problem. In addition, disconnecting the tether and allowing either of the two donor ligands to obtain a *trans* configuration or complete loss of one of the two also favors the Pd^0 as demonstrated in our related work with $(\text{pyr})_2\text{PdXH}^{18}$.

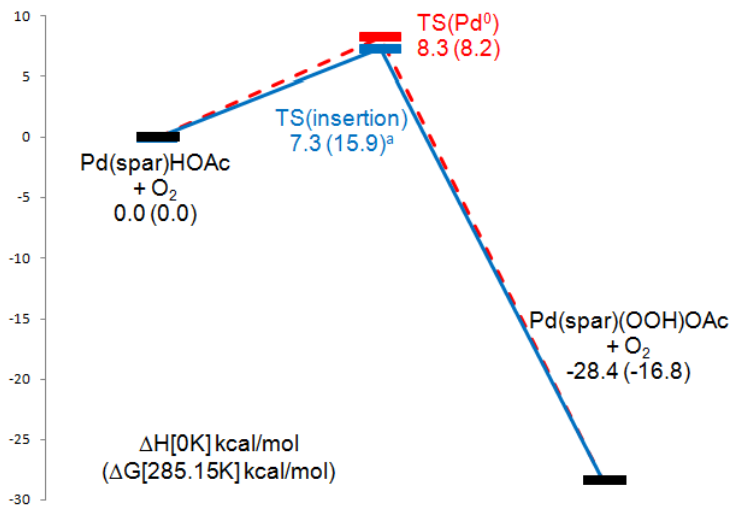


Figure 4.7. Comparison of Pd^0 (dotted line) and insertion (solid line) energetics for $(\text{spar})\text{PdHOAc} + \text{O}_2 \rightarrow (\text{spar})\text{Pd}(\text{OOH})\text{OAc}$ in toluene

Together with our previous report, we now have a complete picture of the two competing pathways at work in a specific palladium oxidase system along with substantial information as to how the choice of ancillary ligands affects the competition. We expect this to provide a framework for further studies in this area.

¹⁸ See Chapter 5.

Chapter 5

Activation of Molecular Oxygen by (Pyridine)₂Pd(OAc)H: Pd⁰ vs. Direct Insertion

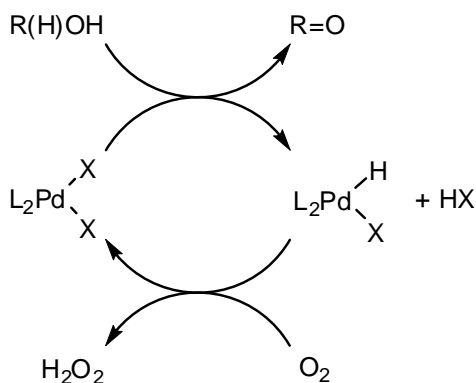
5.1 Introduction

Palladium oxidation catalysis employing molecular oxygen as the stoichiometric oxidant has become ubiquitous in the literature [4, 23, 30, 31, 40-41]. Oxygen is inexpensive, abundant, noncorrosive, and environmentally benign making it the ideal oxidant for green chemistry. Thus, enabling the use of molecular oxygen is highly desirable. Indeed, Pd/O₂ systems have been developed for selective oxidation of alcohols [1b, 1e, 31], intermolecular oxidative amination of alkenes [32], oxidative C-C bond cleavage in tertiary alcohols [33], intermolecular heterocyclization of alkenes [34], and the synthesis of hydrogen peroxide [35]. Nevertheless, only a fraction of the important reactions involving Pd systems utilize oxygen, leaving numerous reactions where the use of oxygen as the stoichiometric oxidant would be valuable [4a, 23, 30].

These palladium-catalyzed oxidations are believed to proceed through an “oxidase” pathway, in which oxidation of the substrate by the palladium species occurs first, followed by reoxidation of palladium by O₂ (Scheme 5.1) [23, 30a]. Despite this knowledge of the

mechanism, the specific details of the reoxidation are actively debated which significantly hinders the rational design of new catalysts. Consequently, much work has been performed in an effort to ascertain the mechanism or mechanisms involved and has narrowed the discussion down to two main pathways for the majority of the systems involved [4a, 5b–c, 23, 24, 30, 36–38, 40–41]^{19,20}.

Scheme 5.1



The first of these two pathways involves the direct insertion of O_2 into a Pd^{II} -hydride brought about by the abstraction of the hydrogen atom by O_2 followed by rearrangement of the $HOO\bullet$ fragment and spin conversion (Figure 5.1, “Direct Insertion”), whereas the other involves the formation of Pd^0 through the reductive elimination of HX followed by reaction with O_2 (Figure 5.1, “ Pd^0 ”). In particular, multiple experimental studies on the direct reaction of Pd^0 with O_2 have been reported, demonstrating both the formation of a stable η^2 -peroxo Pd^{II} complex and the eventual products hydrogen peroxide and $Pd^{II}X_2$, after treatment with HX [5b–c, 36–37]. This demonstrates the feasibility of the Pd^0 pathway under select conditions, although this is not conclusive proof. In addition to the

¹⁹ See Chapter 1–4.

²⁰ Two additional pathways proposed for this process are: 1) The oxidative addition of O_2 to form an octahedral Pd^{IV} complex; 2) The substitution of O_2 for the X -ligand forming a cationic $LPd^{III}H$ -superoxide. In our efforts and those of others these pathways have been eliminated due to unreasonably high energy intermediates and will not be examined here. For more information, including a computational examination of these pathways, see Popp and Stahl [41].

experimental work, Landis and co-workers used density functional theory (DFT) to examine the feasibility of a spin crossover for several Pd^0 systems and showed that first a triplet Pd^{I} -superoxide complex is formed followed by conversion to a singlet Pd^{II} -peroxo complex which is significantly downhill, making the barrier for the spin-crossing practically negligible [37].

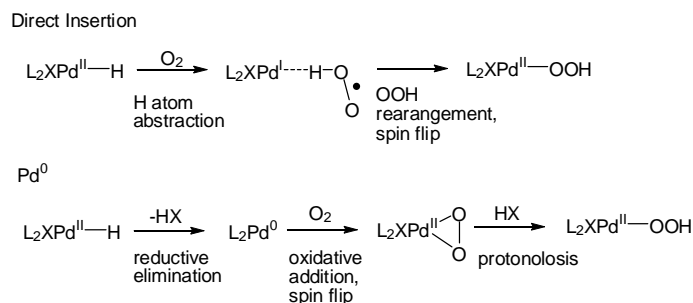


Figure 5.1. The two feasible mechanisms previously shown to be at work for the aerobic oxidation of L_2PdHX

Studies on the direct insertion are only now becoming common. Our group first demonstrated the feasibility through DFT studies on a (spar) PdHCl system used in enantioselective oxidation of alcohols, where the direct insertion was calculated to be favored ($\Delta\Delta H^\ddagger = 6.2$ kcal/mol, $\Delta\Delta G^\ddagger = 7.5$ kcal/mol)²¹. The insertion mechanism reported therein proceeds through the abstraction of a hydrogen atom by oxygen to form a Pd^{I} radical T-complex and $\text{HOO}\cdot$, which subsequently leads to the formation of triplet palladium hydroperoxo species. After undergoing a spin flip to form the singlet hydroperoxo species the reaction proceeds through the addition of a proton to form H_2O_2 and the corresponding PdCl_2 . We concluded that the re-formation of the two radical species and the existence of the *cis* hydrogen bond acceptor were intimately correlated and removal of the *cis* hydrogen bond acceptor substantially increased the reaction barrier as the radical pair must first undergo a spin conversion before directly forming the singlet hydroperoxo species en route to completing the catalytic cycle. Our work with (spar) PdHCl demonstrated that the direct insertion pathway is indeed the favored route most likely due to the bidentate character of the ligand which prevents the formation of a linear Pd^0 species

and the need for an exogenous base²¹. This preference was then reversed with the substitution of OAc ion due to its ability to chelate to the metal after the reductive elimination and eliminating the need for the exogenous base²². Our previous work also demonstrated similar results for the spin conversion as Landis and coworkers, by calculating feasible minimum energy crossing points between the singlet and triplet palladium hydroperoxo and between several bound and unbound O₂ and OOH fragments.

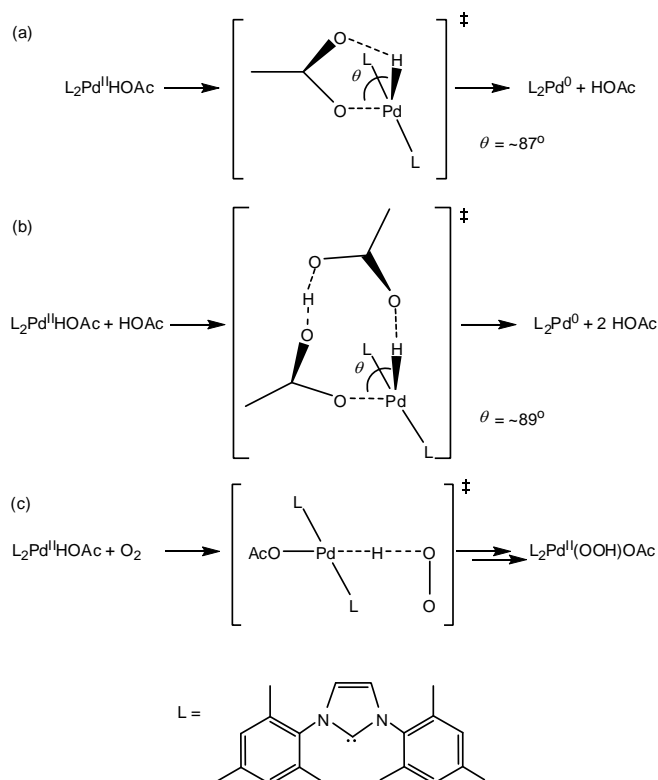


Figure 5.2. Transition state structures presented in study of *trans*-(IMes)₂PdHOAc + O₂ by Popp and Stahl [41].

Submitted shortly before our results completing the (spar)PdClH study, Popp and Stahl published a thorough examination of (IMes)₂PdHOAc (Figure 5.2) [41]. Based on their calculations they demonstrate that the direct insertion mechanism is lower in energy than

²¹ See Chapters 1 and 3.

²² See Chapter 4.

the Pd^0 pathway ($\Delta\Delta H^\ddagger = 12.3$ kcal/mol, $\Delta\Delta G^\ddagger = 4.8$ kcal/mol) although they term this difference as “exhibit[ing] barriers that are very similar in energy” and they conclude that the “HX reductive elimination pathway is the most likely mechanism for catalyst oxidation under typical reaction conditions” in glaring contradiction to their calculated results. They rationalize this discrepancy by alluding to the “tentative” results for the addition of exogenous carboxylic acid which they found to lower the barrier for the Pd^0 pathway ~ 1 kcal/mol on the ΔE surface, a result that would seemingly be more than counteracted with the inclusion of entropy. Simplified drawings of their three main transition state structures are shown in Figure 5.2.

As a possible solution to these confounding results we suggest that the conclusions and chemical intuition are sound and that only a few simple issues in their computational picture are the culprit. First note the angle θ in transition states **a** and **b** in Figure 5.2. In **a** $\theta = \sim 87^\circ$ and most likely contributes a considerable amount of the energy to the barrier ($\theta = \sim 180^\circ$ in the reactant) and the inclusion of an additional HOAc molecule only results in an increase of θ from ~ 87 to ~ 89 . This seems strange as the additional acid molecule should allow the transition state to relax further toward 180° . One possibility for this, if it is indeed an error, could be that the additional molecule was simply added to the previously optimized seesaw transition state and then optimized further instead of looking for the acid-assisted pathway that corresponds to the square planar structure.

Another possible source for the missing low-energy direct insertion mechanism could possibly be the failure to examine any transition states arising from *cis* structures. Although Konnick et al. synthesized the *trans* species in their experimental work [24b] there is reason to believe that both the *cis* and the *trans* species could be active in the catalytic systems. Evidence for this can be seen in the necessity of a *cis* ligand system for the β -hydride elimination mechanism for the reduction of alcohols by Pd^{II} complexes resulting in the formation of *cis*- $\text{L}_2\text{Pd}^{\text{II}}\text{H}$ -alkoxide and subsequently what is thought to be *cis*-

$L_2Pd^{II}HX^{23}$. Despite the prior existence of *cis* species or lack thereof at this point in the reaction mechanism the interconversion between the two must also be examined. Although these suggestions play an important role in the calculations of our pyridine system discussed here it is only speculation that they will make a difference in the much bulkier N-heterocyclic carbene system presented above.

Herein we will present a detailed mechanistic view of the reaction of O_2 with $(pyr)_2PdHOAc$ focusing on direct insertion and Pd^0 mechanisms for both the *cis* and *trans* species as well as the interconversion between the two and the acid-assisted *trans*- Pd^0 pathway that maintains a near square planar structure in the transition state ($\theta = 159.3$). These new results provide a complete picture of both possible pathways for this system thus defining the preferred path and suggest ways to obtain consistent results for related systems.

5.2 Computational Methodology

All calculations were performed using the hybrid DFT functional B3LYP, as implemented by the Jaguar 7.0 program package [44]. This DFT functional utilizes the Becke three-parameter functional (B3) [7] combined with the correlation functional of Lee, Yang, and Parr (LYP) [8] and is known to produce good descriptions of reaction profiles for transition metal containing compounds [9,10]. Pd was described with the LACVP** effective core potential and basis set (18 explicit electrons) [11]. All other elements were described including the core electrons, using the Pople 6-31G** basis set [12], but with 3s combination of the six d-like functions reduced to five.

All geometries were optimized and evaluated for the correct number of imaginary frequencies through vibrational frequency calculations using the analytic Hessian. Zero imaginary frequencies correspond to a local minimum, whereas one imaginary frequency corresponds to a transition structure.

²³ See Appendix.

Implicit solvent effects for toluene were calculated with the Poisson-Boltzmann (PBF) continuum approximation [13], using the parameters $\epsilon = 2.38$ and solvent radius = 2.76 Å. Here we use the solvent-accessible surface of the molecular complex built using standard vdW radii. The solvation effects were calculated at geometries optimized for the gas phase.

Using the analytic Hessian we calculated the zero-point energy corrections at 0 K and added this to the solvation correction and the QM energy ($\Delta[E]$) to obtain the enthalpy at 0 K, $\Delta H[0 \text{ K}]$. Similarly, the vibrational frequencies were used to calculate the entropy and enthalpy corrections to 298.15 K, to obtain $(\Delta H - T\Delta S) = \Delta G[298.15 \text{ K}]$.

On the basis of previous results we expect that relative energies on the $\Delta H[0 \text{ K}]$ surface are accurate to ~ 3 kcal/mol for stable intermediates and to ~ 5 kcal/mol for transition structures. Probably the relative energies on the $\Delta G[298 \text{ K}]$ surface are less accurate, due to the use of the PBF model [14]. This methodology was found to be at an adequate level of theory in our previous study of (sparteine)Pd(Cl)(H) when compared to various other functionals and basis sets²⁴.

DFT is formulated in terms of Slater determinants built from Kohn-Sham orbitals that are calculated self-consistently. This process is consistent for states that are well described with closed-shell orbitals (up and down spins in the same orbitals), the normal situation for most DFT applications. However, in the studies carried out here it was necessary to also include some triplet states. With DFT this is done by having two more spin orbitals with up spin than down spin (unrestricted DFT or UDFT). We refer to this as the triplet state, but it need not be an eigenstate of the spin operator, S^2 . Rather, it is an eigenfunction of S_z , leading to $M_S = 1$. The problem with this formulation occurs when considering a transition between triplet and singlet states, a topic of this paper. Thus, starting with the true triplet orbitals of O₂ and calculating the energy of the singlet state should lead to a component of $^1\Delta_g$ with an excitation energy of 22.5 kcal/mol. In fact, UDFT gives an excitation energy of 10.5 kcal/mol. The reason is that the $M_S = 0$ wavefunction we consider to describe the

²⁴ See Chapter 1.

singlet state also has a mixture of triplet character. This can be treated by applying the spin projection operator, which will lead to a rigorous energy for the singlet-triplet splitting (20.5 kcal/mol) [15a] but neither the orbitals nor the geometry are optimum after spin projection. Bally and Borden have suggested simply doubling the calculated energy gap in order to approximate the true gap, which in this case yields an energy gap of 21.0 kcal/mol for O₂ [15b]. Thus, in the case of O₂ both methods produce similar results. All results reported here are UDFT.

5.3 Results and Discussion

5.3.1 *Cis/Trans* Isomerisation

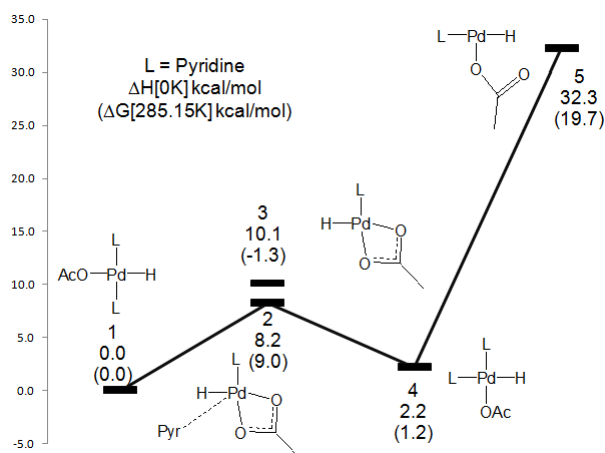


Figure 5.3. Calculated mechanism for *cis/trans* isomerisation for (pyr)₂PdHOAc in toluene

As mentioned above it is our belief that both *cis* and *trans* species (**1** and **4**) are important in these catalytic processes as it is likely that both exist in the reaction mixture. In addition to using both *cis* and *trans* as starting points for the reoxidation we also examined the interconversion between the two (Figure 5.3). A significant aid to this process is the relative stability of structures **2** and **3** ($\Delta H = 8.2$ and 10.1 kcal/mol), which differ only by the inclusion of a free pyridine molecule, with **3** being downhill 1.3 kcal/mol on the free energy surface. This stability is due in large part to the OAc ligands ability to bind η^2

maintaining the square planar Pd^{II} geometry which can be seen by comparing **3** directly with **5** (the result of losing the pyridine *cis* to the acetate in the *trans* species) where the acetate can't bind η^2 and as a result the Pd^{II} T-complex is significantly uphill ($\Delta H = 32.3$ kcal/mol). Rigorous transition states were not found for the conversion between **2** and **1** or **3** but constrained examinations of the surrounding potential energy surface²⁵ give approximate barriers of 15.1 kcal/mol for **2** \rightarrow **1** and 13.8 kcal/mol **2** \rightarrow **3** ($\Delta G^\ddagger_{\text{approx}} = 16.3$ and 14.9 kcal/mol).

5.3.2 Direct Insertion Pathway

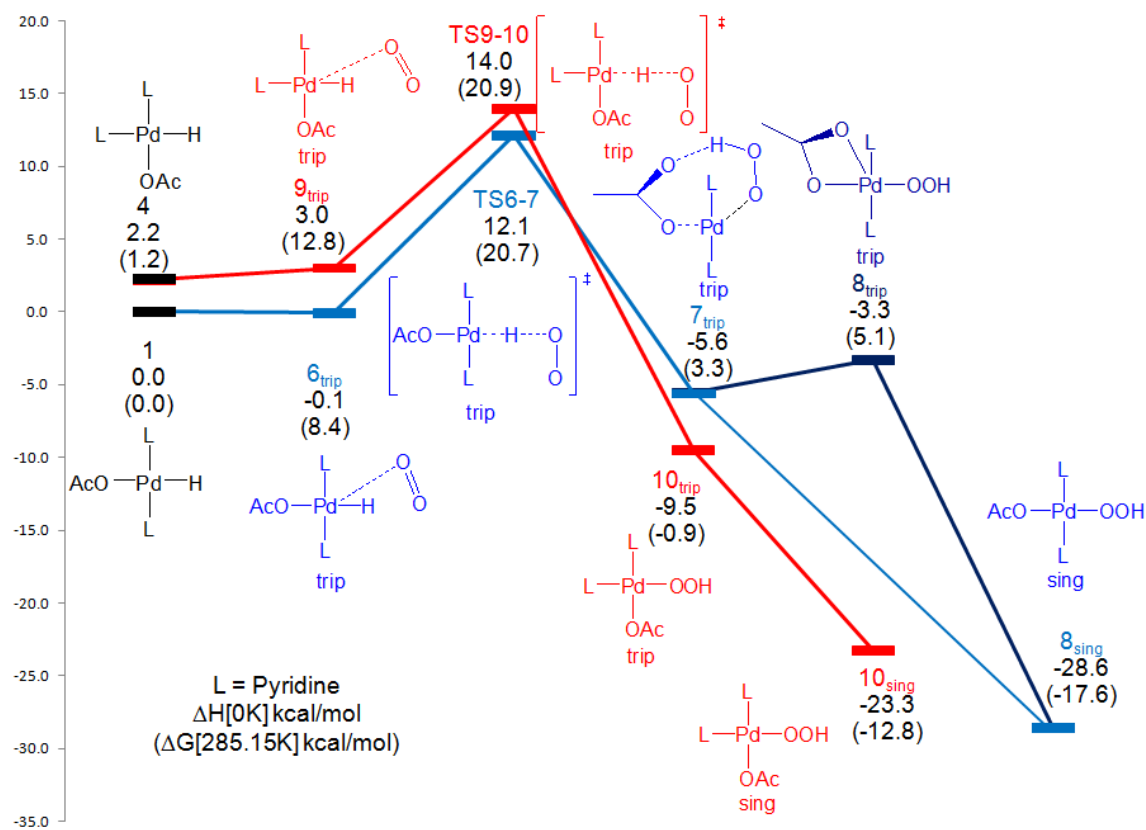


Figure 5.4. Calculated mechanism for the direct O₂ insertion pathway for (pyr)₂PdHOAc + O₂ \rightarrow (pyr)₂Pd(OOH)OAc in toluene for *cis* (red line) and *trans* (blue and navy lines)

²⁵ For both cases the free pyridine in **2** was systematically brought closer to the Pd while being forced to remain 90° from the H for the *trans* case and 90° from the other pyridine for the *cis* case.

5.3.2.1 *Trans* Pathway

Starting from *trans*-(pyridine)₂-Pd^{II}HOAc (**1**, Figure 5.4) we introduced (triplet) molecular oxygen which lead immediately to the formation of a weakly bound van der Waals complex [(pyr)₂PdHCl]•O₂ **6**_{trip} with $\Delta H = -0.1$ kcal/mol. There is negligible electron transfer between the O₂ and the Pd complex. Spin analysis shows that all unpaired spins in **6**_{trip} are on the O₂ fragment (one π^* orbital in the plane, hereafter the σ electron, and the other π^* orbital perpendicular to the plane, hereafter the π electron).

From **6**_{trip} we find transition state for direct O₂ insertion. Here the transition state, **TS6-7** (Figure 5.5 left), has the triplet O₂ positioned to abstract the H from the Pd with $\Delta H^\ddagger = 12.1$ kcal/mol. Thus from **1** to **TS6-7** the Pd-H bond length stretches from 1.55 to 1.68 Å, indicating a decrease in bond order from 1 to ~ 0.7 . At the same time the O-O bond distance increases from 1.20 to 1.27 Å, indicating a decrease in bond order of ~ 0.2 . On the other hand, the O-H distance of 1.30 Å (compared to 0.96 Å in HO₂) indicates the O-H bond has not yet formed. At this point the π unpaired spin (perpendicular to the O₂-H-Pd plane) remains on the O₂, while the σ unpaired spin (in the plane) has partly delocalized onto the Pd d_{x²-y²} orbital (where Pd-H is the x direction and the plane is the xy plane). Spin population for the O₂ moiety is 1.43 (with 0.66 on the O nearest to Pd), and that for Pd is 0.39.

From **TS6-7** the energy falls monotonically by 17.7 kcal/mol while the HO₂ moves out of the square plane toward the OAc ligand to form **7**_{trip} in which the H is now bonded to one O of the O₂ (H-O = 1.06 Å) while the other O is now directed toward the Pd (Pd-O = 2.48 Å). $\Delta H = -5.6$ kcal/mol with respect to **1**. **7**_{trip} is best described as a Pd^I T-complex with unpaired spin in the orbital formerly covalently bonded to the hydride, while the hydrogen in the HO₂• radical is coordinating to the *trans*-OAc moiety (H-O_γOAc = 1.43 Å). The spin density for the O₂ moiety is 1.05 (0.67 of which resides on the O nearest Pd), and that for Pd is 0.78. Since the unpaired orbitals are orthogonal by symmetry and localized on different centers, they have little interaction and **7**_{trip} is a biradical. Indeed,

the Pd-O bond distance of 2.48 Å indicates little bonding at all, compared to the significantly shorter value of 2.00 Å expected for a Pd^{II}-O single bond. The O-O bond distance of 1.33 Å is typical of a peroxy radical species (O-O = 1.33 Å in free HO₂•), halfway between common single and double bond distances of 1.48 and 1.21 Å. The O-H bond distance of 0.97 Å is close to that of free HO₂• (1.00 Å). Finally, the Pd-O_{ac} bond distance of 2.34 Å and the Pd-N distances of 2.15 Å are elongated by 0.26 and 0.06 Å compared to the bond lengths in the corresponding Pd^{II}OOH complex, as expected for a Pd^I center.

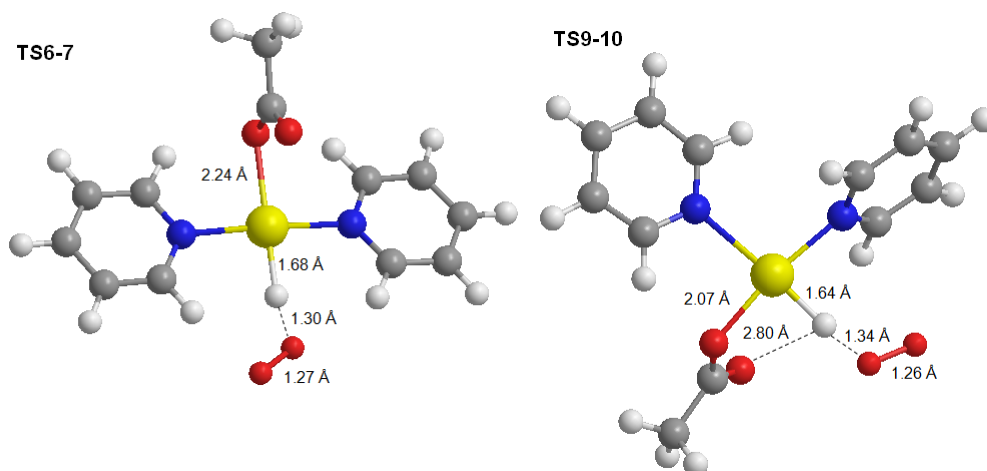


Figure 5.5. Detailed transition state structures along the *trans* (left) and *cis* (right) direct O₂ insertion pathways.

Conversion to the singlet state and relaxation leads to **8_{sing}**, with $\Delta H = -26.8$ kcal/mol. **8_{sing}** is clearly a Pd^{II}OOH complex: the Pd-O bond distance of 2.00 Å is consistent with it being a covalent Pd^{II}-O bond, while the O-O bond distance of 1.45 Å is slightly shorter than a normal single bond distance of 1.48 Å. The O-H bond distance of 0.97 Å is consistent with an O-H bond distance in H₂O₂. The Pd-O_{ac} bond distance of 2.08 Å and the Pd-N distances of 2.09 and 2.10 Å are as expected for Pd^{II}.

As discussed in Section 5.1, spin conversions in related complexes have been thoroughly examined and we feel it is unnecessary to calculate a MECP for the

conversion of **7_{trip}** to **8_{sing}**. Alternatively rearrangement from **7_{trip}** can lead slightly uphill to species **8_{trip}**, $\Delta H = -3.3$ kcal/mol as shown in Figure 5.4. This species is very similar to **7_{trip}** except for the loss of H-bonding between the hydroperoxo H and the OAc group, a decrease in Pd-O distance to 2.06 Å and an increase in the O-Pd-O angle from 120.3° to 168.9°. Conversion to the singlet state and relaxation again leads to **8_{sing}** and we feel it provides no new information to examine the MECP for the conversion of **8_{trip}** to **8_{sing}**. From here reaction with a second equivalent of HOAc completes the catalytic cycle by producing Pd^{II}OAc₂ and H₂O₂.

5.3.2.2 *Cis* Pathway

Starting from *cis*-(pyridine)₂-Pd^{II}HOAc (**4**, Figure 5.4, $\Delta H = 2.2$ kcal/mol) we introduced (triplet) molecular oxygen which lead immediately to the formation of a weakly bound van der Waals complex [(pyr)₂Pd^{II}HCl]•O₂ **9_{trip}** with $\Delta H = -3.0$ kcal/mol. There is negligible electron transfer between the O₂ and the Pd complex. Spin analysis shows that all unpaired spins in **7_{trip}** are on the O₂ fragment (one π^* orbital in the plane, hereafter the σ electron, and the other π^* orbital perpendicular to the plane, hereafter the π electron).

From **7_{trip}** we find the transition state for direct O₂ insertion. Here the transition state, **TS9-10** (Figure 5.5 right), has the triplet O₂ positioned to abstract the H from the Pd with $\Delta H^\ddagger = 14.0$ kcal/mol. Thus from **4** to **TS9-10** the Pd-H bond length stretches from 1.53 to 1.64 Å, indicating a decrease in bond order from 1 to ~ 0.7 . At the same time the O-O bond distance increases from 1.20 to 1.26 Å, indicating a decrease in bond order of ~ 0.2 . On the other hand, the O-H distance of 1.40 Å (compared to 0.96 Å in HO₂) indicates the O-H bond has not yet formed. At this point the π unpaired spin (perpendicular to the O₂-H-Pd plane) remains on the O₂, while the σ unpaired spin (in the plane) has partly delocalized onto the Pd $d_{x^2-y^2}$ orbital (where Pd-H is the x direction and the plane is the xy plane). Spin population for the O₂ moiety is 1.52 (with 0.72 on the O nearest to Pd), and that for Pd is 0.40.

From **TS9-10** the energy falls monotonically by 17.7 kcal/mol while the HO₂ moves out of the square plane toward the OAc ligand to form **10_{trip}** in which the H is now bonded to one O of the O₂ (H-O = 1.09 Å) while the other O is now bound to the Pd (Pd-O = 2.26 Å). $\Delta H = -9.5$ kcal/mol with respect to **1**. **10_{trip}** is best described as a square planar Pd^I complex with unpaired spin in the orbital formerly covalently bonded to the hydride, while the HO₂• is coordinating to the Pd (H-O _{γ} OAc = 1.43 Å). The spin density for the O₂ moiety is 1.04 (0.66 of which resides on the O nearest Pd), and that for Pd is 0.78. Since the unpaired orbitals are orthogonal by symmetry and localized on different centers, they have little interaction and **10_{trip}** is a biradical. Indeed, the Pd-O bond distance of 2.26 Å indicates a weak donor-acceptor bond, compared to the significantly shorter value of 2.00 Å expected for a Pd^{II}-O single bond. The O-O bond distance of 1.33 Å is typical of a peroxy radical species (O-O = 1.33 Å in free HO₂), halfway between common single and double bond distances of 1.48 and 1.21 Å. The O-H bond distance of 1.09 Å is slightly elongated compared to that of free HO₂• (1.00 Å). Finally, the Pd-O _{α} OAc bond distance of 2.27 Å and the Pd-N distances of 2.25 Å for both the *cis* and *trans* N's are elongated by 0.20, 0.10, and 0.12 Å compared to the bond lengths in the corresponding Pd^{II}OOH complex, as expected for a Pd^I center.

Conversion to the singlet state and relaxation leads to **10_{sing}**, with $\Delta H = -23.3$ kcal/mol. **10_{sing}** is clearly a Pd^{II}OOH complex: the Pd-O bond distance of 1.97 Å is consistent with it being a covalent Pd^{II}-O bond, while the O-O bond distance of 1.43 Å is slightly shorter than a normal single bond distance of 1.48 Å. The O-H bond distance of 0.98 Å is consistent with an O-H bond distance in H₂O₂. The Pd-O_{OAc} bond distance of 2.07 Å and the Pd-N distances of 2.15 (*cis* to OAc) and 2.13 Å (*trans* to OAc) are as expected for Pd^{II}. As discussed in earlier spin conversions in related complexes have been thoroughly examined and we feel it is unnecessary to calculate a MECF for the conversion of **10_{trip}** to **10_{sing}**. From here reaction with a second equivalent of HOAc completes the catalytic cycle by producing Pd^{II}OAc₂ and H₂O₂.

5.3.3 Pd⁰ Pathway: Unassisted Reductive Elimination of HOAc

5.3.3.1 *Cis* Pathway

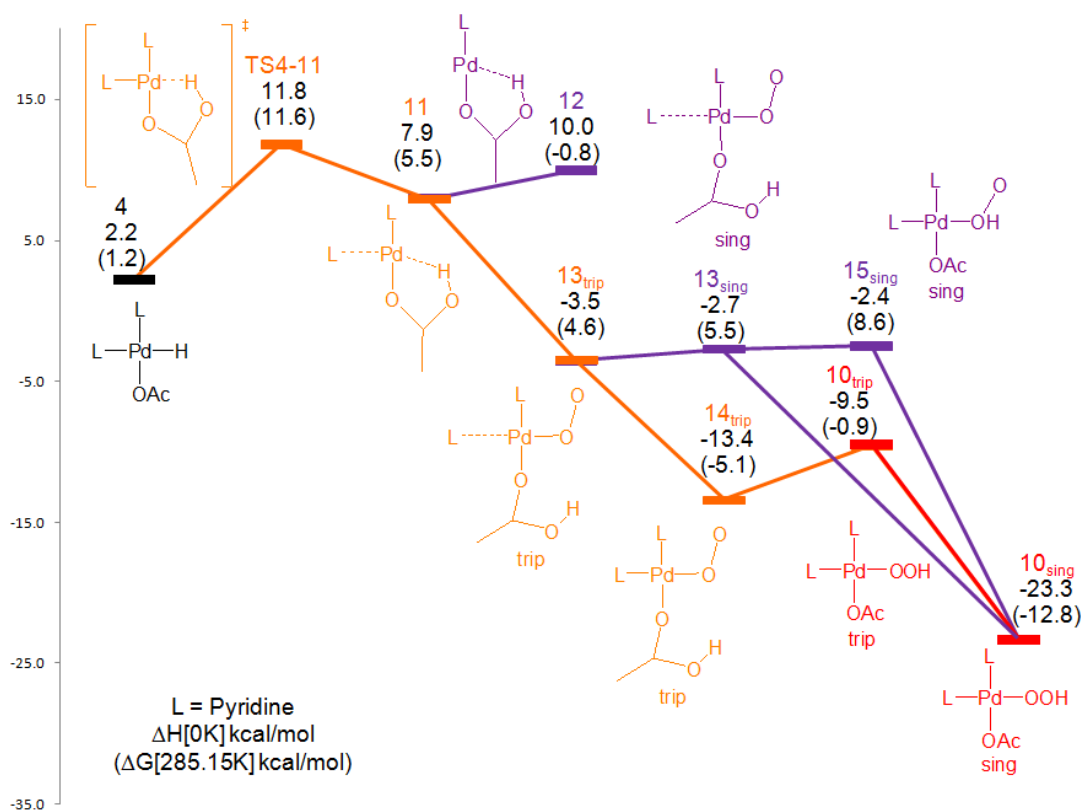


Figure 5.6. Calculated mechanism for the Pd⁰ pathway for *cis*-(pyr)₂PdHOAc + O₂ → *cis*-(pyr)₂Pd(OOH)OAc in toluene

Similar to Section 5.3.2.2, we start from *cis*-(pyridine)₂-Pd^{II}HOAc (4, Figure 5.6). From 4 we found a reductive elimination transition state, TS4-11 (Figure 5.7 left), in which the Pd complex goes through an intermolecular proton transfer from the Pd to the OAc resulting in the formation of a linear (pyr)Pd⁰-acetic acid complex, 11. The ΔH[‡] for TS4-11 is 11.8 kcal/mol. The Pd-H distance has stretched from 1.53 to 1.66 Å, indicating that the Pd-H bond has not completely broken, while the O_γOAc-H distance has decreased from 3.19 to 1.35 Å, indicating that the O_γOAc-H bond is not fully formed. The imaginary frequency corresponds to a mode in which the proton transfers from the Pd to O_γOAc with little other

molecular motion except for slight stretching of the Pd-N (*cis* to OAc) distance. Also of note is that the Pd-N (*cis* to OAc) distance has increased from 2.29 to 2.54 Å, indicating a loss of bonding, consistent with the hybridization of the available orbitals on a d^{10} Pd^0 species. As a result of the change in formal oxidation state of the Pd, the Pd- $\text{O}_{\alpha\text{OAc}}$ distance has increased from 2.04 Å to 2.16 Å.

From **TS4-11** the reaction proceeds to species **11**, a linear Pd^0 complex very similar to the preceding transition state. Indeed, the only significant changes are the further stretching of the Pd-H distance to 2.19 Å, the reduction of the $\text{O}_{\gamma\text{OAc}}\text{-H}$ distance to 1.01 Å, and further stretching of Pd-N (*cis* to OAc) distance to 4.30 Å indicating a complete loss of bonding to the second pyridine molecule. Species **4** is downhill with $\Delta H = 7.9$ kcal/mol. Complete removal of the free pyridine, **12**, is uphill only 2.1 kcal/mol (downhill on the free energy surface), but will not be pursued as reintroduction of the pyridine must immediately occur after introduction of O_2 to the system.

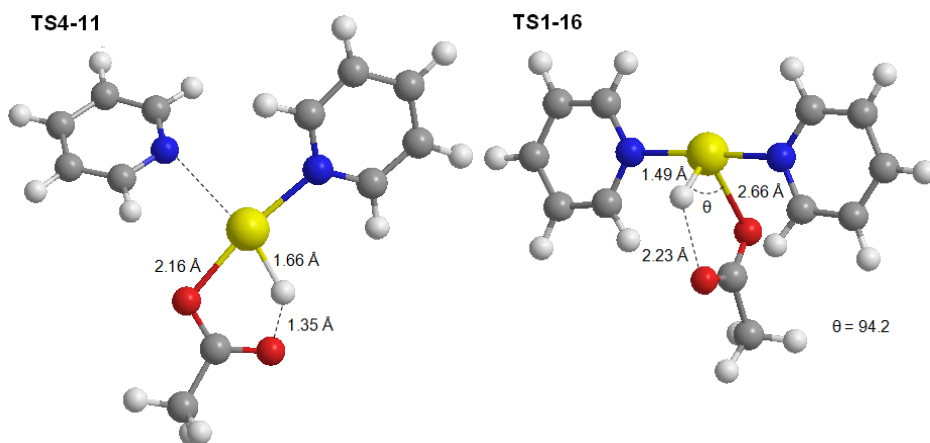


Figure 5.7. Detailed transition state structures along the *cis* (left) and *trans* (right) Pd^0 pathways

Instead of removing pyridine, triplet oxygen was added to **11**. We could not isolate any unbound $\text{Pd}^0\text{-O}_2$ species, as all attempts immediately optimized to a three-coordinate triplet $(\text{pyr})\text{Pd}^{\text{I}}(\eta^1\text{-O}_2)\text{-acetic acid}$ complex, **13_{trip}**, with a ΔH of -3.5 kcal/mol. The new Pd- O_2 bond and the electron transfer to form Pd^{I} are the main factors governing the exothermicity

of this step. In this species the N from the bound pyridine, the $O_{\alpha OAc}$, and the bonding O of the end-on O_2 moiety, and the Pd all reside in the plane. Spin analysis of complex **5_{trip}** shows a spin density of 1.29 on the two oxygens (0.71 on the O α to Pd and 0.58 on the O β to Pd), a spin density of 0.64 on the Pd atom, and the remaining spin density (0.07) distributed over the bound pyridine and HOAc, indicating that this complex should be considered a Pd^I species. The O-O bond of 1.30 Å is typical for a superoxide species (1.33 Å in free O_2^-), halfway between common single- and double-bond distances of 1.48 and 1.21 Å, respectively. The Pd-N distance of 3.97 Å (*cis* to OAc) indicates that the second pyridine remains unbound. The new Pd-O, O-H and $O_{\gamma OAc}$ -H bond lengths are 2.21, 1.55, and 1.12 Å.

At this point coordinating the second pyridine molecule to the Pd center to form species **14_{trip}** is downhill 9.9 kcal/mol (ΔH of -13.4 kcal/mol). The new structure has slightly longer Pd-N bonds of 2.29 Å and a hydrogen bond between the HOAc and the α O of the O_2 with a distance of 1.37 Å (down from 1.55 Å in **13_{trip}**). From here a proton transfer to the β O of the O_2 results in species **10_{trip}** presented above in Section 5.3.2.2 and will not be discussed further. Attempts to transfer the proton to the α O of the O_2 while maintaining the triplet spin configuration (**14_{trip}**, not shown) were unsuccessful and collapsed to either **10_{trip}** or **14_{trip}**.

As an alternate pathway spin conversion was considered from **13_{trip}** before recoordinating the second pyridine molecule to the Pd resulting in species **13_{sing}** (ΔH of -2.7 kcal/mol). From here a proton transfer to the β O of the O_2 results in species **10_{sing}** presented above in Section 5.3.2.2 and will not be discussed further. Alternatively proton transfer to the α O of O_2 may occur first, **15_{sing}** (ΔH of -2.4 kcal/mol). **15_{sing}** can proceed to species **10_{sing}** through a additional proton transfer to the β O of O_2 or could react with a second equivalent of HOAc completing the catalytic cycle by producing $Pd^{II}OAc_2$ and H_2O_2 .

5.3.3.2 *Trans* Pathway

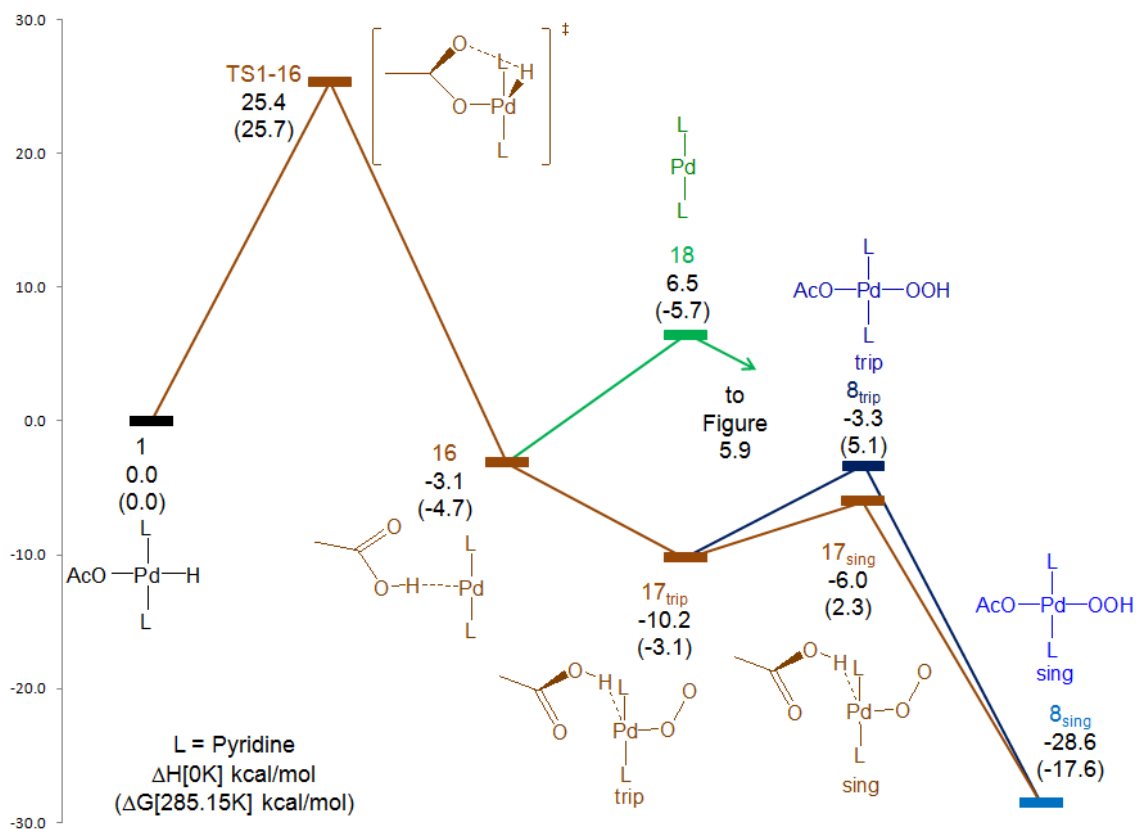


Figure 5.8. Calculated mechanism for the Pd^0 pathway for $\text{trans}-(\text{pyr})_2\text{PdHOAc} + \text{O}_2 \rightarrow \text{trans}-(\text{pyr})_2\text{Pd}(\text{OOH})\text{OAc}$ in toluene (continued from species 13 on Figure 5.9)

Similar to Section 5.3.2.1, we start from $\text{trans}-(\text{pyridine})_2\text{-Pd}^{\text{II}}\text{HOAc}$ (**1**, Figure 5.8). From **4** we found a reductive elimination transition state, **TS1-16** (Figure 5.7 right), in which the Pd complex goes through an intermolecular proton transfer from the Pd to the OAc resulting in the formation of a linear $(\text{pyr})_2\text{Pd}^0$ complex, **16**. The ΔH^\ddagger for **TS1-16** is 25.4 kcal/mol. This relatively high barrier is thought to be the result of considerable distortion from the square planar starting structure ($\theta = 94.2^\circ$) and the elongation of the $\text{Pd}-\text{O}_{\alpha\text{OAc}}$ distance from 2.18 to 2.66 Å required to gain close proximity between the H and the $\text{O}_{\gamma\text{OAc}}$. The $\text{Pd}-\text{H}$ distance has decreased from 1.55 to 1.49 Å, presumably due to the removal of the trans effect from the OAc, while the $\text{O}_{\gamma\text{OAc}}-\text{H}$ distance has decreased from 3.19 to 2.23 Å, indicating that the $\text{O}_{\gamma\text{OAc}}-\text{H}$ bond is not formed. The imaginary frequency corresponds to

a mode in which the proton transfers from the Pd to $O_{\gamma OAc}$ with little other molecular motion. Also of note is that the Pd-N distances have had little change increasing from 2.08 to 2.10 Å²⁶.

From **TS1-16** the reaction proceeds to species **16**, a linear Pd^0 with acetic acid forming a weakly bound van der Waals complex with the H pointed directly at the Pd. The significant changes in this structure compared to the preceding transient state are the further stretching of the Pd-H distance to 2.14 Å, the reduction of the $O_{\gamma OAc}$ -H distance to 1.01 Å, and further stretching of Pd- $O_{\alpha OAc}$ distance to 3.91 Å indicating a complete loss of bonding. Species **16** is downhill with $\Delta H = -3.1$ kcal/mol.

Introduction of triplet oxygen at this point leads directly to a three-coordinate triplet *trans*-(pyr)₂ $Pd^I(\eta^1-O_2)$ species with acetic acid still forming a weakly bound van der Waals complex, **17_{trip}**. We could not isolate any unbound Pd^0-O_2 species, as all attempts immediately optimized to **17_{trip}**, with a ΔH of -10.2 kcal/mol. The new Pd- O_2 bond and the electron transfer to form Pd^I are the main factors governing the exothermicity of this step. Spin analysis of complex **17_{trip}** shows a spin density of 1.56 on the two oxygens (0.79 on the O α to Pd and 0.77 on the O β to Pd), a spin density of 0.40 on the Pd atom, and the remaining spin density (0.04) distributed over the pyridines and the HOAc, suggesting that this complex should be considered a Pd^I species. The O-O bond of 1.27 Å is somewhat shorter than that of superoxide (1.33 Å in free O_2^-), halfway between common single- and double-bond distances of 1.48 and 1.21 Å, respectively. The new Pd-O bond length is 2.34 Å.

At this point spin conversion leads to species **17_{sing}** ($\Delta H = -6.0$ kcal/mol) with almost no change in geometry. From here a proton transfer to the β O of the O_2 results in species **8_{sing}**, presented above in Section 5.3.2.1 and will not be discussed further. Alternatively the

²⁶ It should be pointed out here that this transition state is almost identical to the corresponding transition state for (IMes)₂PdHOAc from ref [42] discussed in Section 5.1.

proton transfer to may occur first to form species **8_{trip}** followed by the spin conversion once again leading to **8_{sing}**.

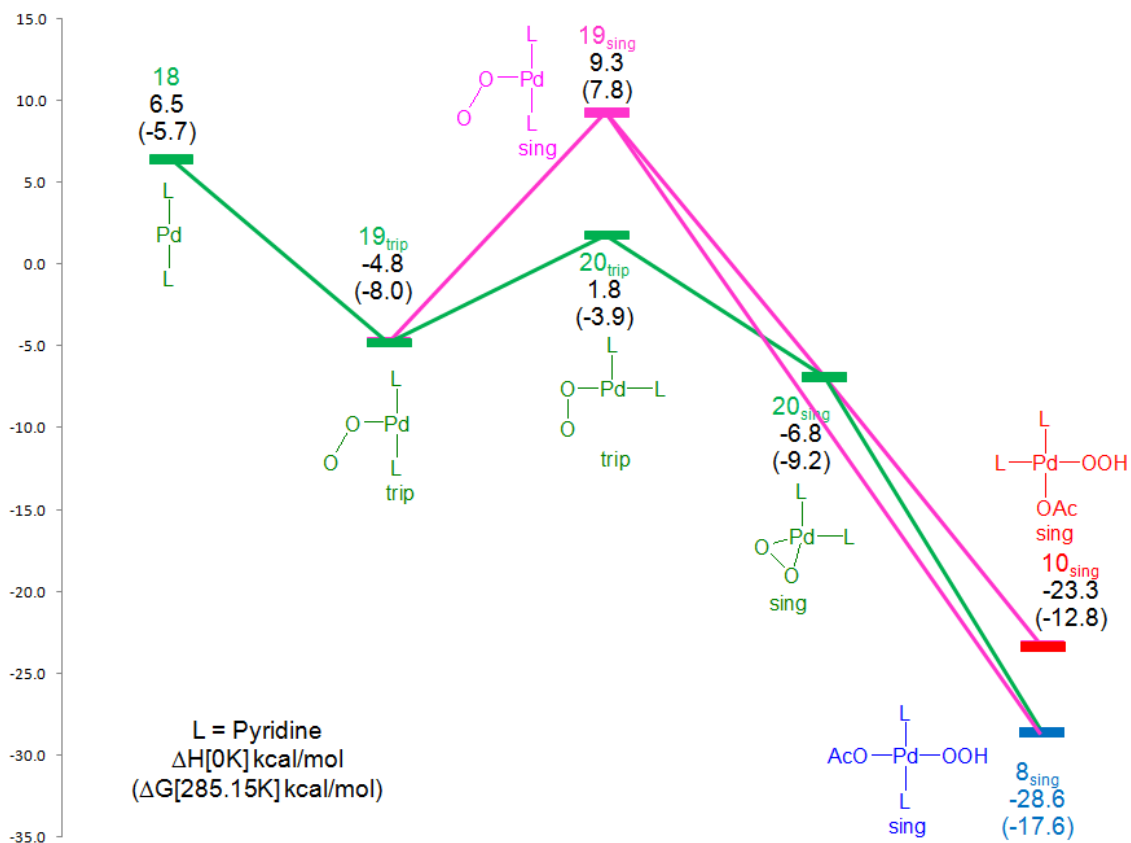


Figure 5.9. Continuation of the calculated mechanism for the Pd^0 pathway from species 13.

As an alternative to proceeding through species **17_{trip}** complete removal of the HOAc from species **16** leads directly to **18** and is uphill 9.6 kcal/mol (downhill 1 kcal/mol on the free energy surface). The geometry of **18** is identical to **16** without the HOAc. From **18** addition of O_2 leads directly to a three-coordinate triplet *trans*-(pyr)₂ $\text{Pd}^{\text{I}}(\eta^1\text{-O}_2)$ species (Figure 5.9). We could not isolate any unbound $\text{Pd}^0\text{-O}_2$ species, as all attempts immediately optimized to **19_{trip}**, with a ΔH of -4.8 kcal/mol. The geometry of **19_{trip}** is identical to **17_{trip}** without the HOAc.

From **19**_{trip} it is uphill 6.6 kcal/mol to the corresponding *cis* species **20**_{trip} ($\Delta H = 1.8$ kcal/mol). Spin analysis of complex **17**_{trip} shows a spin density of 1.40 on the two oxygens (0.76 on the O α to Pd and 0.64 on the O β to Pd), a spin density of 0.54 on the Pd atom, suggesting that this complex should be considered a Pd^I species. The O-O bond of 1.30 Å is similar to that of superoxide (1.33 Å in free O₂⁻), halfway between common single- and double-bond distances of 1.48 and 1.21 Å, respectively. The new Pd-O bond length is 2.06 Å.

At this point spin conversion leads to species **20**_{sing} ($\Delta H = -6.8$ kcal/mol). The new O-O bond distance is slightly longer (1.38 Å) and the new Pd-O bond lengths are 2.00 Å. From here, reaction with HOAc results in either species **8**_{sing} (Section 5.3.2.1) or **10**_{sing} (Section 5.3.2.2) and will not be discussed further. Alternatively spin conversion could occur at **19**_{trip} resulting in **19**_{sing} with $\Delta H = 9.3$ kcal/mol. From here rearrangement to **20**_{sing} is feasible or direct reaction with HOAc result in either species **8**_{sing} or **10**_{sing} and will not be discussed further.

5.3.4 Pd⁰ Pathway: HOAc-Assisted Reductive Elimination HOAc

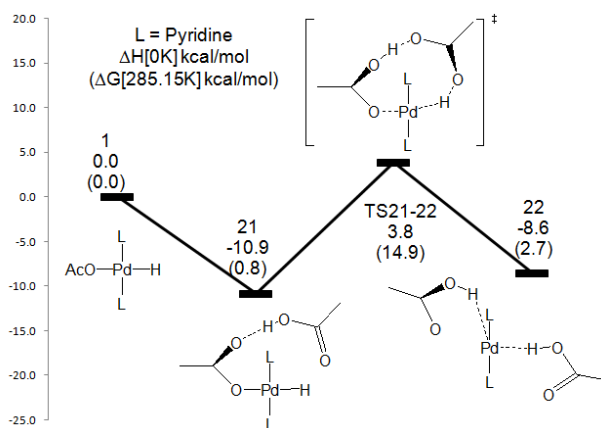


Figure 5.10. Calculated mechanism for the Pd⁰ pathway with the inclusion of an additional HOAc molecule

In Section 5.3.3.2 it was demonstrated that direct reductive elimination of HOAc from *trans*-(pyridine)₂-Pd^{II}HOAc was considerably high in energy. As an alternative pathway for this process, assisted reductive elimination was examined in which an additional HOAc molecule (present in catalytic systems) was added to the optimization. From **4** we first found a stable van der Waals complex between *trans*-(pyr)₂PdHOAc and the addition HOAc (Figure 5.10, **21**). The additional acid molecule lies out of the plan forming hydrogen bonds to the H of the Pd complex (O-H distance = 1.61 Å). ΔH for this is −10.9 kcal/mol (ΔG = 0.8 and further ΔHs for the HOAc-assisted steps will be with respect to this species referred to as ΔH^a).

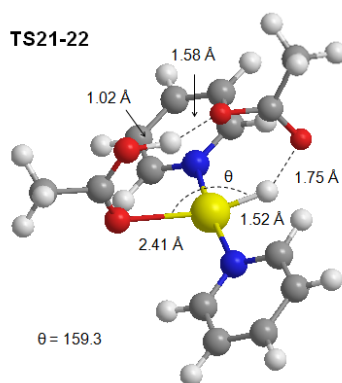


Figure 5.11. Detailed transition state structures along the HOAc-assisted Pd⁰ pathways

Next we find an acid-assisted reductive elimination transition state, **TS21-22** (Figure 5.11), in which the Pd complex goes through a proton transfer from the Pd to the OAc with the aid of the additional HOAc molecule (now HOAc_{add}) resulting in the formation of a linear (pyr)₂Pd⁰ complex, **22**. The ΔH[‡] for **TS21-22** is 3.8 kcal/mol (ΔH^{‡a} = 14.7 kcal/mol). This barrier is considerably lower in energy (both ΔH^a and ΔG) than the unassisted pathway present above. This difference is most likely a result of relaxation toward the square planar starting structure (θ = 159.3°) and the shorter Pd-O_{αOAc} distance of 2.41 Å. The transition state is a distorted nine-member ring consisting of the Pd and both carboxylic acid moieties. The Pd-H distance has now only decreased from 1.55 to 1.52 Å, while the O_{γOAc}-H_{add} distance has decreased from 1.54 to 1.02 Å, indicating that the O_{γOAc}-

H_{add} bond has already formed. The $H_{\text{add}}-O_{\text{add}}$ distance has increased to 1.58 Å on the order of a H-bond while the $O_{\text{add}}-H_{\text{Pd}}$ distance is now 1.75 Å. The imaginary frequency corresponds primarily to a mode in which H_{Pd} transfers from the Pd to O_{add} with $H-O_{\gamma\text{OAc}}$ and $\text{Pd}-O_{\alpha\text{OAc}}$ stretching to a lesser extent. Despite the almost complete transfer of H_{add} in this transition state, it is the concerted dual proton transfer transition state and not simply a proton transfer from $\text{Pd}(\text{HOAc})\text{H}^+$ to OAc^- , as examination of the intermediates directly preceding and following this transition state are indeed **21** and **22**. From **22** this pathway can join the previously presented mechanism at species **16** in Figure 5.8.

5.4 Conclusions

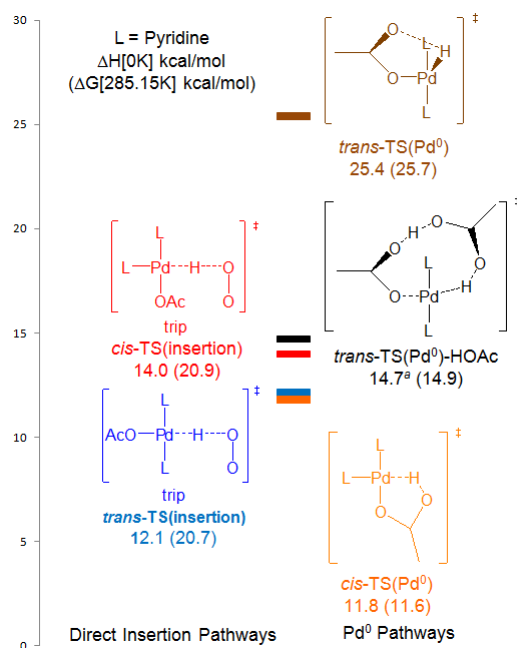


Figure 5.12. Comparison of *cis*- Pd^0 (orange), *trans*- Pd^0 (brown), *trans*- Pd^0 (HOAc assisted, black), *cis*-insertion (red), and *trans*-insertion (blue) transition state energies $(\text{pyr})_2\text{PdHOAc} + \text{O}_2 \rightarrow (\text{spar})\text{Pd}(\text{OOH})\text{OAc}$ in toluene. ^a ΔH value with respect to *trans*-(pyr)₂ $\text{PdHOAc}\cdot\text{HOAc}$.

We conclude that both the Pd^0 and the direct insertion pathways presented above are all indeed feasible for $(\text{pyr})_2\text{PdXOAc}$ and we outlined five competing pathways involving the

cis and *trans* forms of the hydride as well as the incorporation of an additional HOAc molecule. The five different pathways proceed as follows:

Trans-(pyr)₂PdOAcH direct insertion involves first the abstraction of the H atom from the palladium center ($\Delta H^\ddagger = 12.1$ kcal/mol, $\Delta G^\ddagger = 20.7$ kcal/mol, Figure 5.12, **blue**) and the immediate formation of *trans*-(pyr)₂Pd^IOAc/HOO• triplet van der Waals complex. This then undergoes spin conversion to singlet and relaxation to form *trans*-(pyr)₂Pd(OOH)OAc. Reaction with a second equivalent of HOAc completes the catalytic cycle by producing Pd^{II}OAc₂ and H₂O₂.

Cis-(pyr)₂PdOAcH direct insertion involves first the abstraction of the H atom from the palladium center ($\Delta H^\ddagger = 14.0$ kcal/mol, $\Delta G^\ddagger = 20.9$ kcal/mol, Figure 5.12, **red**) and the immediate formation of *cis*-(pyr)₂Pd^I(OOH)OAc triplet. This then undergoes spin conversion to the *cis*-(pyr)₂Pd(OOH)OAc singlet. Reaction with a second equivalent of HOAc completes the catalytic cycle by producing Pd^{II}OAc₂ and H₂O₂.

Cis-(pyr)₂PdOAcH Pd⁰ pathway involves first the intramolecular of the hydride to form HOAc while maintaining the interaction between the OAc moiety and the Pd ($\Delta H^\ddagger = 11.8$ kcal/mol, $\Delta G^\ddagger = 11.6$ kcal/mol, Figure 5.12, **orange**) and the loss of one of the pyridine ligands (initially trans to H) to form *trans*-(pyr)Pd⁰(HOAc). Introduction of O₂ and reattachment of the second pyridine results in the formation of *cis*-(pyr)₂Pd^I(η^1 -O₂)(HOAc) triplet which then undergoes a proton transfer followed by spin conversion to the *cis*-(pyr)₂Pd(OOH)OAc singlet. Reaction with a second equivalent of HOAc completes the catalytic cycle by producing Pd^{II}OAc₂ and H₂O₂.

Unassisted *trans*-(pyr)₂PdOAcH Pd⁰ pathway involves first the reductive elimination of HOAc from a strained seesaw structure ($\Delta H^\ddagger = 25.4$ kcal/mol, $\Delta G^\ddagger = 25.7$ kcal/mol, Figure 5.12 **brown**) to form the corresponding *trans*-(pyr)₂Pd⁰/(HOAc) van der Waals complex. Upon introduction of O₂, reaction with the HOAc fragment and spin conversion, the reaction proceeds to the *trans*-(pyr)₂Pd(OOH)OAc singlet. Reaction

with a second equivalent of HOAc completes the catalytic cycle by producing Pd^{II}OAc₂ and H₂O₂.

HOAc-assisted *trans*-(pyr)₂PdOAcH Pd⁰ pathway involves first the reductive elimination of HOAc from a nearly planar (H-Pd-O angle = 159.3°) through a 9-membered ring transition state with the assistance of a second HOAc molecule ($\Delta H^{\ddagger a} = 14.7$ kcal/mol, $\Delta G^{\ddagger} = 14.9$ kcal/mol, Figure 5.12 **black**) to form the corresponding *trans*-(pyr)₂Pd⁰/(HOAc) van der Waals complex. Upon introduction of O₂, reaction with the HOAc fragment and spin conversion the reaction proceeds to the *trans*-(pyr)₂Pd(OOH)OAc singlet. Reaction with a second equivalent of HOAc completes the catalytic cycle by producing Pd^{II}OAc₂ and H₂O₂.

The barrier for the *cis*-Pd⁰ pathway is lower in energy than that of the direct oxygen insertion mechanism ($\Delta\Delta H^{\ddagger} = 2.2$ kcal/mol, $\Delta\Delta G^{\ddagger} = 9.3$ kcal/mol) and the barrier for the HOAc-assisted *trans*-Pd⁰ pathway is lower in energy than that of the direct oxygen insertion mechanism ($\Delta\Delta H^{\ddagger} = -2.6$ kcal/mol, $\Delta\Delta G^{\ddagger} = 5.8$ kcal/mol). In addition the barrier for *cis*-Pd⁰ pathway is the lowest overall with ($\Delta H^{\ddagger} = 11.8$ kcal/mol, $\Delta G^{\ddagger} = 11.6$ kcal/mol). We also calculated a barrier for the *cis/trans* isomerisation ($\Delta H^{\ddagger} = 15.1$ kcal/mol, $\Delta\Delta G^{\ddagger} = 16.3$ kcal/mol) leading to the conclusion that interconversion doesn't occur before interaction with oxygen for either the *cis* or *trans* case although we still stress the belief that both the *cis* and *trans* species are likely to be present in catalytic systems. We believe these results should apply to all Pd systems which employ two monodentate donor ligands and a basic chelating X-ligand, and that our *cis*-Pd⁰ pathway and HOAc-assisted-Pd⁰ could alleviate some of the issues experienced for calculations of other ligand frameworks by others. Based on these results, we demonstrate that the incorporation of two monodentate ligands significantly favors the Pd⁰ pathways and the chelating HOAc moiety avoids the need of an exogenous base.

Together with our previous reports, we now have a complete picture of the two competing pathways at work in palladium oxidase systems with both a single bidentate

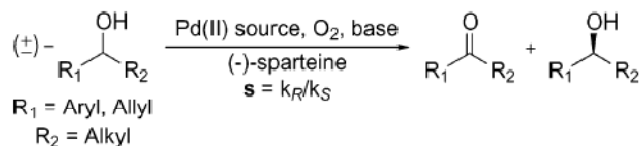
ligand or two monodentate ligands (both *cis* and *trans*) coupled with multiple X-ligands (OAc and Cl) in the presence of both exogenous acid or base consistent with reaction conditions. We expect this report together with our previous studies to provide a thorough framework for reactions of molecular oxygen with palladium hydrides.

Appendix

Enantioselective Oxidations of Secondary Alcohols by (–)-Sparteine-Pd^{II} Complexes

A.1 Introduction

Scheme A.1



²⁷Recent examples of alcohol oxidations by Pd^{II} complexes and molecular oxygen, in the absence of copper co-catalysts, demonstrate increasing efficiency and selectivity. Generally, the metal (ligated to sp² [1–3] or sp³ [4,5] nitrogen, DMSO [6,7], and common anions) and a catalytic amount of excess base enable the dehydrogenation of an organic substrate by O₂, producing water or hydrogen peroxide. A subset of these reactions is the enantioselective oxidation of secondary alcohols to ketones by a (–)-sparteine-PdX₂ catalyst (X = Cl, OAc), generating primarily H₂O₂ (Scheme A.1). Sparteine, an asymmetric

²⁷ Reproduced with permission from *J. Am. Chem. Soc.* **2004**, 126, 7967. Copyright 2004 American Chemical Society.

natural product able to coordinate to Pd by two sp^3 -nitrogen lone pairs, has engendered relative rates between (R) and (S) enantiomers of model aryl substrates of up to 47:1 [4,5]. It has also proven useful in the synthesis of biologically important molecules [8,9]. The aim of this work is to trace the observed characteristics of this catalyst, and less effective ones, to their microscopic causes.

Previous studies by the Stoltz [4] and Sigman [5] groups have shown that an array of natural and synthetic ligands exhibit a wide range of reaction rate and selectivity in kinetic resolutions. Also, systematic variations in the reactivity of the (–)-sparteine-PdX₂ complexes as a function of substrate have been mapped [10]. Basic additives such as Cs₂CO₃ accelerate turnover [11], presumably by aiding the deprotonation of the alcohol. A recent solvent screen [12] has shown chloroform offers rates and selectivities exceeding those previously measured in toluene. We used the specific kinetic data to guide our investigations, which in turn have revealed the atomistic factors that must be present to allow a ligand’s potential selectivity to evidence itself. Using 1-phenylethanol as a representative substrate, we examined the mechanism by which (–)-sparteine-PdCl₂ functions. Then the consequences of changing anions and solvents were studied. The details of the methods are presented in Section A.2. The mechanism is described in Section A.3 while the selectivities are discussed in Section A.4. Further discussion is in Section A.5 with the conclusions in Section A.6.

A.2 Computational Methodology

Reported solution-phase energies (E_{sol}) are the sum of gas-phase electronic energies and solvation energies computed with the Poisson-Boltzmann reactive field method. The gas-phase energy is evaluated with the B3LYP [13] collection of gradient-corrected density functionals using a 6-31G** [14–16] basis set for light atoms (with diffuse functions added to Cl atoms and O atoms in acetate groups), the LACVP [17] relativistic effective core potential for Pd (which treats the 4s, 4p, 4d, and 5s electrons explicitly [18]), and the LAV3P [19] relativistic effective core potential for I (5s and 5p explicitly), augmented with

a d-polarization shell as optimized by Höllwarth et al. [20]. The solvation energy is the difference between solvated and unsolvated calculation performed with the described basis set sans diffuse functions. The solvent is represented as a polarizable continuum (with dielectric ϵ) surrounding the molecular complex at an interface constructed by combining atomic van der Waal radii with the effective probe radius of the solvent. Charges are allowed to develop on this interface according to the electrostatic potential of the solute and ϵ then the polarized reaction field of the solvent acts back on the quantum mechanical description of the solute. The wave function of the complex is relaxed self-consistently with the reaction field to solve the Poisson-Boltzmann (PB) equations. Solvents were represented with the following parameters: toluene, $\epsilon = 2.379$, probe radius (rp) = 2.762 Å; chloroform, $\epsilon = 4.806$, rp = 2.514 Å; 1,2-dichloroethane, $\epsilon = 10.65$, rp = 2.513 Å. Generally the gas-phase structures were used in the solvation calculations. In some cases (the relative energies in Table A.1), the forces on the atoms from the reaction field of the solvent were used to optimize the structure of the solvated complex, allowing us to follow more precisely the effects of the dielectric. In such cases the relative energies are simply energy differences between solvent optimized structures.

Stable intermediates are completely relaxed, while transition states are characterized by no interatomic forces and the presence of exactly one imaginary vibrational frequency. When a transition-state structure included a displaced anion, we often were not able to eliminate an imaginary frequency corresponding to the relative motion of the unbound fragments (in addition to the imaginary frequency of the reaction coordinate.) This probably results from numerical approximations in the methods which make it difficult to completely relax the very soft modes associated with such a loosely bound complex. However, such modes lead to very low force constants and cause only a negligible deviation in the transition-state energy.

A.3 Mechanism

A.3.1 General

Discussions of mechanisms for alcohol oxidations by palladium usually invoke a β -hydride elimination from a Pd-alkoxide formed by substrate coordination and deprotonation. Rather than study an assumed sequence of intermediates, the mechanism for the reaction of interest was determined by hypothesizing and testing many routes, using the predicted energetics to eliminate unlikely steps. 1-Phenylethanol, free sparteine, and (sparteine)PdCl₂ in toluene were taken as reactants (the reference state for energies).

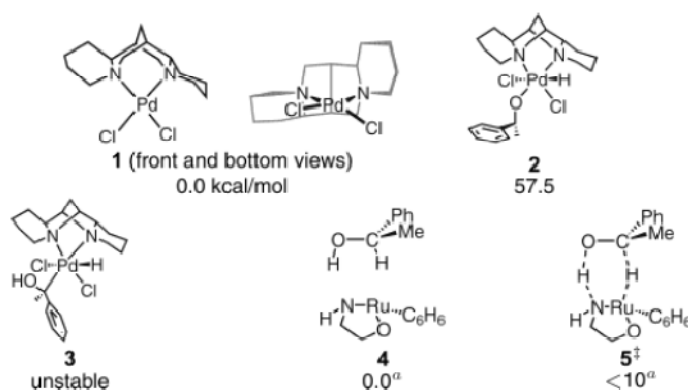


Figure A.1. ((-)-Sparteine)PdCl₂ and intermediates unlikely to participate in the oxidation mechanism. Energies (kcal/mol) for **1–3** are relative to **1** and include PB solvation by toluene ($\epsilon = 2.379$). ^a From [22]

Paths involving oxidative addition to form Pd^{IV} species were found to be quite unfavorable. The products of O-H (**2**) and C-H (**3**) addition lie 58 kcal/mol above the reactants or are altogether unstable (Figure A.1).

A slightly more feasible route comes by analogy to the ruthenium catalyst of Noyori et al. [21], generated from RuCl₂-(η^6 -benzene), β -amino alcohols, or N-tosyl-1,2-diamines, and strong base. That complex (represented by **4**) performs the same net transformation, *sec*-alcohol to ketone, in one pericyclic step, **5[‡]**. Yamakawa's calculations [22] suggest a

barrier of less than 10 kcal/mol must be overcome when reacting methanol with the coordinatively unsaturated compound **4**. There are two striking differences, however, between the Ru^{II} and Pd^{II} complexes: the unsaturation of the Ru atom allows it to immediately accept hydride from the alcohol, and the amido nitrogen can accept a proton without significant geometric rearrangement. No analogous transition state was found involving the Pd^{II} compound, regardless of which base accepted the alcoholic proton: Cl dissociating from Pd, a nitrogen of sparteine dissociating from Pd, or exogenous amine. The structures sampled during the search for a concerted mechanism lie more than 30 kcal/mol above the reactants, suggesting that the reaction on Pd consists of some combination of elementary steps.

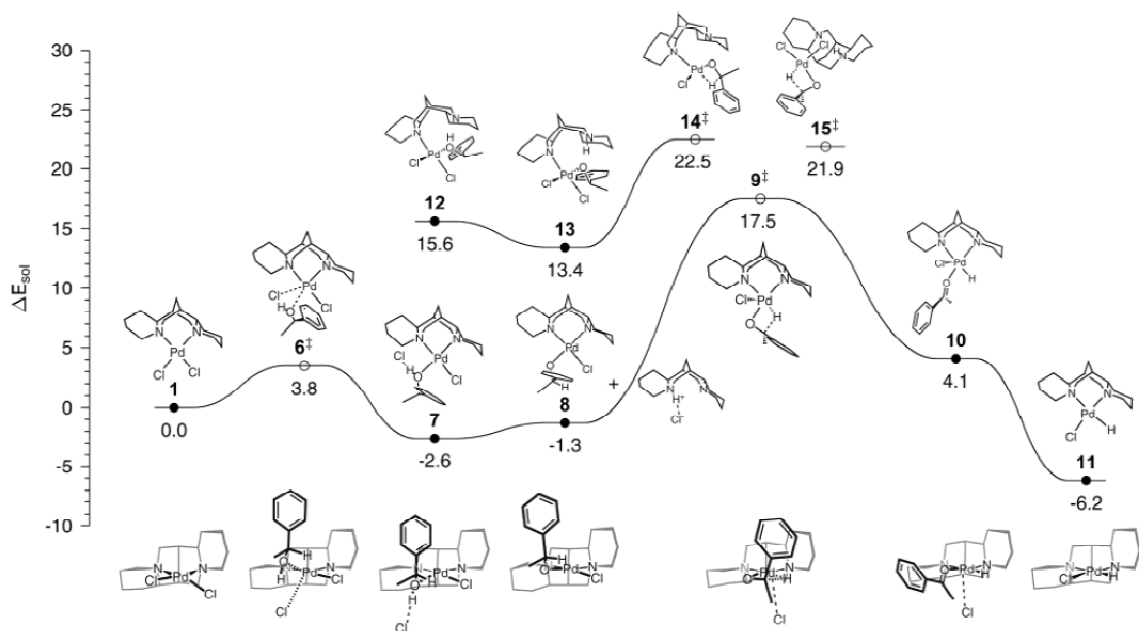


Figure A.2. Mechanism for the oxidation of (*R*)-1-phenylethanol by ((-)-sparteine)PdCl₂. Energies (kcal/mol) are relative to **1** and include PB solvation by toluene ($\epsilon = 2.379$). Images are projections of the 3D structures, with corresponding bottom views aligned below.

Many possible paths involving coordination of alcohol, deprotonation, and C-H activation by β -hydride elimination are imaginable if one allows both Cl and sparteine to be displaced from the metal during the reaction. The lowest-energy route through these steps

is plotted in Figure A.2, along with some energetically competitive alternatives [23]. The alcohol enters the coordination sphere by associative substitution for a Cl^- ion (**1**, **6[‡]**, **7**). The predicted barrier for this displacement ($\Delta E_{\text{sol}}^\ddagger = 3.8$ kcal/mol) is lowered by the $\text{Cl}^- \cdots \text{H-OR}$ hydrogen bond which forms as the substrate approaches. The free Cl^- ion in **7** is not basic enough to deprotonate the bound alcohol alone, but the combination of Cl^- and an exogenous sparteine molecule is. Deprotonation of the coordinated alcohol by free sparteine has not been simulated (due to the large number of atoms and soft degrees of freedom associated with a second, unbound ligand), but the energetic barrier of this step is believed to be much smaller than that of the subsequent β -hydride elimination. (Such is the case for benzyl alcohol [10]). The products of deprotonation in the models are the bound alkoxide **8** and a separate sparteine- H^+Cl^- ion pair, which is predicted to be more stable than separate HCl and sparteine by $\Delta E_{\text{sol}} = 25.2$ kcal/mol. The relevance of structure **8** as an intermediate is supported by the recent X-ray characterization of an analogous species (in which the methyl group of the substrate is fluorinated) with the same structure [24].

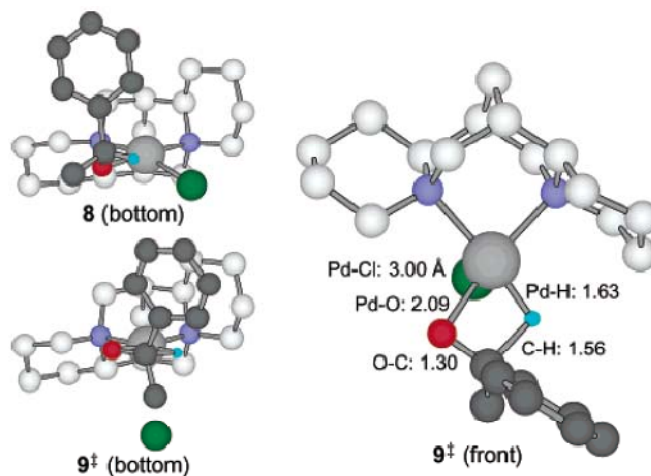


Figure A.3. Pd-alkoxide **8** and β -hydride elimination transition state **9[‡]**. Sparteine carbon atoms in light gray, chlorine in green

The alkoxide **8** is found to undergo β -hydride elimination through a four-coordinate transition state **9[‡]**, in which the remaining Cl atom is displaced to an axial, outer-sphere position 3.00 Å from Pd (Figure A.3). The ketone produced (in **10**) is assumed to be easily

replaced by the Cl atom, generating the more stable Pd-hydride complex **11**. A five-coordinate transition state was sought in which the Cl atom remains bound and the β -hydrogen approaches Pd from out of the square plane to replace the Pd-O bond. That such a structure could not be found is consistent with the fact that palladium's d-orbitals are correctly organized to allow a "2 + 2" metathesis reaction in the four-coordinate geometry **9**[‡], but not in a five-coordinate geometry [25]. Attempts to find a five-coordinate transition state relaxed to the four-coordinate structure by displacing the Cl atom from the metal.

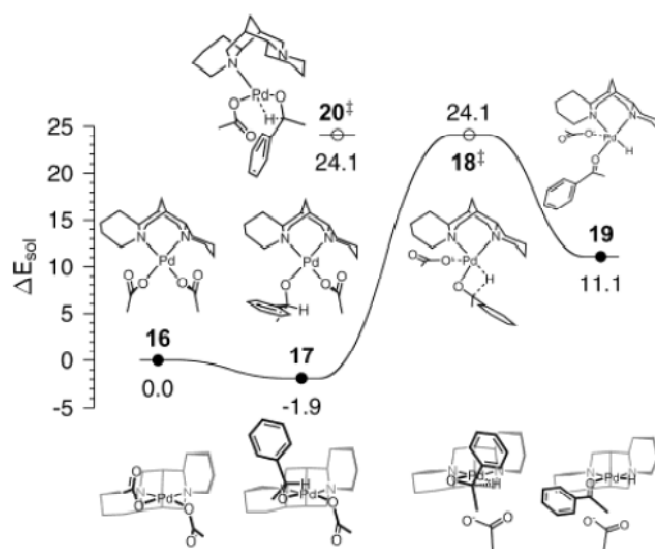


Figure A.4. Abbreviated mechanism for the oxidation of (*R*)-1-phenylethanol by ((-)-sparteine)Pd(OAc)₂. Energies (kcal/mol) include PB solvation by toluene ($\epsilon = 2.379$.) Bottom views are aligned below.

It is most intuitive to assume that the sparteine ligand imparts chirality to the metal center by remaining bidentate throughout the reaction and breaking the symmetry of the coordination sphere. Nonetheless, we also considered the dissociation of one or both N atoms of sparteine. A general result of the calculations is that the proximity of the nitrogen lone pairs and the bulk and rigidity of the ligand render it possible but unfavorable for sparteine to be bound to palladium by only one nitrogen. This is borne out by the peripheral structures in Figure A.2. **12–14**[‡] belong to a mechanism featuring monodentate sparteine, and a low-energy β -hydride elimination transition state **15**[‡] was found in which both Cl

atoms remain bound to Pd while protonated sparteine is present as a counter ion. Besides being energetically less favorable than 9^\ddagger , a mechanism including 14^\ddagger or 15^\ddagger likely suffers kinetically since sparteine must be removed from the metal. We speculate that sparteine possesses unusual kinetic stability; in addition to its chelation, its bulk hinders associative substitution mechanisms, and its rigidity hinders stepwise breaking of the N-Pd bonds. Finally, these alternate paths are not predicted to yield the enantioselectivity observed experimentally (*vide infra*).

The reoxidation of L_2PdXH species to L_2PdX_2 by O_2 , a reaction general to many catalytic cycles besides the present one, warrants separate attention. This step is apparently not rate limiting in oxidations featuring nitrogen-bound ligands under an oxygen atmosphere, and presently we find either of two suggestions plausible. O_2 may add across the Pd-H bond to produce a hydroperoxide complex, as proposed previously [1,26,27]. A hydroperoxide complex is expected to readily join the $1 \rightleftharpoons 7 \rightleftharpoons 8$ equilibrium after protonation by a new alcohol or sparteine- H^+Cl^- and liberation of H_2O_2 . Alternatively, Stahl [28] has demonstrated that $(bc)Pd^0(\eta^2\text{-olefin})$ (bc = bathocuproine) yields $(bc)Pd^{II}X_2$ and H_2O_2 (via a stable $(bc)Pd^{II}(\eta^2\text{-peroxo})$ intermediate) upon attack by molecular oxygen and an acid, HX . If an analogous reduced species such as $(sparteine)Pd^0(\eta^2\text{-ketone})$ can be attained, perhaps by deprotonation of **10**, a similar mechanism should yield the starting material **1**.

The result of our studies is a mechanism that involves the same sequence of steps proposed by Mueller et al. [29], whose observations of the same model reaction strongly support rate limitation by either deprotonation (at low sparteine loading) or β -hydride elimination (at high sparteine loading). Mueller found no reaction when no excess ligand was present, but as sparteine was added, the rate approached an asymptote at high loading. Also, when the α -hydrogen of 1-phenylethanol was replaced with deuterium, Mueller observed a kinetic isotope effect only under sparteine-saturated conditions. In light of these observations, we focus on the deprotonation (DP) and β -hydride elimination (β HE)

elementary steps, their dependence on the catalyst's composition, and their control of the observed selectivity.

A.3.2 Chloride vs. Acetate

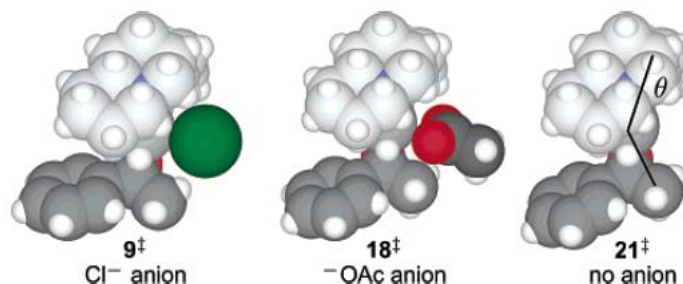


Figure A.5. β -Hydride elimination transition states incorporating chloride (9^\ddagger), acetate (18^\ddagger), and no anion (21^\ddagger), optimized in toluene. The anion nestles between the ligand and substrate, increasing the $C_{\text{sparteine}}\text{-Pd-}C_{\text{methyl}}$ angle θ .

The thermodynamics in Figure A.2 suggest that deprotonation of **7** is driven by the concentration of reactants, not by an energetic force. As mentioned, excess sparteine (or other base) is required for reaction to occur using a dichloride Pd source. When ^-OAc replaces Cl^- in the catalyst, however, the calculations predict that the ^-OAc group displaced by the substrate deprotonates the alcohol directly, without the aid of an exogenous base (Figure A.4). No stable analogue of structure **7** containing ^-OAc was found; instead the proton hops from the alcohol to the acetate ion during the energy minimization. We find that the alkoxide **17** is more stable ($\Delta E_{\text{sol}} = -1.9$ kcal/mol) than the sparteine- $\text{Pd}(\text{OAc})_2$ starting material **16**. (Again we consider that the acetic acid generated forms a hydrogen-bound complex with free sparteine, predicted to be only 10.2 kcal/mol more stable than separate acetic acid and sparteine.) Consequently we expect the alkoxide to play a larger role in the $\mathbf{16} \rightleftharpoons \mathbf{17}$ equilibrium when ^-OAc replaces Cl^- , leaving the overall reaction rate to be determined by the β -hydride elimination step at a lower concentration of base. Acetate's greater basicity is confirmed by the observation of modest reactivity when employing (sparteine) $\text{Pd}(\text{OAc})_2$ with no added base [10].

β HE transition-state structures and energies were found for 1-phenylethanol incorporating both Cl^- and ^-OAc as the anion. They reveal the important role of X-groups in determining the selectivity and rate of elimination-limited reactions. The sample structures in Figure A.5 illustrate that there is little direct interaction between the substrate and ligand. Instead, the temporarily displaced X-group lies between the two in a pocket lined by -CH groups of sparteine and the alcohol's methyl group. We believe that the role of the anion at this point in the mechanism is to communicate steric interactions between ligand and substrate, while not covalently bound but held in place by electrostatic forces. The $\text{C}_{\text{sparteine}}\text{-Pd-C}_{\text{methyl}}$ angle θ shown in Figure A.5 increases from 135° in **21** ‡ to 139° in **18** ‡ to 146° in **9** ‡ to accommodate the counter ions. By filling the space between the methyl group and ligand differently, the two anions present the same substrate with slightly different environments. The asymmetry of sparteine ensures that R and S alcohols face different combinations of steric interference as they pass through this transition state, hence the selectivity.

To validate the role of these diastereomeric transition-state structures, their energies were used to predict enantioselectivities (s_{calc}) of reactions limited by β -hydride elimination using the method of the following section. A selectivity factor of $s_{\text{calc}} = 17.7$ is calculated for 1-phenylethanol in toluene at 60°C when $\text{X} = \text{Cl}^-$, and $s_{\text{calc}} = 7.4$ at 80°C in toluene and $s_{\text{calc}} = 14.9$ at 60°C in 1,2-dichloroethane when $\text{X} = ^-\text{OAc}$. Bagdanoff et al. [11] report $s_{\text{exp}} = 20.0$ at 60°C using (norbornadiene) PdCl_2 as a palladium source. (This datum is interpreted here as representing the β -hydride elimination-controlled regime because of the excess base, Cs_2CO_3 , present.) Starting with $\text{Pd}(\text{OAc})_2$, Ferreira and Stoltz [4] report $s_{\text{exp}} = 8.8$ at 80°C in toluene and Jensen et al. [5] report $s_{\text{exp}} = 13.0$ at 60°C in dichloroethane.

To further emphasize the anion's role in the β -hydride elimination step, transition states were found for (R)- and (S)- 1-phenylethanol with no anion present. The separation of charge implied by removing the anion from the resulting cationic complex (e.g., **21** ‡ in Figure A.5) is energetically unrealistic in a low-dielectric medium such as toluene. Higher elimination barriers ($\Delta E_{\text{sol}}^\ddagger = 36.4$ kcal/mol relative to reactants) are predicted when Cl^- is

solvated separately than when Cl^- is allowed to remain close to the reaction center. More striking is that practically no discrimination between enantiomers is predicted ($s_{\text{calc}} = 1.5$), suggesting no selectivity would be observed if the anion were not present between the ligand and substrate to amplify it.

A.4 Selectivity

A.4.1 General

The enantioselectivity displayed by a catalyst/substrate pair is a convolution of the relative rates of the coordination (e.g., $1 \rightarrow 7$), deprotonation ($7 \rightarrow 8$), and β -hydride elimination ($8 \rightarrow 10$) events. An algebraic expression for selectivity in terms of these rates (k_{Coord} , k_{DP} , $k_{\beta\text{HE}}$) and their associated equilibrium constants depends on one's choice of rate law and the conditions employed in the reaction and cannot be written down a priori. We find that selectivities observed in kinetic resolutions of racemic mixtures under base-rich conditions are accurately described by

$$s_{\text{calc}} = \frac{\text{rate}_R}{\text{rate}_S} = \frac{A_o \sum_R \exp\left(-\frac{\Delta E_{\text{sol}}^\ddagger}{RT}\right)}{A_o \sum_S \exp\left(-\frac{\Delta E_{\text{sol}}^\ddagger}{RT}\right)} \quad (1)$$

when $\Delta E_{\text{sol}}^\ddagger$ is the calculated energy of a βHE transition state relative to the reactants (Figure A.6). Since the asymmetry of sparteine makes the two sites occupied by Cl atoms in the resting state incongruent, two βHE transition states exist for each enantiomer. Distinguished by which Cl atom is initially displaced by the alcohol, we consider these two structures (e.g., **R1** and **R2** or **S1** and **S2** in Table A.1) to belong to separate reaction pathways. (Four additional isomers, analogues of **R1**- **S2**, can be generated by swapping the methyl and aryl groups of the substrate so that the anion resides adjacent the aryl group

instead of the methyl group. For 1-phenylethanol, the unfavorable interaction of the anion with the δ -electrons of the aryl group causes the energies of these isomers to lie 2.5–4 kcal/mol above their analogues **R1-S2**, and these isomers were subsequently ignored.) Hence, the sums in (eq. 1) contain two terms per enantiomer. Equal prefactors A_0 are assumed. By the same reasoning, experimental and calculated selectivities can be transformed into effective $\Delta\Delta G^\ddagger$ s (a measure of the degree to which a catalyst distinguishes between enantiomers) for a substrate/anion/solvent combination according to $\Delta\Delta G^\ddagger_{\text{eff}} = RT \ln(s)$. Using only sparteine as a ligand, Jensen et al. found that the selectivity between (R)- and (S)-1-phenylethanol ranged from 2.6 to 17.5, depending on their palladium source and reaction conditions [5]. Although the models only contain information regarding the substrate, X-group, solvent, and temperature, they are able to consistently reproduce the selectivities observed in elimination-limited reactions.

Equation 1 is consistent with an expression such as

$$s = \frac{K_{\text{Coord,R}}K_{\text{DP,R}}k_{\beta\text{HE,R}}}{K_{\text{Coord,S}}K_{\text{DP,S}}k_{\beta\text{HE,S}}}$$

in which all steps prior to βHE reach preequilibrium. Expressions derived from more complex mechanisms cannot, however, be excluded. The selectivity observed in the DP-limited regime differs from that in βHE -limited reactions for a given catalyst and is likely described by $s = K_{\text{Coord,R}}k_{\text{DP,R}}/K_{\text{Coord,S}}k_{\text{DP,S}}$. We focus on selectivity in the βHE -limited regime for two reasons. Barring a change in mechanism, new catalysts will achieve their highest rates under these conditions. Also, the βHE step may be more amenable to tuning with new ligands than deprotonation. An experimental combinatorial study [30] found that Pd complexes of both chiral and achiral ligands yielded functioning catalysts in the presence of sparteine (acting only as a chiral deprotonating agent). Unfortunately, selectivities resulting from these asymmetric deprotonations were not improved over sparteine-Pd complexes operating in the βHE -limited regime.

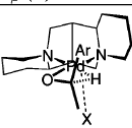
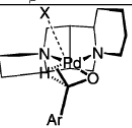
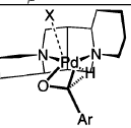
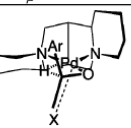
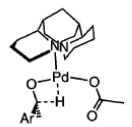
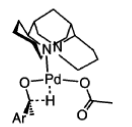
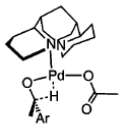
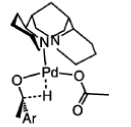
Entry	Substrate Anion	Solvent Temp	E_{sol}^a ($\Delta E_{\text{sol}}^{\ddagger b}$), kcal/mol		E_{sol}		E_{sol}		E_{sol}		s_{calc}^c s_{exp}^e	$\Delta\Delta G_{\text{eff,calc}}^e$ $\Delta\Delta G_{\text{eff,exp}}^e$
			C-H $_{\beta}$ (Å)	Pd...X ^d (Å)	C-H $_{\beta}$	Pd...X	C-H $_{\beta}$	Pd...X	C-H $_{\beta}$	Pd...X		
<div><div></div><div></div><div></div><div></div></div> <p>bidentate sparteine</p> <p>R1 R2 S1 S2</p>												
1	Ar = C ₆ H ₅ X = Cl ⁻	toluene 60°C	0.0 (17.5) 1.61	3.11	1.73 1.64	3.23	2.82 1.52	3.11	2.03 1.62	3.28	17.7 20.0 ^f	1.9 2.0
2	Ar = <i>p</i> -MeOC ₆ H ₄ X = Cl ⁻	toluene 60°C	0.0 (16.6) 1.58	3.25	1.21 1.61	3.28	2.65 1.48	3.12	1.82 1.59	3.31	14.1 14.9 ^f	1.8 1.8
3	Ar = <i>p</i> -FC ₆ H ₄ X = Cl ⁻	toluene 60°C	0.0 (17.8) 1.61	3.24	1.18 1.64	3.23	2.36 1.53	3.11	1.63 1.62	3.31	10.3 12.1 ^f	1.5 1.6
4	Ar = 2-Naphthyl X = Cl ⁻	toluene 60°C	0.0 (15.7) 1.59	3.11	2.28 1.64	3.23	2.87 1.52	3.11	2.13 1.62	3.29	19.5 15.8 ^f	2.0 1.8
5	Ar = C ₆ H ₅ X = ⁻ OAc	toluene 80°C	0.0 (24.1) 1.64	2.83	2.38 1.65	2.84	2.85 1.59	2.65	1.47 1.66	2.90	7.4 8.8 ^g	1.4 1.5
6	Ar = C ₆ H ₅ None	toluene 60°C	0.0 (—) 1.50	—	1.55 1.55	—	0.28 1.50	—	1.54 1.55	—	1.5 NA	0.3 NA
7	Ar = C ₆ H ₅ X = I ⁻	toluene 60°C	0.0 (14.5) 1.56	3.42	1.72 1.61	3.82	2.48 1.53	3.93	2.04 1.61	3.64	15.5 NA	1.8 NA
8	Ar = C ₆ H ₅ X = Cl ⁻	gas phase 60°C	0.0 (23.4) 1.56	3.00	1.54 1.62	3.09	3.55 1.50	3.01	1.64 1.60	3.07	12.5 NA	1.7 NA
9	Ar = C ₆ H ₅ X = Cl ⁻	chloroform 23°C	0.0 (14.6) 1.62	3.22	2.34 1.67	3.32	2.85 1.56	3.23	2.08 1.64	3.31	27.7 30.7 ^h	2.0 2.0
10	Ar = C ₆ H ₅ X = ⁻ OAc	1,2-DCE 60°C	0.0 (26.5) 1.64	3.05	3.21 1.66	3.00	2.45 1.58	3.21	2.08 1.66	3.00	14.9 13.0 ⁱ	1.8 1.7
<div><div></div><div></div><div></div><div></div></div> <p>monodentate sparteine</p> <p>R3 R4 S3 S4</p>												
11	Ar = C ₆ H ₅ X = ⁻ OAc	toluene 60°C	0.60 (24.7) 1.58	2.08	0.07 1.58	2.08	1.23 1.61	2.09	0.0 1.60	2.08	1.1 NA	0.1 NA

Table A.1. Energetic and structural data of diastereomeric β -hydride elimination transition states. ^a Relative to lowest-energy isomer. ^b Activation energy relative to reactants. ^c From (eq. 1). ^d When X = ⁻OAc, distance to nearest O atom. ^e Data best representing elimination-determined selectivities (i.e., base-rich reaction conditions) is used for comparison. ^fFrom [11]. ^gFrom [4]. ^hFrom [12]. ⁱFrom [5]

Four β HE transition states were located for a sampling of substrates (1-substituted ethanols), solvents, and X-groups. The energetic and structural data collected in Table A.1 show that configurations **R1** and **S2** provide the lowest-energy routes to the (R) and (S) substrates, respectively, although none of the four paths is negligible. We find the relative energies of the isomers are determined by three factors. First, transition-state energies are lower if the anion is displaced to the open face of the ligand (below Pd in Table A.1) than if it moves to the occluded face (above Pd). The rightmost piperidine ring of sparteine (as

drawn) disrupts the coordination sphere of Pd by interfering with both the adjacent equatorial site (e.g., the adjacent chlorine in **1** is bent out of the square plane) and upper axial site (e.g., the anion in structure **S1**). Whether the oxygen of the substrate bonds to the left or right site on Pd is another factor. In the favorable site (R1, S1), oxygen abuts the less obtrusive, leftmost piperidine ring. This effect is most clearly seen in entry **6**, in which no anion is present to otherwise affect the relative energies. Third, as mentioned, displacing the anion toward the aryl group of the substrate requires more energy than displacing it toward the methyl group. By combining the favorable aspects of each of these factors, structure **R1** provides (R) substrates with the fastest oxidation pathway.

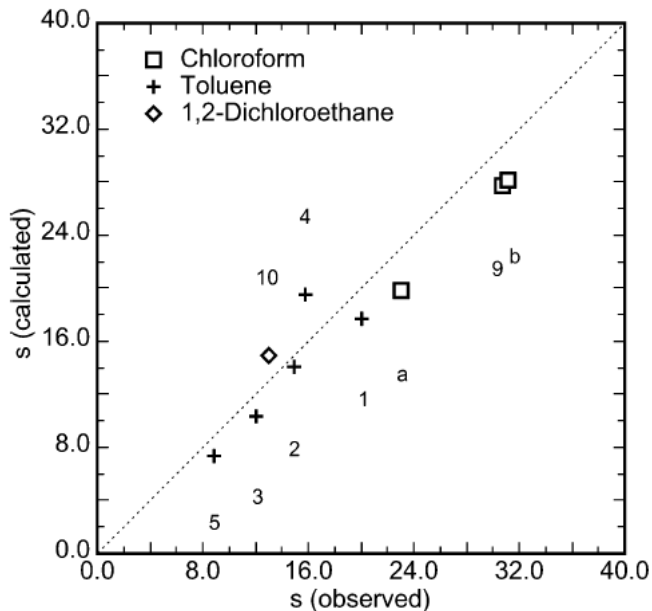


Figure A.6. Calculated and experimental enantioselectivities. Labels denote corresponding entry in Table A.1; a and b correspond to 1-(*p*-FC₆H₄)ethanol and 1-(2-naphthyl)ethanol, respectively, in chloroform at 23 °C, X = Cl[−].

Selectivity predictions based on the combination of gas-phase optimized transition-state energies and single-point solvation energies only qualitatively matched the experimental observations. In particular, this approach failed to capture the high selectivities observed when chloroform is used as solvent. This suggested that solvent-induced geometric relaxation plays a significant role in addition to electronic relaxation. Therefore, all

structures **R1** through **S2** were optimized within the continuum solvent model, allowing the geometries and relative energies to more accurately reflect the action of the particular solvent.

A.4.2 Solvent Effects

Many organic solvents have proved competent for kinetic resolutions using sparteine-PdCl₂, with reactions in halomethanes excelling in both rate and selectivity [12]. Although the advantages associated with different solvents may also concern solubilities and the oxidation of the Pd-hydride intermediate, the effect of the dielectric on the β HE step is revealed by the evolution of the transition states in the different virtual solvents. The β -hydrogen displaces the remaining anion from its site as the C-H $_{\beta}$ bond breaks. Since breaking the polar Pd-X bond requires further separation of charge between the positively charged Pd center and the anion, it follows that a medium of increased dielectric strength should facilitate the process. The activation energies calculated for (R)-1-phenylethanol (traversing state **R1**, X = Cl⁻) in a vacuum, toluene ($\epsilon = 2.4$), and chloroform ($\epsilon = 4.8$) are 23.4, 17.5, and 14.6 kcal/ mol, respectively. We find this trend to be general of all substrates. (When X = ⁻OAc, the predicted activation energies increase with the dielectric constant, but the sparteine-HOAc byproduct is responsible for reversal of this trend. Unlike the sparteine-H⁺Cl⁻ complex, the acetic acid complex formed during the deprotonation of the bound alcohol is not polar enough to generate a large solvation energy. Consequently, reactants (16) are favored over later intermediates as the dielectric increases. However, the energy difference between the alkoxide and β HE states is decreased by increasing dielectric strength whether X = Cl⁻ or ⁻OAc.) That the solvent is stabilizing the charge separation is manifest in the increasing Mulliken population of the Cl⁻ ion: -0.65 |e⁻| in a vacuum, -0.74 |e⁻| in toluene, and -0.79 |e⁻| in chloroform (structures **R1** of entries **8**, **1**, and **9**).

The increase in reaction rate observed in chloroform (relative to toluene) is apparently also the primary factor responsible for the observed increase in selectivity. A facile kinetic resolution can be performed at lower temperatures, where a catalyst's discrimination

between enantiomers (i.e., $\Delta\Delta G_{\text{eff}}^\ddagger$) leads to a higher selectivity factor. For example, Bagdanoff, using a dichloride catalyst and 1-phenylethanol, reported a selectivity of 20.0 in toluene [11] at 60 °C and 31 in chloroform [12] at 23 °C, suggesting the same $\Delta\Delta G_{\text{eff}}^\ddagger$ of 2.0 kcal/mol in each solvent. However, a second mechanism is also at work, by which the solvent influences $\Delta\Delta G_{\text{eff}}^\ddagger$ directly. 1-(*p*-fluoro)phenylethanol exhibited a selectivity of 12.1 at 60 °C in toluene [11] and 23 at 23 °C in chloroform [12], yielding disparate $\Delta\Delta G_{\text{eff}}^\ddagger$ s of 1.65 and 1.84 kcal/mol, respectively. (Both increases and decreases in $\Delta\Delta G_{\text{eff}}^\ddagger$ are observed among the substrates.) Although possibly due to a difference in the activation entropies of enantiomers, this more subtle effect may also be mediated by the response of the displaced anion to more polar solvents. Two trends regarding the anion are clear in the calculations. One is the aforementioned accumulation of charge allowed by higher dielectrics. The second is the increase in the Pd...X distance in transition states optimized in more polarizable media. (See entries **8**, **1**, and **9**, or **5** and **10**.) In stabilizing the forming dipole the solvent draws the charged species further into solution. Together, these two effects allow the solvent to influence the effective size and position of the X-group. Since the X-group is responsible for communicating steric interactions from ligand to substrate, it follows that the solvent's influence should extend to the discrimination between enantiomers. An additional selectivity prediction using dichloromethane as solvent (for 1-phenylethanol at 60 °C, X = Cl⁻, ϵ = 9.1) yielded s_{calc} = 13.1. The β HE structures relaxed in this dielectric show that the chloride ion moves still farther from the palladium center, and this is likely the cause of the decrease in calculated selectivity from chloroform to dichloromethane. We propose that there is a critical dielectric constant above which (with the help of entropy) the anion would be solvated entirely separate from the cationic complex. For example, using a dielectric of 80.4 to represent water we find the separate ions Cl⁻ and **21**[‡] have a slightly lower energy than the complex **9**[‡]. Were the reactants still soluble in so polar a medium, enantioselectivity would be lost.

A.4.3 Substrate and Ions

The oxidation rates of substituted benzylic alcohols in the presence of excess sparteine were observed to increase with the electron-donating strength of the substituent [10]. This was attributed to a rate-limiting β HE step in which negative charge is drawn from the alkoxide to the resulting Pd-hydride complex. Our calculations involving *para*-substituted 1-phenylethanols (entries **1–3**) show the same behavior; that is, the activation energies $\Delta E_{\text{sol}}^{\ddagger}$ increase with the Hammett parameters of the substrates. In accordance with the Hammond postulate, we find that transition-state structures of less easily oxidized substrates are more product-like. For example, the C-H $_{\beta}$ bond being broken in each transition state incorporating 1-(*p*-fluoro)phenylethanol is at least 0.03 Å longer than the corresponding C-H $_{\beta}$ bond in 1-(*p*-methoxy)phenylethanol.

To explore the properties of other counter ions, chlorine was replaced with iodine in the model reaction, and the key energetics were calculated. The predicted selectivity ($s_{\text{calc}} = 15.5$ at 60 °C, entry **7**) is no greater than that of the dichloride catalyst, but the activation energy of the lowest β HE transition state ($\Delta E_{\text{sol,I,R1}}^{\ddagger}$) 14.5 kcal/mol) is lower (cf $\Delta E_{\text{sol,Cl,R1}}^{\ddagger} = 17.5$). This reflects the ground-state destabilization of the initial (sparteine)PdI₂ complex; the crowding of sparteine and the large iodine atoms around Pd effectively weakens the Pd-X bonds which must be broken during the cycle. High activity can be translated into higher selectivity by operating at a lower temperature, as noted.

When X = ⁻OAc, β HE transition states incorporating monodentate sparteine (entry **11**) are as energetically accessible as those with the ligand chelated (entry **5**). In this geometry the ligand dominates the coordination sphere even less than when bidentate, and the variation in energy among the isomers (and hence the predicted selectivity) is correspondingly small. Still another group of isomers exists in which the oxygen of the substrate bonds *trans* to monodentate sparteine, but the activation energies associated with this geometry are 8 kcal/ mol higher than those for the structures shown.

A.4.4 Thermodynamics

The discussion above relies on solution phase energies rather than enthalpies or free energies. Accurate gas-phase thermodynamic properties for the various intermediates can be calculated by applying the appropriate formulas of statistical mechanics to frequency spectra derived from calculated (gas phase) Hessians. Solution-phase enthalpies are accessible from the gas-phase values by subtracting PV and including the calculated solvation energies. This assumes the six hindered translational and rotational modes still behave classically and contribute $6/2kT$ to the total energy and the vibrational frequencies do not change appreciably in solution. In this manner solution-phase enthalpies H_{sol} at 298 K were calculated for the model reaction. This yielded: reactants (**1**), 0.0 kcal/mol; substitution transition state (**6[‡]**), 5.2; alcohol complex (**7**), -1.1; alkoxide complex (**8**), 1.3; and β HE transition state (**9[‡]**), 16.2. (The last value can be compared to the activation enthalpy of 16.8 kcal/mol measured by Mueller and Sigman [10] using an Eyring plot from 30 to 65 °C.) Since the “reactants” state is composed of three separate molecules (alcohol, sparteine-PdCl₂, and free sparteine) and subsequent stages of the oxidation involve only two (Pd-substrate complex and sparteine-H⁺Cl⁻ complex), the free energy of the reactants will be even lower relative to that of the other intermediates because of their greater entropy. This explains the observation of a first-order dependence of reaction rate on substrate concentration under all conditions. As long as the reactants are lowest in free energy, increased alcohol concentration will drive more palladium from state **1** to states **7** and onward.

The relative solution-phase enthalpies of the β HE transition states incorporating 1-phenylethanol and chloride (entry **1**) are 0.0 (**R1**), 1.7 (**R2**), 2.8 (**S1**), and 2.1 (**S2**). In general, we find that selectivity predictions based on solution-phase enthalpies yield qualitatively similar results to those based on energies but with more variation from the experimental measurements. The gas-phase entropies of the same four species are within 1 eu of one another, and for other substrates the variation is less than 5 eu. Therefore, we conclude that energy (or enthalpy) differences alone are sufficient to explain

enantioselectivities derived from β HE. Thus, we rely on solution-phase energies, reaching the same conclusions and avoiding the assumptions associated with gas-phase Hessians.

A.5 Discussion

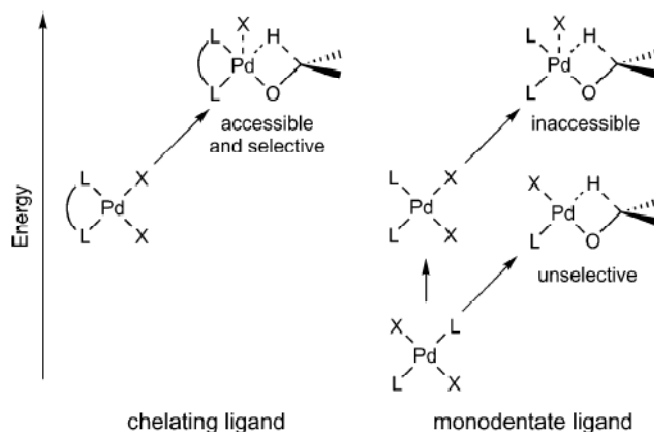
The ligands which have proved less selective than sparteine in kinetic resolutions of sec-alcohols are too numerous and complex to study individually. However, their structures and comparisons of the experimental and theoretical observations allow speculation regarding which motifs may be responsible for reaction rates and selectivities in current and future catalysts.

Brucine [4], (+)-Troger's base, quinine (OTBS), and (S)- nicotine [5] each yielded higher rates than sparteine in the $\text{Pd}(\text{OAc})_2$ -catalyzed oxidation of 1-phenylethanol under similar conditions. Their enantioselectivities, however, were unobservable or small. The former two in this group have only sp^3 N lone pairs available for bonding to Pd (neglecting oxygen atoms), while the latter two possess both sp^3 and sp^2 N atoms and O atoms. The geometries of all four dictate that they bond to Pd through only one N at a time. (S,S)-Ph-BOX [5], (S,S)-Ph-PyBOX [4,5], cinchonidine [4], and others displayed no selectivity and lower rates than sparteine when tested. Possibly multidentate, these ligands provide either sp^2 (Ph-BOX, Ph-PyBOX) or both sp^2 and sp^3 N lone pairs. The chiral phosphine BINAP also showed rates similar to those of sparteine and no enantioselectivity.

Sparteine's rigid structure forces it to chelate in a *cis*, bidentate fashion, while L_2PdX_2 -type compounds generally prefer a *trans* arrangement. If, for monodentate ligands, the alkoxide requires two of the four Pd sites during β HE, then the lowest-energy transition structure will have either the form $\text{LXPd}(\text{alkoxide})$ or $\text{L}_2\text{Pd}(\text{alkoxide})$. The former case is likely unselective for other ligands, as it is for sparteine. The latter case, which would require extra mechanistic steps to rearrange the ligands from a *trans* configuration, may be energetically inaccessible from the (more stable) *trans* resting state (Scheme A.2), so it

would seem only a catalyst with a *cis* resting state can lead to an accessible and selective β HE transition state.

Scheme A.2



Our work joins a number of increasingly quantitative calculations of the outcome of stereoselective reactions in solution and in proteins. Many algorithms have been applied to this problem, employing a variety of methods for the evaluation of energies (force fields [31], DFT [32], empirical correlations [33]) and structural models (explicit transition states or more abstract concepts [34]). Some factors which aid the reliability of predictions, however, are recurrent. Relative reaction rates often result from a flux of chiral or prochiral molecules through not only two transition states (e.g., (R) and (S)) but through a collection of diastereomeric states. A computational model should reflect this by averaging over an ensemble of all thermodynamically relevant reaction paths. Also, variations in the solvent-accessible surface of these isomeric transition states can contribute to or even determine [33] selectivity. A model of solvation is therefore helpful or necessary, depending upon the reaction in question.

A.6 Conclusions

The mechanism for oxidation of sec-alcohols by ((-)-sparteine)PdX₂ compounds begins with the facile substitution of an alcohol for an anion, followed by the deprotonation of the bound alcohol. Chloride is too weak a base to drive this step alone and requires free

sparteine or a basic additive to form a Pd-alkoxide. Acetate and stronger bases can perform the deprotonation alone or in conjunction with sparteine at rates dependent on their basicity and concentration.

Once the ensuing β -hydride elimination step becomes rate limiting, the enantioselectivity displayed by a catalyst in the presence of a racemic substrate is a function of the relative energies of an ensemble of diastereomeric β HE transition-state structures. The anion plays a critical role in these transition states by mediating the interaction between the otherwise estranged ligand and substrate. Solvents influence rate and selectivity during the elimination by accommodating an increase in charge on the anion. In addition to aiding the interpretation of existing results, the ability to compute activation energies and enantioselectivities provides a tool for screening new catalyst/substrate combinations.

Bibliography

- [1] (a) Peterson, K. P.; Larock, R. C. *J. Org. Chem.* **1998**, *63*, 3185.
(b) Ferreira, E. M.; Stoltz, B. M. *J. Am. Chem. Soc.* **2001**, *123*, 7725.
(c) Jensen, D. R.; Pugsley, J. S.; Sigman, M. S. *J. Am. Chem. Soc.* **2001**, *123*, 7475.
(d) Steinhoff, B. A.; Fix, S. R.; Stahl, S. S. *J. Am. Chem. Soc.* **2002**, *124*, 766.
(e) Steinhoff, B. A.; Stahl, S. S. *Org. Lett.* **2002**, *4*, 4179.
- [2] ten Brink, G.-J.; Arends, I. W. C. E.; Sheldon, R. A. *Science* **2000**, *287*, 1636.
- [3] Bortolo, R.; Bianchi, D.; D'Aloisio R.; Querci, C.; Ricci, M. *J. Mol. Catal. A* **2000**, *153*, 25.
- [4] (a) Nishimura, T.; Uemura, S. *Synlett* **2004**, *2*, 201.
(b) Nishimura, T.; Onoue, T.; Ohe, K.; Uemura, S. *J. Org. Chem.* **1999**, *64*, 6750.
(c) Nishimura, T.; Onoue, T.; Ohe, K.; Uemura, S. *Tetrahedron Lett.* **1998**, *39*, 6011.
(d) Hosokawa, T.; Murahashi, S.-I. *Acc. Chem. Res.* **1990**, *23*, 49.
- [5] (a) Steinhoff, B. A.; Guzei, I. A.; Stahl, S. S. *J. Am. Chem. Soc.* **2004**, *126*, 11268.

- (b) Konnick, M. M.; Guzei, I. A.; Stahl, S. S. *J. Am. Chem. Soc.* **2004**, *126*, 10212.
- (c) Stahl, S. S.; Thorman, J. L.; Nelson, R. C.; Kozee, M. A. *J. Am. Chem. Soc.* **2001**, *123*, 7188.
- [6] *Jaguar 5.5*; Schrodinger, Inc.: Portland, OR, 2003.
- [7] Becke, A. D. *J. Chem. Phys.* **1993**, *98*, 5648.
- [8] Lee, C.; Yang, W.; Parr, R. G. *Phys. Rev. B* **1988**, *37*, 785.
- [9] Baker, J.; Muir, M.; Andzelm, J.; Scheiner, A. In *Chemical Applications of Density-Functional Theory*; Laird, B. B., Ross, R. B., Ziegler, T., Eds.; ACS Symposium Series 629; American Chemical Society: Washington, DC, 1996.
- [10] Niu, S.; Hall, B. M. *Chem. Rev.* **2000**, *100*, 353.
- [11] (a) Hay, P. J.; Wadt, W. R. *J. Chem. Phys.* **1985**, *82*, 299.
- (b) Goddard, W. A., III. *Phys. Rev.* **1968**, *174*, 659.
- (c) Melius, C. F.; Olafson, B. O.; Goddard, W. A., III. *Chem. Phys. Lett.* **1974**, *28*, 457.
- [12] (a) Hariharan, P. C.; Pople, J. A. *Chem. Phys. Lett.* **1972**, *16*, 217.
- (b) Francel, M. M.; Pietro, W. J.; Hehre, W. J.; Binkley, J. S.; Gordon, M. S.; DeFrees, D. J.; Pople, J. A. *J. Chem. Phys.* **1982**, *77*, 3654.
- [13] (a) Tannor, D. J.; Marten, B.; Murphy, R.; Friesner, R. A.; Sitkoff, D.; Nicholls, A.; Ringnalda, M.; Goddard, W. A., III; Honig, B. *J. Am. Chem. Soc.* **1994**, *116*, 11875.
- (b) Marten, B.; Kim, K.; Cortis, C.; Friesner, R. A.; Murphy, R. B.; Ringnalda, M. N.; Sitkoff, D.; Honig, B. *J. Phys. Chem.* **1996**, *100*, 11775.

- [14] (a) Truong, T. N.; Truong, T. T.; Stefanovich, E. V. *J. Chem. Phys.* **1997**, *107*, 1881.
- (b) Cramer, C. J.; Thrular, D. G. *Chem. Rev.* **1999**, *99*, 2161.
- (c) Oxgaard, J.; Muller, R. P.; Periana, R. A.; Goddard, W. A. III. *J. Am. Chem. Soc.* **2004**, *126*, 352
- [15] (a) Xu, X.; Goddard W. A. *Proc. Natl. Acad. Sci. U.S.A.* **1996**, *99*, 15308.
- Wittbrodt, J. M.; Schlegel, H. B. *J. Chem. Phys.* **1996**, *105*, 6574.
- (b) For methods on correcting spin contamination in DFT, see: Bally, T.; Borden, W. T. *Rev. Comput. Chem.* **1999**, *13*, 1.
- [16] Kitamura, C.; Inoue, T.; Kawatsuki, N.; Yoneda, A. *Anal. Sci.* **2005**, *21*, x15.
- [17] Dey, S.; Jain, V. K.; Knoedler, A. *Anal. Sci.* **2004**, *20*, x127.
- [18] (a) Igersheim, F.; Mimoun, H. *Nouv. J. Chim.* **1980**, *4*, 711.
- (b) Muto, S.; Kamiya, Y. *Bull. Chem. Soc. Jpn.* **1976**, *49*, 2587.
- [19] For a similar simplification on the experimental front, see: ten Brink G.-J.; Arends I. W. C. E.; Hoogenraad, M.; Verspui, G.; Sheldon, R. A. *Adv. Synth. Catal.* **2003**, *345*, 497.
- [20] Harvey, J. N.; Aschi, M.; Schwarz, H.; Koch, W. *Theor. Chem. Acc.* **1998**, *99*, 95.
- [21] Carreón-Macedo, J.-L.; Harvey, J. N. *J. Am. Chem. Soc.* **2004**, *126*, 5789.
- [22] Fan, Y.; Hall, M. B. *Chem. Eur. J.* **2004**, *10*, 1805.
- [23] Stahl, S. S. *Angew. Chem., Int. Ed.* **2004**, *43*, 3400 and references cited therein.

- [24] (a) Denny, M. C.; Smythe, N. A.; Cetto, K. L.; Kemp, R. A.; Goldberg, K. I. *J. Am. Chem. Soc.* **2006**, *128*, 2508.
- (b) A second paper appearing shortly after (a) also reports insertion of molecular oxygen into a Pd^{II}-H bond: Konnick, M. M.; Gandhi, B. A.; Guzei, I. A.; Stahl, S. *S. Angew. Chem., Int. Ed.* **2006**, *45*, 2904.
- [25] *Jaguar 6.5*; Schrodinger, Inc.: Portland, OR, 2005.
- [26] (a) Smith, K. M.; Poli, R.; Harvey, J. N. *Chem.–Eur. J.* **2001**, *7*, 1679.
- (b) Poli, R.; Harvey, J. N. *Chem. Soc. Rev.* **2003**, *32*, 1.
- [27] Skodje, R. T.; Truhlar, D. G. *J. Phys. Chem.* **1981**, *85*, 624.
- [28] For a more in-depth discussion of this, see, for example: Churchill, D. G.; Janak, K. E.; Wittenberg, J. S.; Parkin, G. *J. Am. Chem. Soc.* **2003**, *125*, 1403.
- [30] (a) Punniyamurthy, T.; Velusamy, S.; Iqbal, J. *Chem. Rev.* **2005**, *105*, 2329.
- (b) Gligorich, K. M.; Sigman, M. S. *Angew. Chem., Int. Ed.* **2006**, *45*, 6612.
- (c) Stoltz, B. M. *Chem. Lett.* **2004**, 362.
- (d) Sigman, M. S.; Schultz, M. J. *Org. Biomol. Chem.* **2004**, *2*, 2551.
- (e) Stahl, S. *Science* **2005**, *309*, 1824.
- (f) Muzart, J. *Chem. Asian J.* **2006**, *1*, 508.
- [31] (a) Sigman, M. S.; Jensen, D. R. *Acc. Chem. Res.* **2006**, *39*, 221.
- (b) Bagdanoff, J. T.; Stoltz, B. M. *Angew. Chem., Int. Ed.* **2004**, *43*, 353.

- (c) Jensen, D. R.; Schultz, M. J.; Mueller, J. A.; Sigman, M. S. *Angew. Chem. Int. Ed.* **2003**, *42*, 3810.
- (d) Schultz, M. J.; Park, C. C.; Sigman, M. S. *Chem. Commun.* **2002**, 3034.
- (e) Bagdanoff, J. T.; Ferreira, E. M.; Stoltz, B. M. *Org. Lett.* **2003**, *5*, 835.
- (f) Jensen, D. R.; Sigman, M. S. *Org. Lett.* **2003**, *5*, 63.
- [32] (a) Rogers, M. M.; Wendlandt, J. E.; Guzei, I. A.; Stahl, S. S. *Org. Lett.* **2006**, *8*, 2257.
- (b) Lee, J. M.; Ahn, D. S.; Jung, D. Y.; Lee, J.; Do, Y.; Kim, S. K.; Chang, S. K. *J. Am. Chem. Soc.* **2006**, *128*, 12954.
- (c) Streuff, J.; Hovellmann, C. H.; Nieger, M.; Muniz, K. *J. Am. Chem. Soc.* **2005**, *127*, 14586.
- (d) Brice, J. L.; Harang, J. E.; Timokhin, V. I.; Anastasi, N. R.; Stahl, S. S. *J. Am. Chem. Soc.* **2005**, *127*, 2868.
- (e) Timokhin, V. I.; Anastasi, N. R.; Stahl, S. S. *J. Am. Chem. Soc.* **2003**, *125*, 12996.
- [33] (a) Nishimura, T.; Araki, H.; Maeda, Y.; Uemura, S. *Org. Lett.* **2003**, *5*, 2997.
- (b) Matsumura, S.; Maeda, Y.; Nishimura, T.; Uemura, S. *J. Am. Chem. Soc.* **2003**, *125*, 8862.
- (c) Nishimura, T.; Matsumura, S.; Maeda, Y.; Uemura, S. *Tetrahedron Lett.* **2002**, *43*, 3037.
- (d) Nishimura, T.; Ohe, K.; Uemura, S. *J. Am. Chem. Soc.* **1999**, *121*, 2645.
- [34] (a) Piera, J.; Narhi, K.; Backvall, J. E. *Angew. Chem., Int. Ed.* **2006**, *45*, 6914.

- (b) Trend, R. M.; Ramtohul, Y. K.; Ferreira, E. M.; Stoltz, B. M. *Angew. Chem., Int. Ed.* **2003**, *42*, 2892.
- [35] Bianchi, D.; Bortolo, R.; D'Aloisio, R.; Ricci, M. *Angew. Chem., Int. Ed.* **1999**, *38*, 706.
- [36] Clegg, W.; Eastham, G. R.; Elsegood, M. R. J.; Heaton, B. T.; Iggo, J. A.; Tooze, R. P.; Whyman, R.; Zacchini, S. *J. Chem. Soc., Dalton. Trans.* **2002**, 3300.
- [37] (a) Landis, C. R.; Morales, C. M.; Stahl, S. S. *J. Am. Chem. Soc.* **2004**, *126*, 16302.
- (b) Popp, B. V.; Wendlandt, J. E.; Landis, C. R.; Stahl, S. S. *Angew. Chem. Int. Ed.* **2007**, *46*, 601.
- [38] Privalov, T.; Linde, C.; Zetterberg, K.; Moberg, C. *Organometallics* **2005**, *24*, 885.
- [39] Nielsen, R. J.; Goddard, W. A., III. *J. Am. Chem. Soc.* **2006**, *128*, 9651.
- [40] (a) Sheldon, R. A.; Arends, I. W. C. E.; ten Brink, G.-J.; Dijksman, A. *Acc. Chem. Res.* **2002**, *35*, 774.
- (b) Toyota, M.; Ihara, M. *Synlett* **2002**, 1211.
- [41] Popp, B. V.; Stahl, S. S. *J. Am. Chem. Soc.* **2007**, *129*, 4410.
- [42] Oxgaard, J.; Bhalla, G.; Periana, R. A.; Goddard, W. A., III. *Organometallics*, **2006**, *25*, 1618.
- [43] Chowdhury, S.; Rivalta, I.; Russo, N.; Sicilia, E. *Chem. Phys. Lett.*, **2007**, *443*, 183.
- [44] *Jaguar 7.0*; Schrodinger, Inc.: Portland, OR, 2005.